

A STUDY OF THE ADSORPTION OF Ni(II)
ONTO AN AMORPHOUS SILICA SURFACE
BY CHEMICAL AND NMR METHODS

Thesis by
James R. Young

In Partial Fulfillment of the Requirements
for the Degree of
Doctor of Philosophy

California Institute of Technology
Pasadena, California
1982

(Submitted August 12, 1981)

ACKNOWLEDGEMENTS

There are many people who have given much of themselves to make these years at Caltech an unmatched learning experience which extends far beyond the scope of this thesis. Most importantly, the patience and support of my advisor, James J. Morgan, are greatly appreciated. Our discussions have been very helpful and his counsel has proven to be sound.

I would like to acknowledge the contribution of Sunney Chan who spent much time teaching me about NMR and provided an opportunity to conduct NMR experiments in his laboratory.

I owe a debt of thanks to Stan Manatt and Stan Sander for their assistance in facilitating the NMR experiments conducted at JPL. Bill Croasmun has given his time and talents to the same end here at Caltech.

The following people deserve credit for providing the technical assistance necessary to complete this work: Sylvia Garcia, Michaela Garvey, Anna Huff and Lorraine Moberly. I am especially grateful to Pat Coin, who slaved over a cranky spectrometer, and John Faughnan (programmer extraordinaire) for installing the surface chemistry subroutines necessary to create SURFEQL.

The Caltech staff is incomparable. Elton Daly, Joe Fontana, Rich Eastvedt, Dave Byrum, and Leonard Montenegro have never failed to help repair the inevitable (and always critical) late afternoon breakdowns. The Environmental Engineering Librarians, Rayma Harrison and Gunilla Hastrup, are very proficient and, above all, wonderful people to know. The department secretaries, especially Elaine Granger, Joan Mathews, and

Adelaide Massengale, have continually helped me with typing, copying and a multitude of other necessary tasks.

I must say thanks to these fellow students and associates for their friendship and help: Mike Barcelona, Jim Hunt, Alan Stone, Windsor Sung and especially to my most recent office mates, Lisa Anderson, Jim Ouimette and Connie Senior for helping to keep each crisis in its proper perspective and maintaining a necessary level of craziness, for balance.

I appreciate and acknowledge the following organizations' generous support of Caltech and this work: The U.S. Environmental Protection Agency, National Institute of Environmental Health Sciences, Foremost-McKesson, Inc., Union Oil Company, General Motors, the President's Fund, the President's Venture Fund, the Jesse Smith Noyes Foundation, Inc. and lastly, the National Science Foundation whose support of the Southern California Regional NMR Facility through grant number CHE-7916324 made instrument time available on the WM-500 spectrometer.

Lastly, I must express my deepest feelings of gratitude to my parents, Robert and Bernice Young, for supporting me to the fullest in all of my decisions and through some difficult times, to my fiancée, Bea Meyerhofer, for her patience and love during these last few months and to Peg Meyerhofer for her invaluable help during the final weeks of the preparation of this thesis.

ABSTRACT

The physical structure of the electrical double layer at a metal-oxide surface is not well-known. Adsorption models, which require a knowledge of the location of the adsorbed species, have integrated different descriptions of the electrical double layer into a common coordination chemistry framework.

The goal of this work was to determine the hydration number of Ni(II) species adsorbed onto a silica surface by extending a nuclear magnetic resonance (NMR) technique used to determine the hydration number of paramagnetic metal ions in solution. Information about the environment of the adsorbed Ni(II) species at the molecular level could then be incorporated into state-of-the-art adsorption models.

In order to conduct the NMR experiment, it was necessary to determine the speciation of a Ni(II)-silica system at a high metal-ion loading. Titrations, in 0.1 N NaClO_4 , were conducted on silica suspensions, nickel solutions and a system where the total amount of Ni(II) was twice the total number of available surface binding sites. The pH dependence of the adsorption process and the maximum adsorption density achievable were investigated.

The amount of charge on a silica surface was found to increase logarithmically with pH. Formation of surface complexes with Na^+ provided the necessary mechanism to account for this behavior. All of the Ni(II) present in the Ni(II)-silica system was removed by adsorption processes at a pH of approximately 8. In the same system, removal of Ni(II) by a precipitation process does not occur until $\text{Ni(OH)}_2(\text{s})$ forms at a pH of

approximately 8.5. The adsorption process was not limited by the number of surface hydroxyl groups present. It was shown that the NiOH moiety of a hydrolyzed nickel surface complex could provide the new adsorption centers necessary for a multilayer adsorption process, if the NiOH group functions chemically like an SiOH group. The observation of adsorption of Ni(II) onto a silica surface at coverages greater than one monolayer indicates siliceous soils and sediments may have a greater capacity to bind Ni(II) than previously thought.

The capability of the NMR spectroscopic technique to determine hydration numbers of adsorbed metal ions was demonstrated. Usefulness of the technique was limited by the slowness of water exchange between the first coordination sphere of the adsorbed Ni(II) species and bulk solution. A lower limit for the hydration number of the adsorbed Ni(II) species was calculated to be 4.4. This is at the lower end of the predicted range for this value (4.5 to 6.0). Suggestions were made to improve upon the design of the NMR experiment so as to overcome the limitations encountered.

TABLE OF CONTENTS

<u>Chapter</u>		<u>Page</u>
	NOTATIONS	xiv
1	INTRODUCTION	1
	1.1 Adsorption Models	1
	1.2 Nuclear Magnetic Resonance	4
	1.3 Reasons for the Choice of Nickel and Silica	6
2	THEORY	8
	2.1 Adsorption	8
	2.1.1 Introduction	8
	2.1.2 Coordination Chemistry on the Surface	9
	2.1.2.1 Hydrolysis of Surface Groups	9
	2.1.2.2 Adsorption of Trace Metals, Major Cations and Major Anions	11
	2.1.3 Physical Descriptions of the Electrical Double Layer	12
	2.1.4 Charge and Potential Relationships	16
	2.1.4.1 The Triple Layer Model	16
	2.1.4.2 The Constant Capacitance Model	18
	2.1.5 Surface Equilibrium Constants Corrected for Electrostatic Effects	19 19
	2.1.6 Computer Modeling	21
	2.2 Nuclear Magnetic Resonance Spectroscopy	21
	2.2.1 Introduction	21
	2.2.2 Prior Applications of Spectroscopic Techniques to the Study of Metal Ions in Solution and Metal Ions Adsorbed onto Surfaces	22
	2.2.3 Exchange-averaging of Two NMR Lines	25
	2.2.4 The Contact Shift	27
	2.3 Implications of these Theoretical Considerations for Experimental Design	28
3	EXPERIMENTAL METHODS	30
	3.1 Description of Materials and Reagents	30
	3.1.1 Silica	30

TABLE OF CONTENTS (Continued)

<u>Chapter</u>		<u>Page</u>
	3.1.2 Chemicals	30
	3.1.3 Labware	32
3.2	Analytical Methods	32
	3.2.1 pH	32
	3.2.2 Atomic Absorption Spectroscopy	35
	3.2.3 Silica	35
3.3	Experiments	35
	3.3.1 Adsorption	36
	3.3.1.1 Batch Experiments	36
	3.3.1.2 Titrations	37
	3.3.2 Nuclear Magnetic Resonance	38
	3.3.2.1 Apparatus	38
	3.3.2.2 Susceptibility Corrections	39
4	ADSORPTIVE BEHAVIOR OF Ni(II) ON SILICA	41
	4.1 Introduction	41
	4.2 Design Considerations	41
	4.3 Silica Titrations	42
	4.3.1 Choice of the Solid Phase	42
	4.3.2 Physical and Chemical Characteristics of Silica	43
	4.3.2.1 Solution Chemistry	43
	4.3.2.2 Surface Chemistry	44
	4.3.2.3 Surface Site Density	46
	4.3.3 Previous Studies of the Silica Surface	47
	4.3.4 Experimental Results	48
	4.3.5 Modeling the Observed Surface Charge	53
	4.3.6 Discussion	56
	4.4 Nickel Hydroxide Solubility Studies	64
	4.4.1 Introduction	64
	4.4.2 Results and Discussion	64

TABLE OF CONTENTS (Continued)

<u>Chapter</u>	<u>Page</u>
4.5 Adsorption Experiments	70
4.5.1 Adsorption Density Measurements	70
4.5.1.1 Results	71
4.5.1.2 Discussion	73
4.5.2 pH dependence Studies	73
4.5.2.1 Previous Work on Nickel Adsorption on Silica	74
4.5.2.2 Prediction of the pH dependence of Nickel Adsorption on Silica	75
4.5.2.3 Batch Experiments	76
4.5.2.4 Titrations	79
4.5.2.4.1 Results	79
4.5.2.4.2 Discussion	87
4.6 Summary	102
5 NUCLEAR MAGNETIC RESONANCE EXPERIMENTS	105
5.1 Introduction	105
5.2 Referencing of Spectra	105
5.3 Concentration-dependent Experiments	106
5.3.1 Investigation of the Chemical Shift of the Exchange-averaged Water Line in Diamagnetic and Paramagnetic Systems	106
5.3.1.1 Results	106
5.3.1.2 Discussion	109
5.3.2 Determination of the Hyperfine Coupling Constant	110
5.3.2.1 Introduction	110
5.3.2.2 Results	111
5.4 Temperature-dependent Experiments	114
5.4.1 Introduction	114
5.4.2 Results	114
5.4.3 Discussion	122
5.4.3.1 Water	122
5.4.3.2 The Ni ²⁺ Solution	122

TABLE OF CONTENTS (Continued)

<u>Chapter</u>		<u>Page</u>
	5.4.3.3 The Ni(II)-Silica System	124
	5.5 Summary	129
6	CONCLUSIONS	131
	6.1 The Adsorption of Ni(II) onto a Silica Surface	131
	6.2 NMR Spectroscopy	131
	REFERENCES	135

LIST OF FIGURES

<u>Figure</u>		<u>Page</u>
1.1	Representations of various surface complexes between a metal ion, Me, and surface groups.	3
2.1	Potential vs. distance curves for the solid/solution interface as defined by the Constant Capacitance Model and the Triple Layer Model.	14
2.2	Schematic representation of hydrated cations, anions, and bivalent metal ions in the proximity of a surface.	15
2.3	Schematic representation of an NMR spectrum of a solution of paramagnetic cations under conditions of slow exchange (dotted line) and exchange-averaging (solid line).	26
3.1	Sketch of the reaction vessel for titration experiments.	33
4.1	Measured dissolved silica plotted as a function of time at 2 different pH values.	49
4.2	Titration data for 1 g/L silica suspensions titrated with 0.1 N NaOH. Calculated titration curves for various equilibrium systems are shown for comparison.	50
4.3	Surface charge calculations for titrations LM12 and LM13 compared to literature values for equivalent systems.	52
4.4	A comparison of values predicted for σ by the CCM and the TLM to calculated values from titration LM13.	55
4.5	A comparison of values predicted for σ by the CCM' to calculated values from titration LM13.	57
4.6	Calculations from Figure 4.3 replotted as $\log -\sigma$ vs. pH.	58
4.7	The logarithm of the fraction of surface sites neutralized, α , is plotted against p_cH .	60
4.8	The distribution of surface species SiO^- and SiO^-Na^+ as a function of p_cH .	61
4.9	Titration of 0.357 mM $Ni(ClO_4)_2$ in 0.1 M $NaClO_4$ with 0.1 N NaOH under N_2 in the absence of silica.	66

LIST OF FIGURES (Continued)

<u>Figure</u>		<u>Page</u>
4.10	pH change with time is shown after selected additions of C_B during titration LM10.	67
4.11	pH change with time is shown for each addition of C_B during titration LM10.	68
4.12	Adsorption density of Ni^{2+} on silica is plotted against the total concentration of nickel present.	72
4.13	Predicted behavior of Ni^{2+} adsorbing onto silica at $\rho = 0.0023$.	77
4.14	pH dependence of Ni^{2+} adsorbing on silica as determined by batch experiments.	78
4.15	Forward and back titration of Ni^{2+} in the presence of an 0.16 g/L suspension of silica.	80
4.16	pH change as a function of time for each addition of titrant in titration LM15.	82
4.17	Direct comparisons of pH vs. time curves for titrations of nickel in the presence of silica (LM15) and in the absence of silica (LM10) at C_B total of 200 μeq (4.17a) and 300 μeq (4.17b).	85
4.18	Percent adsorption calculations for titration LM15 at the equilibrium times shown.	86
4.19	Plots of adsorption density Γ versus the total concentration of adsorbate for Langmuir (a) and BET (b) isotherms.	96
4.20	Linearized BET plots of adsorption data from Figure 4.12.	97
4.21	The shape and location of the adsorption edge predicted using SURFEQL when regeneration of adsorption centers is included.	100
4.22	Adsorption edge predictions using the unmodified version of SURFEQL.	101
5.1	The absolute value of the log of the chemical shift of the water resonance for the components listed plotted against the log of their concentrations.	108

LIST OF FIGURES (Continued)

<u>Figure</u>		<u>Page</u>
5.2	Chemical shifts for $\text{Ni}(\text{ClO}_4)_2$ solutions measured on both the HA-100 and WM-500 spectrometers, plotted against the fraction of coordinated water molecules in each solution studied.	112
5.3	Chemical shifts are plotted against inverse temperature for the three systems listed. Measurements were made on the HA-100 spectrometer.	116
5.4	Chemical shifts are plotted against inverse temperature for the three systems listed. Measurements were made on the WM-500 spectrometer.	117
5.5	Linewidths of the water resonance in an 0.0274 M $\text{Ni}(\text{ClO}_4)_2$ solution are plotted against inverse temperature. Measurements were made on the HA-100 spectrometer (5.5a) and the WM-500 spectrometer (5.5b).	120
5.6	Linewidths for the water resonance in the adsorbed Ni(II) system are plotted against inverse temperature. Measurements were made using the HA-100 spectrometer (5.6a) and the WM-500 spectrometer (5.6b).	121

LIST OF TABLES

<u>Table</u>		<u>Page</u>
1.1	Predicted values for hydration numbers of adsorbed metal ion surface complexes.	5
2.1	Surface equilibrium constants and electrostatic corrections for the CCM and the TLM.	20
2.2	Published values of the rate constant for exchange between the first coordination sphere of Ni ²⁺ and bulk solution at 25°C.	23
3.1	Physical properties and chemical composition of Aerosil 200.	31
3.2	BET measurements on Aerosil 200.	31
4.1	Solution equilibria for selected silica species at 25°C, I = 0.	45
4.2	Solution equilibria for nickel hydroxo species at 25°C, I = 0, from Smith and Martell (1976).	69
4.3	Percent nickel removed by adsorption processes as a function of time.	88
5.1	Contact shift values as a function of the working frequency of the spectrometer.	109
5.2	Concentrations, densities, and f_{coor} values for the five nickel solutions investigated in the NMR experiments.	113
5.3	Linear regression parameters describing the variation of chemical shifts with temperature ⁻¹ .	118
5.4	Calculation of the hydration number of the adsorbed Ni(II) species at higher temperatures.	128

NOTATIONS

[]	solution phase concentration, moles/L.
{ }	surface concentration, moles/kg.
X_T	total concentration of component X.
a	activity, moles/L.
A	electron-nuclear hyperfine coupling constant, sec^{-1} .
A^-	general electrolyte anion.
\AA	angstrom, 10^{-10} meter.
C	coulomb, 6.24×10^{18} charges.
C^+	general electrolyte cation.
C_1	inner layer capacitance, Farads/ m^2 .
C_2	outer layer capacitance, Farads/ m^2 .
C_A	amount of strong acid added to a system, μmoles .
C_B	amount of strong base added to a system, μmoles .
C_s	saturation concentration.
$D_{[\text{Ni}]}$	density of a $\text{Ni}(\text{ClO}_4)_2$ solution, g/L.
eq	equivalents.
f_{coor}	fraction of water molecules coordinated to a metal ion.
F	Faraday, 96487 coulombs/equivalent.
Farad	coulomb/volt.
g	gram.
g_{eff}	effective electronic g factor.
g_N	nuclear g factor.
G	Gibb's free energy.

NOTATIONS (Continued)

G'	contribution to G due to the presence of an electric field.
h_n	hydration number.
I	ionic strength, mole/L.
J	joule.
k	Boltzmann's constant, 1.38×10^{-16} erg/ $^{\circ}$ K.
k_1	rate constant for exchange of water molecules between the first coordination sphere of a hydrated metal ion and bulk solution, sec^{-1} .
cK	equilibrium constant based on concentration.
*K	equilibrium constant for reaction with a protonated ligand.
K^s	surface equilibrium constant
L	liter.
m	meter.
M	molarity, moles/L.
Me^{2+}	bivalent metal ion.
n	charge of a chemical species or compound.
\bar{n}	ratio of protons released per nickel ion removed from solution.
N	normality, equivalents/L.
Ni(II)	nickel in the +2 oxidation state.
pH_{zpc}	pH of the zero point of charge.
p_aH	$-\log a_{\text{H}}$.
p_cH	$-\log [\text{H}^+]$.
R	gas constant, 8.314 joules/mole $^{\circ}$ K.
R_{ω}	ratio of the chemical shift for an adsorbed Ni(II) system to that for a Ni^{2+} solution.

NOTATIONS (Continued)

S	total electron spin.
SA	surface area, m^2/L .
T	absolute temperature, $^{\circ}K$.
T_2	transverse or spin-spin relaxation time, sec.
x	distance from a surface.
z_i	$F\psi_i/RT$.
α	fraction of surface sites neutralized.
β	Bohr magneton.
β_N	nuclear magneton.
γ	activity coefficient.
Γ	adsorption density, $\mu\text{moles/cm}^2$.
Γ_{max}	maximum adsorption density.
δ_{H_2O}	linewidth of an NMR signal, Hz.
ϵ	dielectric constant, C/Jm.
ϵ_0	permittivity of free space, C/Jm.
ζ	zeta potential, volts.
μ	chemical potential.
μ°	standard state chemical potential.
$\bar{\mu}$	the electrochemical potential.
ρ	the ratio, $Ni_T/SiOH_T$, in an experimental system.
σ_0	surface charge, C/cm^2 .
σ_1	charge in the mean plane of specifically adsorbing ions, C/cm^2 .
σ_d	diffuse layer charge, C/cm^2 .

NOTATIONS (Continued)

- χ_v volume magnetic susceptibility.
- ψ_x electrostatic potential at a distance x from a surface, volts.
- ψ_0 surface potential, volts.
- ψ_1 potential in the mean plane of specifically adsorbing ions, volts.
- ψ_d diffuse layer potential, volts.
- ω frequency in radians (sec^{-1}).
- $\Delta\omega$ contact shift.
- $\Delta\omega_{\text{std}}$ chemical shift referenced to some standard compound.
- $\Delta\omega_{\text{H}_2\text{O}}$ chemical shift referenced to pure water.

CHAPTER 1

INTRODUCTION

The need to quantitatively understand adsorption as applied to the fields of natural water chemistry (limnology, oceanography) and environmental pollution control has grown in recent years. As detailed speciation studies have been carried out on both natural systems and well-defined laboratory systems, adsorption oftentimes has been invoked to explain deviations of metal ion and anion concentrations in solution from those predicted by solubility equilibria. In many aquatic systems adsorption phenomena have been postulated as mechanisms by which trace metals are removed from solution by particles and sediments. Adsorption is thought to play a part in the control of trace metal transport and availability in soils and sediments. Likewise, adsorption has potential for removing pollutants, both organic and inorganic, from municipal and industrial waste waters. It has become increasingly evident that a detailed understanding of this process is necessary to describe the nature of these systems more completely and accurately.

1.1 Adsorption Models

Speciation models for systems containing oxide surfaces and sorbable ions have been the main thrust of much research in the field of surface chemistry. Models have become increasingly complex in trying to account for experimentally-observable system behavior. Yet, quite different assumptions in the models concerning the microscopic environment within the electrical double layer allow one to interpret the macroscopic adsorptive behavior equally well.

The most comprehensive adsorption model currently available is presented in a series of papers by Davis et al. (1978) and Davis and Leckie (1978,1980). It attempts to describe adsorption of dilute solutes from swamping electrolyte solutions. This model combines concepts from previous models of two kinds: those which stress physical and electrical double layer effects on the distribution of solutes within a system (see, for example, James and Healy 1972c) and those which emphasize the formation of surface complexes through specific chemical interactions based on a coordination chemistry framework (Hohl and Stumm 1976 and Schindler et al. 1976).

Modeling laboratory experiments is accomplished by adjusting parameters of the model and formation equilibrium constants for a set of postulated surface species until agreement between output and experimental data is reached. The set of surface species chosen is somewhat arbitrary as no direct experimental evidence is available which specifies the number and types of such species present in any given system. For each surface species, one can construct representations of inner and outer sphere surface complexes between adsorbed ions and surface groups (Figure 1.1). Formation of inner sphere complexes involves the displacement of water molecules from the first coordination sphere of an ion as it is adsorbed. Formation of outer sphere complexes does not require the disruption of the primary hydration sheath and leaves the metal center farther from the surface. Inner sphere complexes are most often associated with coordination chemistry descriptions of surface interactions. Outer sphere complexes are more often linked to physical interpretations in which emphasis is placed on the position of the

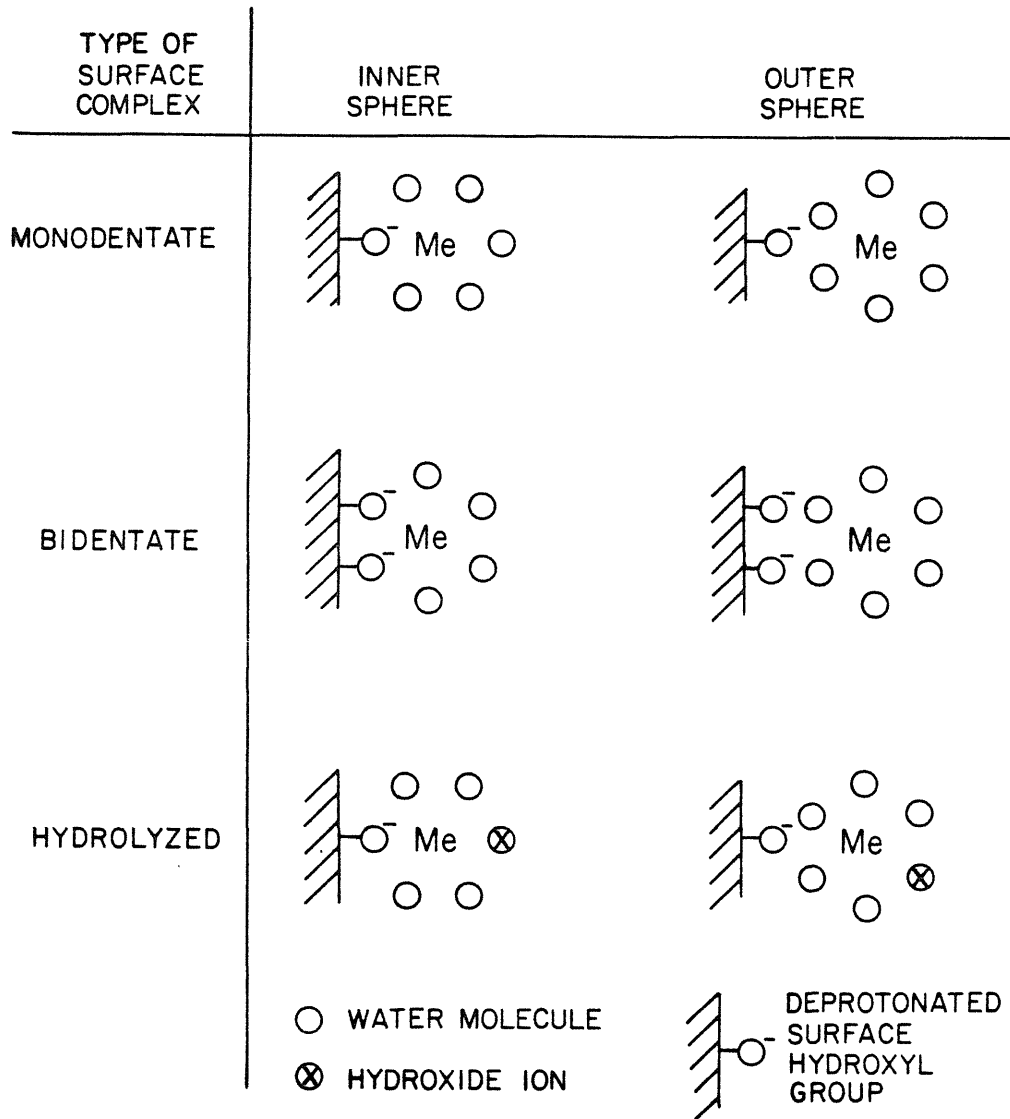


Figure 1.1 Representations of various surface complexes between a metal ion, Me, and surface groups. Details of the charge have been omitted for simplicity.

adsorbed ion in the double layer. Direct experimental evidence, at the molecular level, showing the existence or nonexistence of certain of the species in Figure 1.1 will provide some basis on which to justify a definite choice of surface species and, possibly, give some support to one or another of the physical descriptions of the structure of the solid/solution interface proposed in various adsorption models.

1.2 Nuclear Magnetic Resonance

Information about the physical and chemical environments of an adsorbed metal ion is obtainable at the molecular level by performing an appropriate magnetic resonance experiment. Nuclear magnetic resonance (NMR) spectroscopy is well suited for use as a microscopic probe. Ideally, a peak in an NMR spectrum represents a collection of nuclei in the same electromagnetic environment. Different chemical environments for a particular nucleus will produce resonances at different frequencies or field strengths. This phenomenon is referred to as a chemical shift. Chemical shift data alone can give a first order description of the number and types of chemically different nuclear environments in a given system.

Paramagnetic species in solution are known to significantly affect chemical shifts of nuclei associated with them; the large electric field, resulting from unpaired electron spin, radically changes the local magnetic field. In particular, paramagnetic first-row transition series metal ions in aqueous solution shift the resonant frequency of water molecule protons located in the first coordination sphere of these metal ions. The fact that water molecules in the first coordination sphere

and water molecules in bulk solution are in different environments for solutions of paramagnetic ions, makes NMR the experimental method of choice for determining hydration numbers of transition metal ions in solution.

An NMR experiment, measuring the chemical shift and linewidth of the resonance line of water molecules in suspensions of silica on which nickel ions had been adsorbed, was used in this work to measure the hydration number of an adsorbed paramagnetic nickel ion. Information concerning the number and types of surface complexes present can be determined from this hydration number. Defining the hydration number of an adsorbed surface complex as one half the number of protons found in the first coordination sphere (two protons are bound to each water molecule), then surface complexes illustrated in Figure 1.1 would have the hydration numbers shown in Table 1.1.

Table 1.1

type of surface complex	inner sphere	outer sphere
monodentate	5	6
bidentate	4	6
hydrolyzed	4.5	5.5

A determination of the hydration number of an adsorbed metal ion thus has the possibility to provide the information needed at the molecular level to resolve the difficulties mentioned in section 1.2 in applying adsorption models to systems of environmental and experimental interest.

1.3 Reasons for the Choice of Nickel and Silica

The choice of nickel and silica as components of the experimental system was made with both their adsorptive and magnetic properties in mind.

Nickel was chosen largely due to several favorable properties in the context of the NMR experiment.

- 1) Ni(II) species are paramagnetic, with two unpaired electron spins.
- 2) Nickel ion forms regular octahedral complexes in solution. Specifically, the hexaquo complex, $\text{Ni}(\text{H}_2\text{O})_6^{2+}$, consists of six equivalent water molecules octahedrally arranged around the central Ni^{2+} ion.
- 3) There is a considerable body of literature which describes the results of NMR studies of the solvation shell of aqueous nickel ions.
- 4) Values for two important constants, the rate constant for ligand exchange between bulk solution and the first coordination sphere and the electron-nuclear hyperfine coupling constant have been reported.
- 5) The ligand exchange rate for nickel ion is slow compared to that of other transition metals. This provides a better opportunity to conduct experiments under conditions of slow and fast exchange (see section 2.2.3 for details).

Ni(II) also possesses certain advantageous solution properties under the conditions at which the adsorption reactions were carried out.

- 1) The +2 oxidation state is the only stable one for soluble nickel species.
- 2) The equilibrium constants for the potentially important hydrolysis products, NiOH^+ and $\text{Ni}_4(\text{OH})_4^{4+}$, are well known.

One disadvantage was the necessity to investigate independently the

solubility behavior of the solid phase, $\text{Ni}(\text{OH})_2(\text{s})$, as its reported solubility product ranges over 2.5 orders of magnitude.

Silica was chosen because of its surface chemical properties. The absence of a positively charged surface hydroxyl group under the experimental conditions employed decreased the number of possible surface complexes and thus simplified both the analysis of data from the NMR hydration number determination and the modeling of results from the nickel adsorption experiments.

CHAPTER 2

THEORY

2.1 Adsorption2.1.1 Introduction

Chemical processes describing adsorptive behavior have been largely agreed upon in recent years. This is evidenced by the similar treatments given them in current models such as the triple layer model (TLM) developed by Davis et al. (1978) and Davis and Leckie (1978) and the constant capacitance model (CCM) of Hohl and Stumm (1976) and Schindler et al. (1976). All surface reactions are formulated in a coordination chemistry framework which is modified by electrostatic energy terms.

Complications arise when a consistent form of the electrostatic correction to the free energy term is sought. There is a lack of agreement among the adsorption modelers as to the proper physical description of the electrical double layer, especially with regard to the location of mean planes of adsorption of different classes of adsorbates. These differences manifest themselves in the way in which the equilibrium constants are written for surface complex formation reactions.

Westall and Hohl (1980) examined five different electrostatic models with respect to their ability to represent experimental data. They found that a large range of parameter values could provide an optimal fit. The modeling exercise, however, does not unambiguously provide for a separation of adsorption energies into chemical and electrostatic components, nor does it lend any validity to one physical

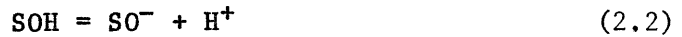
description of the solid-solution interface over another.

Surface equilibrium constants will be defined and their differences examined using the interpretation of appropriate electrostatic corrections to chemical free energies of adsorption in the constant capacitance model and the triple layer model.

2.1.2 Coordination Chemistry on the Surface

2.1.2.1 Hydrolysis of Surface Groups

Protolytic behavior of metal oxides can be described by the acid-base nature of surface hydroxyl groups. A rather simple case is analogous to a diprotic acid in solution. Surface hydrolysis reactions can be written,



where, S stands for some ion that is a part of the solid substrate, and the first and second surface acidity constants, K_{a1}^s and K_{a2}^s , can be defined

$$K_{a1}^s = \frac{\{\text{SOH}\}[\text{H}^+]_o}{\{\text{SOH}_2^+\}} \cdot \frac{\gamma_o \gamma_H}{\gamma_+} \quad (2.3)$$

$$K_{a2}^s = \frac{\{\text{SO}^-\}[\text{H}^+]_o}{\{\text{SOH}\}} \cdot \frac{\gamma_- \gamma_H}{\gamma_o} \quad (2.4)$$

where: [] represent concentrations in the solution phase (moles/L), { } represent concentrations on the surface (moles/kg), γ_H , γ_+ , γ_o and γ_- are the activity coefficients of H^+ , SOH_2^+ , SOH and SO^- , respectively, and subscripts on terms in square brackets indicate the location of an

ion with respect to the surface, e.g., $[i]_0$ is the concentration of the i th soluble species at the surface. The superscript s denotes a surface equilibrium constant. Notation is that used by Schindler (1980). Other stability constant notation follows Sillén and Martell (1964).

These equilibrium constants can be related to calculable intrinsic constants, which describe the microscopic behavior of an isolated surface group, by assuming: i) a relationship between measurable bulk proton concentrations and proton concentrations on the surface (which are experimentally unknowable) and ii) that activity coefficients for all types of surface species are equal.

The proton concentration used in the evaluation of these thermodynamically sound equilibrium constants would be that at the surface under the influence of an electrostatic potential. Measurements of proton concentration can only be made in bulk solution. If one considers a Boltzmann distribution of charge, one can calculate an ion's concentration at any distance x from the surface from its bulk concentration value as follows:

$$[i]_x = [i] \exp(-nF\psi_x/RT) \quad (2.5)$$

where: n is the charge of the i th species, F the Faraday, R the gas constant, T the absolute temperature, and ψ_x the potential at position x . As there is no formalism for calculating activity coefficients for surface species, it will be assumed that they are equal, i.e., $\gamma_+ = \gamma_0 = \gamma_-$. Chan et al. (1975) have offered evidence supporting this assumption. At constant ionic strength, the activity coefficient of the proton in bulk solution will be a constant and can be incorporated into the

value of the equilibrium constant. Then, defining z_i as $(F\psi_i/RT)$ and substituting equation 2.5 into 2.3 and 2.4 one can write equations for the resulting intrinsic concentration constants as follows:

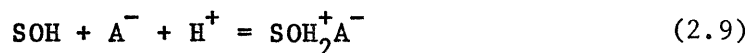
$$c_{K_{a1}}^s(\text{int}) = \frac{\{\text{SOH}\}[\text{H}^+]_o}{\{\text{SOH}_2^+\}} \cdot \exp(-z_o) \quad (2.6)$$

$$c_{K_{a2}}^s(\text{int}) = \frac{\{\text{SO}^-\}[\text{H}^+]_o}{\{\text{SOH}\}} \cdot \exp(-z_o) \quad (2.7)$$

the superscript c indicating an equilibrium constant determined using concentrations rather than activities.

2.1.2.2 Adsorption of Trace Metals, Major Cations and Major Anions

The formulation of mass action laws and equilibrium constants for the adsorption of bivalent metal ions, Me^{2+} , major electrolyte cations, C^+ , and major electrolyte anions, A^- , can be described in a manner analogous to that used for surface groups. Background electrolyte cations and anions react with neutral surface species according to:



The cationic reaction displaces a proton from the surface and the anionic reaction consumes a proton. The equilibrium constants for these reactions are written as

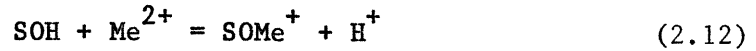
$$c_{K_C}^*{}^s(\text{int}) = \frac{\{\text{SO}^-\text{C}^+\}[\text{H}^+]}{\{\text{SOH}\}[\text{C}^+]} \cdot \exp(z_x - z_o) \quad (2.10)$$

$$c_{A}^{*K_A^S}(\text{int}) = \frac{\{\text{SOH}_2^+ \text{A}^-\}}{\{\text{SOH}\}[\text{A}^-][\text{H}^+]} \cdot \exp(z_o - z_x) \quad (2.11)$$

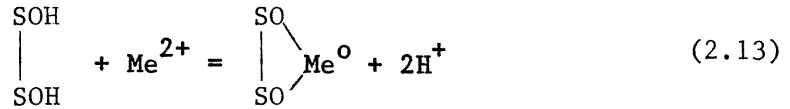
Protons again are located at the surface under the influence of a potential ψ_o . The location of other adsorbing ions is defined, in this general case, to be at a distance x from the surface. The star notation indicates reaction with a protonated ligand, in this case, SOH.

Three possible surface species containing trace metals will be considered and defined as,

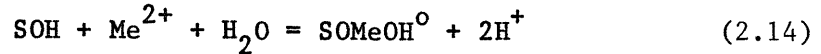
monodentate,



bidentate,



and hydrolyzed



Their corresponding intrinsic concentration constants are,

$$c_{K_1^S}^*(\text{int}) = \frac{\{\text{SOMe}^+\}[\text{H}^+]}{\{\text{SOH}\}[\text{Me}^{2+}]} \cdot \exp(2z_x - z_o) \quad (2.15)$$

$$c_{\beta_2^S}^*(\text{int}) = \frac{\left\{ \begin{array}{c} \text{SO} \\ | \quad \diagup \\ \text{SO} \end{array} \text{Me}^o \right\} [\text{H}^+]^2}{\left\{ \begin{array}{c} \text{SOH} \\ | \\ \text{SOH} \end{array} \right\} [\text{Me}^{2+}]} \cdot \exp(2z_x - 2z_o) \quad (2.16)$$

$$c_{K_{\text{MeOH}}}^*(\text{int}) = \frac{\{\text{SOMeOH}^o\}[\text{H}^+]^2}{\{\text{SOH}\}[\text{Me}^+]} \cdot \exp(2z_x - 2z_o) \quad (2.17)$$

2.1.3 Physical Descriptions of the Electrical Double Layer

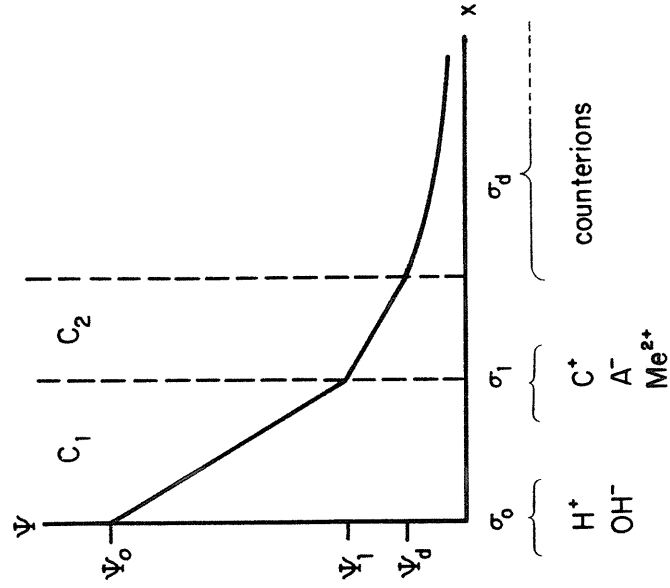
The application of electrostatic corrections to surface

equilibrium constants ultimately rests on the position within some double layer structure at which one places adsorbed species. The concept of placing ions in discrete planes located some distance from the surface was initially described by Stern (1924) and elaborated upon by Grahame (1947). Detailed descriptions of the physical picture of the structure of the solid-solution interface as presented in the constant capacitance model (CCM) and the triple-layer model (TLM) will be discussed. The resultant electrostatic corrections will be combined with the mass law equations for surface complexation already presented.

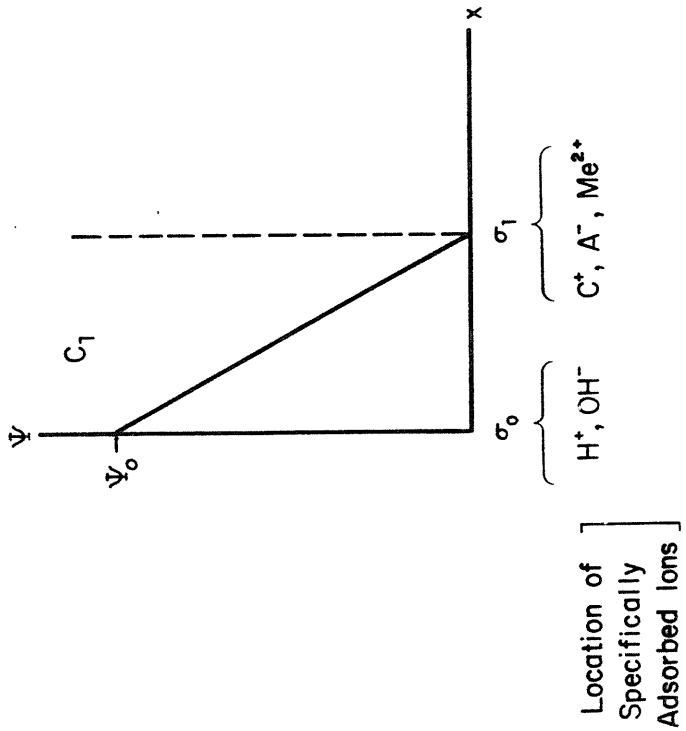
Visual representations of the models are shown in Figure 2.1. Electrostatic potential is plotted against distance from the surface. Mean planes of adsorption at which charge is calculated are represented by vertical lines. Ions located at these planes which contribute to the charge calculated there are listed under the lines.

The two models agree in their assignment of ions to mean planes of adsorption. The potential determining ions, H^+ and OH^- , are located at the solid surface in the σ_0 plane and background electrolyte ions and adsorbing trace metals are placed in the σ_1 plane some distance from the surface. These ions are located at different distances from the surface because their abilities to approach the surface differ. This phenomenon is depicted schematically in Figure 2.2. The species C^+ , A^- , Me^{2+} , H^+ , OH^- , SO^- and SOH_2^+ and the components SOH and H_2O are shown in the proximity of a solid surface. Three simplifying assumptions have been made regarding ion sizes in constructing this figure: i) the radii of H_3O^+ , H_2O , OH^- , SOH_2^+ , SOH and SO^- are the same, ii) the radii of C^+ , A^- and Me^{2+} (including first coordination sphere water molecules) are the same

TRIPLE LAYER MODEL



CONSTANT CAPACITANCE MODEL



Location of
Specifically
Adsorbed Ions

Figure 2.1 Potential vs. distance curves for the solid/solution interface as defined by the Constant Capacitance Model and the Triple Layer Model.

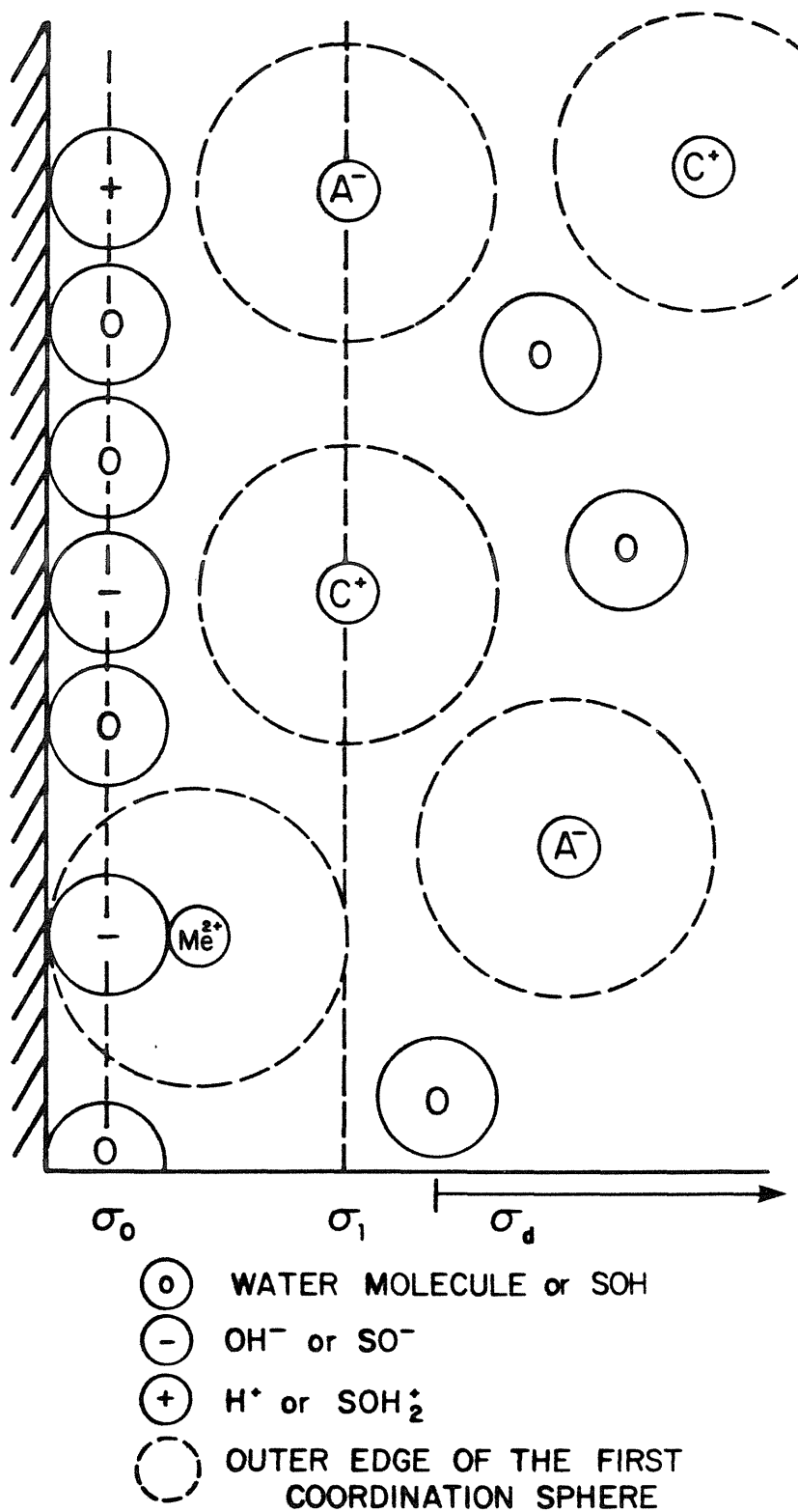


Figure 2.2 Schematic representation of hydrated cations, anions, and bivalent metal ions in the proximity of a surface.

and iii) the unhydrated radii of C^+ , A^- and Me^{2+} are one half that of water molecules. A layer of silanol groups and water molecules is shown at the surface. The σ_0 plane is located at the center of this layer. Hydrated cations, anions and metal ions cannot get this close to the surface (water molecules in their first coordination spheres prevent this). Even inner sphere complexes (an example is shown in the lower left of Figure 2.2) do not allow a metal ion to approach the surface as closely as do H^+ and OH^- . Therefore, the mean plane representing the center of charge for the hydrated species, σ_1 , is located farther from the surface than is the σ_0 plane. The σ_1 plane would be located nearer the surface than is shown in Figure 2.2 if the surface concentration of inner sphere complexes was comparable to the surface concentration of major cation and anion complexes.

The models differ in the degree of complexity involved in their descriptions of the electrical properties of the double layer. This can be seen in the different ways in which charge and potential are defined and related.

2.1.4 Charge and Potential Relationships

2.1.4.1 The Triple Layer Model

The TLM was designed to describe adsorption of trace constituents from both swamping electrolyte solutions and from dilute solutions. The charge at each plane is calculated by summing the concentration of those charged species which have been assigned to that plane. One can write equations for the surface charge, σ_0 and the charge in the mean plane of specifically adsorbing counterions, σ_1 , for

a system containing a solid suspended in an electrolyte solution. They are

$$\sigma_o = F/(SA) ([SOH_2^+] + [SOH_2^+A^-] - [SO^-] - [SO^-C^+]) \quad (2.18)$$

$$\sigma_1 = F/(SA) ([SO^-C^+] - [SOH_2^+A^-]) \quad (2.19)$$

σ_d , the diffuse layer charge, can be calculated from Gouy-Chapman diffuse layer theory, and is found to be, for a monovalent electrolyte,

$$\sigma_d = (8\epsilon\epsilon_oRTI)^{1/2} \sinh(F\psi_d/2RT) \quad (2.20)$$

where: σ_o , σ_1 , and σ_d have units of C/m^2 , (SA) is the surface area in cm^2/L , I is the ionic strength in moles/L, and ϵ and ϵ_o are the dielectric constant and permittivity of free space respectively, in (C/Jm). When trace metals are present, the surface charge is increased by the formation of surface complexes containing an SOH_2^+ group and decreased when species containing an SO^- group are formed. σ_1 is also affected. Species having positively charged ions located in the σ_1 plane add to the value of σ_1 . Likewise, surface complexes having negatively charged ions in the σ_1 plane decrease σ_1 . Electroneutrality of the interface must be maintained so,

$$\sigma_o + \sigma_1 + \sigma_d = 0 \quad (2.21)$$

The charge at planes and the potential difference across layers of the interface are related by the capacitance. When a constant capacitance is assumed between planes of adsorbed ions, each layer behaves as a Helmholtz capacitor. Then the charge/potential relationships are

defined as

$$\sigma_o = C_1(\psi_o - \psi_1) \quad (2.22)$$

$$\sigma_d = C_2(\psi_d - \psi_1) \quad (2.23)$$

where C_1 and C_2 , shown in Figure 2.1, are the integral capacitances of the inner and outer layers in Farads/m².

These six equations, 2.18 to 2.23, and associated parameters, C_1 and C_2 , allow one to describe the electrical properties of the surface solution interface as defined by the TLM.

2.1.4.2 The Constant Capacitance Model

The CCM presents a much simpler picture of the solid/solution interface. It was designed to describe the properties of the interface under conditions of high ionic strength where the diffuse layer thickness and potential are small. This was accomplished by assuming ψ_1 to be zero and eliminating the diffuse layer concept altogether. Formation of complexes between surface groups and background electrolyte ions is not considered. Rather, surface hydrolysis constants must be determined for each electrolyte concentration of interest. The surface charge is then comprised only of protonated and deprotonated surface hydroxyl groups.

$$\sigma_o = F/(SA) ([SOH_2^+] - [SO^-]) \quad (2.24)$$

The addition of a trace metal affects the surface charge in the same way as was described for the TLM. As an example, Ni(II) surface complexes produce a more negative surface charge as seen below

$$\sigma_o = F/(SA) ([SOH_2^+] - [SO^-] - [SONi^+] - [SONiOH^0] - 2[\begin{array}{c} SO \\ | \\ Ni^0 \\ | \\ SO \end{array}]) \quad (2.25)$$

Electroneutrality is simply expressed as

$$\sigma_o = -\sigma_1 \quad (2.26)$$

and the charge/potential relationship, assuming constant capacitance, is

$$\sigma_o = C_1\psi_o \quad (2.27)$$

because $\psi_1 = 0$.

The three equations (2.24, 2.26 and 2.27) and only one parameter (C_1) are necessary to model the electrical properties of the interface using the CCM.

2.1.5 Surface Equilibrium Constants Corrected for Electrostatic Effects

We now have all the information needed to include the appropriate model-dependent potentials into the equilibrium constants previously defined in Equations 2.6, 2.7, 2.10, 2.11, and 2.15 to 2.17. These corrected constants are listed in Table 2.1.

The exponential terms associated with the CCM all have the same form, $\exp(-nF\psi_o/RT)$, as only the release or consumption of protons during the formation of a surface complex is subject to electrostatic correction.

Electrostatic terms in the TLM are unique for each surface reaction considered here. There exists then, in the TLM, the possibility to differentiate among several possible surface complexes by modeling experi-

Table 2.1

Surface equilibrium constants and electrostatic corrections

for the CCM and the TLM

	Symbols	Equilibrium Quotient	Electrostatic Terms	
			CCM	TLM
Surface hydrolysis	$c_{K_{a1}}^s$	$\frac{\{SOH\}[H^+]}{\{SOH_2^+\}}$	$\exp(-F\psi_o/RT)$	$\exp(-F\psi_o/RT)$
	$c_{K_{a2}}^s$	$\frac{\{SO^-\}[H^+]}{\{SOH\}}$	$\exp(-F\psi_o/RT)$	$\exp(-F\psi_o/RT)$
Surface complex formation with major cations and anions	$c_{K_C}^*$	$\frac{\{SO^-C^+\}[H^+]}{\{SOH\}[C^+]}$	NA	$\exp(-\frac{F}{RT}(\psi_o - \psi_1))$
	$c_{K_A}^*$	$\frac{\{SOH_2^+A^-\}}{\{SOH\}[A^-][H^+]}$	NA	$\exp(-\frac{F}{RT}(\psi_1 - \psi_o))$
Surface complex formation with trace metals	$c_{K_{1Me}}^* s$	$\frac{\{SOMe^+\}[H^+]}{\{SOH\}[Me^{2+}]}$	$\exp(-F\psi_o/RT)$	$\exp(-\frac{F}{RT}(\psi_o - 2\psi_1))$
	$c_{\beta_2}^* s$	$\frac{\left\{ \begin{array}{c} SO \\ \\ SO \end{array} \right\} Me^{\circ} [H^+]^2}{\left\{ \begin{array}{c} SOH \\ \\ SOH \end{array} \right\} [Me^{2+}]}$	$\exp(-2F\psi_o/RT)$	$\exp(-\frac{F}{RT}(2\psi_o - 2\psi_1))$
	$c_{K_{MeOH}}^* s$	$\frac{\{SOMeOH^{\circ}\}[H^+]^2}{\{SOH\}[Me^{2+}]}$	$\exp(-1F\psi_o/RT)$	$\exp(-\frac{F}{RT}(\psi_o - \psi_1))$

NA not applicable

mental data. This is not so fully realized in the CCM.

2.1.6 Computer Modeling

All of the adsorption and titration data has been modeled using the equilibrium thermodynamic computer program MINEQL developed by Westall et al. (1976). When surface equilibria were considered, additional modifications as described by Westall and Hohl (1980) were incorporated. The resulting program will be referred to herein as SURFEQL.

SURFEQL has the adaptability to easily include any number of adsorption models. The adaptability is due largely to a consistent chemical framework and the ease with which different electrostatic models can be incorporated. Capabilities to model adsorption data using the CCM and the TLM have been installed.

2.2 Nuclear Magnetic Resonance Spectroscopy

2.2.1 Introduction

Nuclear magnetic resonance (NMR) spectroscopy has been successfully applied to the study of the hydration shell of paramagnetic metal ions in aqueous solution by many investigators. Both oxygen-17 and proton magnetic resonance techniques have been employed to determine such quantities, relevant to this study, as: i) the hydration number of aqueous metal ions, ii) the rate constant for exchange of solvent molecules between the first coordination sphere of a metal ion and bulk solution and iii) the electron-nuclear hyperfine coupling constant which describes the interaction between the unpaired electrons of the paramagnetic species and solvent nuclei.

2.2.2 Prior Applications of Spectroscopic Techniques to the Study of Metal Ions in Solution and Metal Ions Adsorbed onto a Surface

The hydration number of Ni^{2+} in aqueous solution was first determined by Connick and Fiat (1966). They directly observed an ^{17}O NMR signal from water molecules in the first coordination sphere of the Ni^{2+} ion. Their results were consistent with a coordination number of either 4 or 6. Swift and Weinberger (1968), using proton magnetic resonance, found the hydration number of the Ni^{2+} ion to be 6.0 ± 0.2 at -30°C . Chmelnick and Fiat (1971) and Neely and Connick (1972), improving on the experimental technique of Connick and Fiat (1966), reported the existence of six equivalent water molecules in the first coordination sphere of Ni^{2+} . These results held over the temperature range -30 to $+200^\circ\text{C}$. All of these experiments were performed with concentrated (greater than 1 M) $\text{Ni}(\text{NO}_3)_2$ or $\text{Ni}(\text{ClO}_4)_2$ solutions.

The rate constant for exchange of water molecules between bulk solution and the coordination sphere of a hexaquo nickel ion, k_1 , has been measured by both proton and oxygen-17 NMR spectroscopy. ^1H magnetic resonance measures the proton exchange rate and ^{17}O NMR measures the exchange rate for entire water molecules. Values for k_1 reported in the literature are tabulated in Table 2.2. The value $3 \times 10^4 \text{ sec}^{-1}$ is reported most often and considered to be the most reliable. The fact that the value for the exchange rate is the same when determined by ^{17}O and ^1H NMR indicates that proton exchange occurs through the exchange of entire water molecules.

Three values for the electron-nuclear hyperfine coupling constant, A , have been reported in the literature. Luz and Shulman (1965),

Table 2.2

Published values of the rate constant for exchange
between the first coordination sphere
of Ni^{2+} and bulk solution at 25°C

$k_1 \times 10^{-4} \text{ sec}^{-1}$	Reference
3 *	Hausser and Laukin (1959)
2.7 †	Swift and Connick (1962)
3.0 ± 0.3 †	Connick and Fiat (1966)
9 ± 1 *	Swift and Stephenson (1966)
3 ± 1 *	Swift and Weinburger (1968)
4.4 ± 0.2 †	Desai, Dodgen and Hunt (1969)
3 *	Granot, Achlama and Fiat (1974)
30.7 ± 0.5 †	Rablen, Dodgen and Hunt (1976)
3.14 ± 0.06 †	Bechtold, Liu, Dodgen and Hunt (1978)

* measured by proton NMR

† measured by oxygen-17 NMR

measuring the chemical shift of $\text{Ni}(\text{ClO}_4)_2$ solutions over the temperature range 0 to 110 °C note that, at 60 MHz, fast exchange is only observed at the higher temperatures. They calculate a value for A of $12 \times 10^5 \text{ sec}^{-1}$ at 110°C. Wayland and Rice (1966) report a value of $(6.9 \pm 0.6) \times 10^5 \text{ sec}^{-1}$ for A by measuring the chemical shifts of 0.41 to 0.83 M $\text{Ni}(\text{ClO}_4)_2$ solutions at 43°C. Most recently, Granot et al. (1974), working with a 4.0 molal $\text{Ni}(\text{ClO}_4)_2$ solution at temperatures from -10 to -30 °C, directly measured the chemical shift between bulk and coordinated water molecules as a function of temperature. They calculate A to be $(8.2 \pm 0.6) \times 10^5 \text{ sec}^{-1}$.

Spectroscopic studies that have looked at paramagnetic metal ions adsorbed onto a surface have produced results that are chemically inconsistent with available adsorption theories. Using electronic spectroscopy Hathaway and Lewis (1969) report, ". . . when nickel (II) complexes are adsorbed upon hydrated silica gel, the nickel (II) ions are in an environment comparable with that in aqueous solution and are free to move over the layer of physically bound water which covers the surface". Electron paramagnetic resonance (EPR) studies of copper (II) adsorbed on a silica surface by Cozar et al. (1976) provide similar results, that is, at room temperature, the hydrated complex of copper (II) adsorbed on the silica surface, ". . . can move freely and the resulting EPR spectrum will appear homogeneously averaged as in liquid water. . .". This freedom of movement of the adsorbed species seems to preclude detection of any specific chemical interaction between metal ions and surface hydroxyl groups in these systems. However, these studies were carried out on rehydrated silica gels without the presence of a bulk aqueous

phase. It is not clear whether the results are applicable to aqueous systems.

2.2.3 Exchange-averaging of Two NMR Lines

Ideally, in solutions of paramagnetic metal ions, NMR would provide separate resonance signals for solvent molecules in bulk solution and for those coordinated to metal ions. This condition is not easily obtained in aqueous solution for several reasons: i) exchange of solvent molecules between bulk solution and the coordination sphere of paramagnetic ions is rapid, ii) NMR lines of coordinated water molecules are wide compared to bulk water molecule lines, iii) the chemical shift between bound and bulk water molecule lines is not always large compared to the widths of these signals and iv) concentrated solutions of paramagnetic ions (greater than 1 M) are necessary to produce measurable signals from coordinated water molecules.

The exchange-averaging process, in which separate NMR lines coalesce into a single averaged line, occurs when the rate constant for exchange of nuclei between two environments exceeds the value of the chemical shift, $\Delta\omega$, between the two NMR lines. The result of this process on a spectrum with two resolvable lines is shown schematically in Figure 2.3. A spectrum of paramagnetic ions in solution taken under conditions of slow exchange ($k_1 < \Delta\omega$) is represented by the dotted line. Two signals are present. The resonance located at frequency, ω_M , is that of water molecules coordinated to the paramagnetic metal ion. The resonance at ω_{H_2O} is that of bulk water molecules. Exchange-averaging produces the solid line. It is located at a frequency ω , which is the

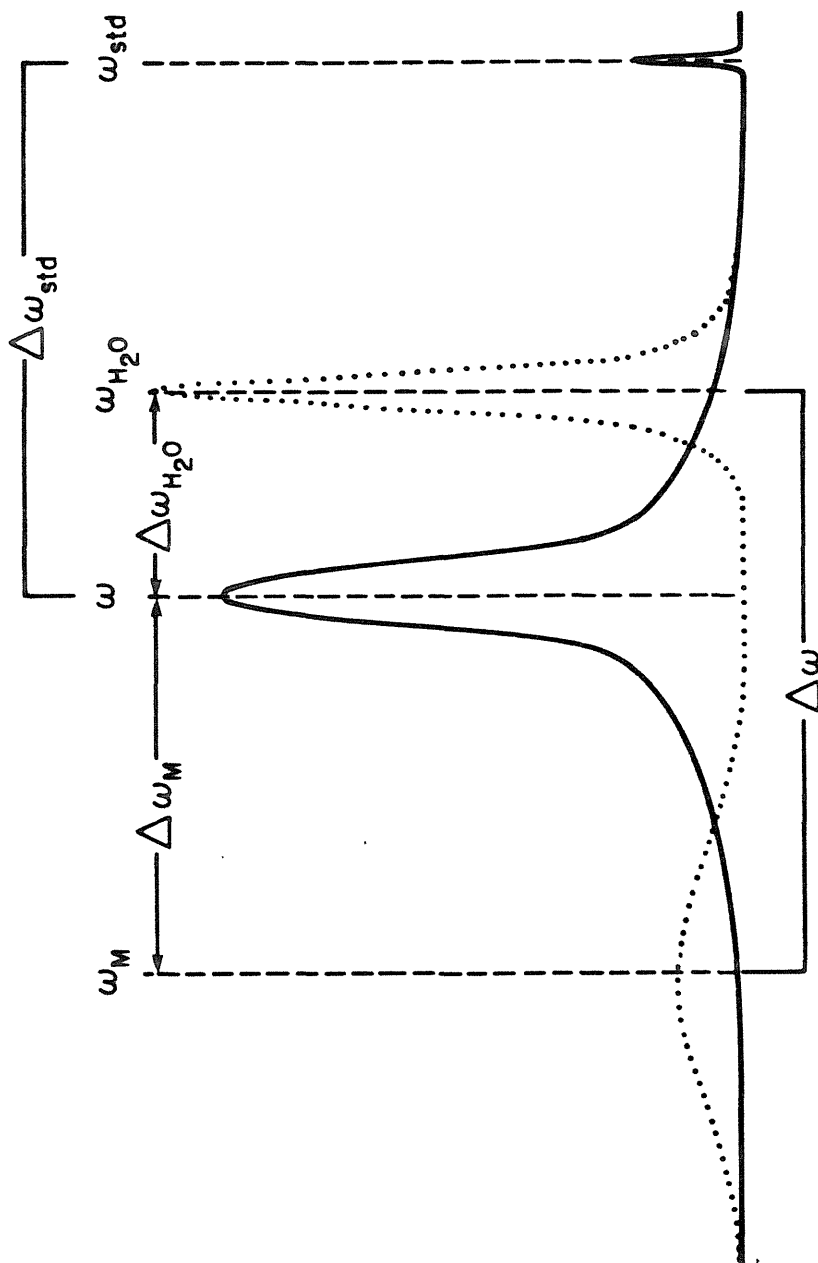


Figure 2.3 Schematic representation of an NMR spectrum of a solution of paramagnetic cations under conditions of slow exchange (dotted line) and exchange-averaging (solid line).

average of the frequencies of the signals located at ω_M and ω_{H_2O} , weighted by the fractional population of each environment. Various chemical shift measurements in such an exchange-averaged system are also designated on the figure.

2.2.4 The Contact Shift

The NMR spectrum of a resonating nucleus will be influenced by the presence of any paramagnetic species. Unpaired electron spin density contacting the resonating nucleus will change the magnitude of the local magnetic field producing a frequency shift of the resonance line. This contact shift, $\Delta\omega$, pictured in Figure 2.3, has been described by Bloembergen (1957) and can be calculated as shown below

$$\frac{\Delta\omega}{\omega} = -A \frac{g_{\text{eff}} \beta S(S+1)}{g_N \beta_N 3kT} \quad (2.28)$$

where: ω is the working frequency, g_{eff} and g_N are the unpaired electron and nuclear g factors, β and β_N the Bohr and nuclear magnetons, S the total electron spin and k the Boltzmann constant. The shift of an exchange-averaged line, referenced to the pure water resonance, as a function of the concentration of metal ion in solution is given by

$$\Delta\omega_{H_2O} = (\Delta\omega) f_{\text{coor}} \quad (2.29)$$

where f_{coor} is the fraction of water molecules coordinated to the metal ion. Substituting the equation 2.29 into 2.28 and rearranging gives

$$\Delta\omega_{H_2O} = \left[-A\omega \frac{g_{\text{eff}} \beta S(S+1)}{g_N \beta_N 3kT} \right] f_{\text{coor}} \quad (2.30)$$

In order to transform the measured value of the chemical shift,

$\Delta\omega_{\text{H}_2\text{O}}$ into a hydration number, an accurate value of A must be known as must the speciation of the paramagnetic metal ion in the experimental system. The latter provides the necessary information to properly convert f_{coor} into a hydration number.

2.3 Implications of these Theoretical Considerations for Experimental Design

Under conditions of slow exchange, hydration numbers of paramagnetic metal ions in solution are directly obtainable by integration of the NMR signal corresponding to the first coordination sphere water molecules. Hydration numbers can be indirectly obtained in exchange-averaged systems by measuring the chemical shift of the exchange-averaged water line, $\Delta\omega_{\text{H}_2\text{O}}$. Data are then analyzed using the Bloembergen equation modified to describe an exchange-averaged system (equation 2.30).

In order to analyze NMR data in this study it was necessary to know the chemical speciation of the Ni(II)-SiO₂ system. In addition, constraints imposed by the NMR experiment dictated a particular configuration of this system; maximum adsorption density was needed to overcome sensitivity problems and close to 100% adsorption was desired to minimize the concentration of the solution species Ni(H₂O)₆²⁺. As literature data do not provide values for the equilibrium constants or physical parameters necessary to accurately predict the pH dependence and maximum adsorption density of nickel interacting with a silica surface, an experimental program was undertaken to measure them for the Ni(II)-SiO₂ system. The results of this program are described in Chapter 4.

It was also judged necessary to conduct the following NMR experi-

ments, for the reasons listed:

- i) a comparison of the magnitude of the chemical shifts due to paramagnetic and diamagnetic species was performed to quantify the contribution of each to the total chemical shift.
- ii) a redetermination of the value of the hyperfine coupling constant was made because of the limited number of previous measurements (3) and their lack of constancy (values vary by a factor of 2).
- iii) measurements of the chemical shift and the linewidth of the exchange-averaged line were recorded as a function of temperature in each system studied in order to assess the degree to which the assumption of exchange-averaging holds over the temperature range studied and the spectrometer frequencies used.

Results of these NMR experiments are described in Chapter 5.

CHAPTER 3

EXPERIMENTAL METHODS

3.1 Description of Materials and Reagents3.1.1 Silica

The silica used throughout was a pyrogenic commercial product, Aerosil 200, manufactured by Degussa Corporation. The physical and chemical properties, as reported by the manufacturer, are listed in Table 3.1.

Aerosil was dried at 110°C before use and stored in a dessicator. Preliminary adsorption experiments indicated no significant difference in the adsorption properties between cleaned and uncleaned silica. The cleaning procedure was that used by Vuceta (1976). It consisted of heating a quantity of Aerosil to 500°C for 24 hours, refluxing in concentrated HNO_3 , washing with distilled water until the suspension reached pH 6, rinsing with 4 N NH_4OH , rewashing with distilled water to pH 8, and, finally, drying at 110°C. Subsequently, uncleaned silica was used in all experiments.

Results of surface area measurements performed on Aerosil 200 using the BET method of Brunauer et al. (1938) are shown in Table 3.2. Results were within manufacturers specifications. The value for the specific surface area of Aerosil used in all calculations was 182 m^2/g .

3.1.2 Chemicals

Reagent grade chemicals were used in all experiments. Perchlorate salts, perchloric acid and redistilled nitric acid were purchased from G. Frederick Smith Co. Hygroscopic salts were dried at

Table 3.1

Physical Properties of Aerosil 200

BET Surface Area (m ² /g)	200 ± 25
Absorbed Moisture (%)	1
pH (4% w/w in water)	3.6 to 4.3
Average Primary Particle Size (nm)	12
Density (g/cm ³)	2.2
Solubility in Water (mg/L)	150
SiOH Density (sites/nm ²)	3.5 ± 2

Chemical Composition

SiO ₂ *	99.8%
Al ₂ O ₃	500 ppm
Fe ₂ O ₃	30 ppm
TiO ₂	300 ppm
HCl	250 ppm

* dried for 2 hours at 105°C

Table 3.2

BET Measurements on Aerosil 200

Sample	Weight Loss (%) 24 hrs., 25°C	Surface Area m ² /g
Aerosil	0.2	181.5
Cleaned Aerosil	2.3	174.4
Cleaned Aerosil	2.8(110°C)	173.8

BET analyses were performed by C. Moran
of the Jet Propulsion Laboratory, Pasadena, CA

110°C for 24 hours prior to use and stored in a dessicator.

The water used throughout was freshly distilled, deionized water (DDW). Particulate impurities were removed from freshly prepared solutions by filtering through 0.45 µm Millipore filters (type HA). The filters were soaked in DDW for 24 hours before use and conditioned with 50 to 100 mLs of the solution to be filtered. Ni²⁺ stock solutions were prepared by dissolving the appropriate amount of Ni(ClO₄)₂·6H₂O in DDW. Concentrated perchloric acid was added to produce a final concentration of 0.01 N. NaClO₄, a non-interactive background electrolyte, was added to give a final ionic strength of 0.1 M. Stock solutions were diluted with 0.1 M NaClO₄ to the desired concentrations immediately before use.

3.1.3 Labware and Reaction Vessels

Reaction vessels consisted of 50 mL polyallomar Oak Ridge type centrifuge tubes for the batch experiments and jacketed glass beakers for all titrations. The 1000 mL borosilicate glass jacketed beaker was sandwiched between plexiglass plates. The upper plate contained five openings to accept electrodes, a thermometer, a disposable pipette delivering prepurified gases, and provide a sampling and titrant delivery port. The system is pictured in Figure 3.1.

3.2 Analytical Methods

3.2.1 pH

pH measurements were made with an Orion Research digital pH meter (model 801) and were recorded with an Orion Research digital printer (model 751). Three electrode systems were employed. When space

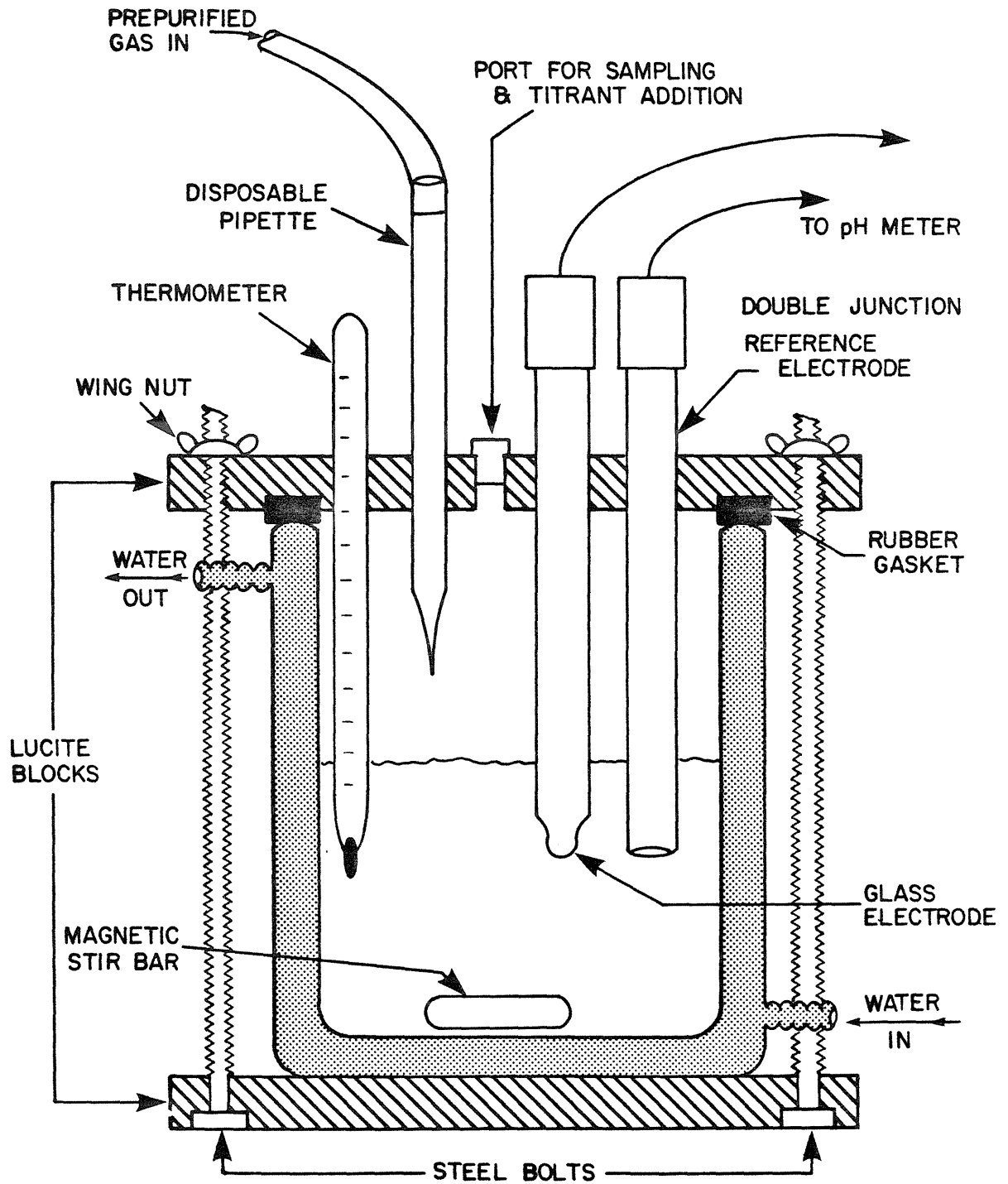


Figure 3.1 Sketch of the reaction vessel for titration experiments.

in the reaction vessel was not a constraint, a Beckman Instruments glass electrode (model 39099) and an Orion Research double junction reference electrode (model 90-02-00) were used. A Broadley-James Corporation 6 mm diameter combination electrode (model 9124) was used to measure pH values of solutions in centrifuge tubes. A Microelectrodes Inc. 2.5 mm diameter combination electrode (model MI-412) was used to measure pH values of solutions in NMR tubes. Calibrations were performed daily with a pair of NBS standard buffers with pH values of 4.0 and 7.0. When alkaline range calibrations were necessary, buffers having pH values of 9.18, 10.00 and 12.45 were used.

Conversion from p_aH to p_cH (from activity to concentration) was accomplished using published values of the apparent ion product of water, ${}^cK_w = [H^+][OH^-]$. Baes and Mesmer (1976) list a value for $\log {}^cK_w$ at 25°C in 0.1 M $NaClO_4$ of -13.78. Smith and Martell (1976) report $\log {}^cK_w = -13.78 \pm 0.01$ at 25°C and $I = 0.1$ M. The relationship between p_cH and p_aH can be derived. By definition,

$$p_aH = -\log a_H \quad (3.1)$$

and

$$a_H = \gamma_H [H^+] \quad (3.2)$$

where a denotes an activity. Substituting equation 3.2 into 3.1,

$$p_aH = -\log(\gamma_H [H^+]) \quad (3.3)$$

$$p_aH = p_cH - \log \gamma_H \quad (3.4)$$

$\log \gamma_H$ can be calculated theoretically by means of the Davies equation resulting in a value of -0.11 at 25°C and $I = 0.1$ M (Stumm and Morgan

Morgan 1981). It can also be determined from experimental values of K_w and c_{K_w} . Assuming $a_{H_2O} = 1$ and $\gamma_H = \gamma_{OH}$, $\log \gamma_H = -0.11$ at $I = 0.1$ M. Thus,

$$p_a^H = p_c^H + 0.11 \quad (3.5)$$

3.2.2 Atomic Absorption Spectroscopy

Nickel in solution was analyzed by flame atomic absorption spectroscopy on a Varian atomic absorption spectrophotometer (model AA-5). Standards of 0.5, 1, 2, and 5 ppm were prepared by dilution of a 1000 ppm Ni standard solution (Varian Techtron) with 0.1 N HNO_3 . Concentrations greater than 5 ppm deviated from otherwise linear calibration curves, $r^2 > 0.99$. Sensitivity was 0.1 ppm giving a working concentration range of 2 to 85 μ M. Absorbance readings were taken directly from the DI-30 digital display. The instrument was recalibrated every 15 to 20 minutes. The accuracy of a single measurement was 2.6% (± 2 standard deviations).

3.2.3 Silica

Silica in solution was measured colorimetrically using the modified molybdenum blue method of Fanning and Pilson (1973). Standard silica solutions were prepared using a precisely weighed amount of $NaSiF_6$. Dilutions and blanks were made with 0.1 M $NaClO_4$. Spectra were recorded on a Hewlett-Packard 8450A UV-VIS spectrophotometer. The average absorbance between 790 and 800 nm was recorded.

3.3 Experiments

3.3.1 Adsorption

Adsorption isotherms and the pH-dependent adsorptive behavior of Ni(II) on silica were determined by means of batch experiments and by potentiometric titrations. All experiments were conducted in unbuffered media in an effort to minimize the number of possible environments for water molecules.

Batch experiments were conducted initially. Titrations followed to differentiate between precipitative and adsorptive removal mechanisms.

3.3.1.1 Batch Experiments

Experiments were conducted either under an atmosphere of purified N₂ gas or a CO₂/N₂ unanalyzed gas mixture from Matheson Gas Co. The concentration of CO₂ in the mixture was 350 ± 35 ppm. Gases were passed through a gas washing train before use. The nitrogen was bubbled through 1 N NaOH, 0.1 N HClO₄ and DDW. The CO₂/N₂ mixture used the same train but excluded the 1N NaOH. A Matheson flowmeter (model 603) was in line to monitor gas flow rates. A glass manifold with eight stopcocks was used when it was necessary to deliver gas to more than one sample simultaneously.

Typically, 30 mL of Ni²⁺ stock solution which had been diluted to between 0.1 to 2.0 mM Ni²⁺ was added to 50 mg of Aerosil 200. A predetermined volume of CO₂-free NaOH was then added along with 0.1 mL of 0.0475 M NaHCO₃. If the experiment was run in the absence of CO₂, the bicarbonate addition was eliminated. A stirring bar was added and the tube and contents were weighed. Experiments were run in triplicate at each [Ni²⁺].

Approach of the system to equilibrium was monitored by measuring the pH of the stirred suspension. One hour prior to and during pH measurements, an appropriate atmosphere of N_2 gas or a CO_2/N_2 gas mixture was provided. Samples were sealed at all other times.

Samples were brought to the desired pH with 0.1 N and 0.01 N NaOH and/or $HClO_4$. The amount of NaOH added was adjusted to keep the pH below the value at which $Ni(OH)_2(s)$ would precipitate at all times. Samples were sonicated for 1 hour and shaken overnight between each pH adjustment.

Separation of the Aerosil from suspension was accomplished by centrifugation. At the completion of the pH equilibration, samples were spun at 4100 rpm for four hours in an International Equipment Company refrigerated centrifuge (model PR-2) maintained at $25^\circ C$. Samples were allowed to sit quiescently for one week prior to atomic absorption analysis of the supernatant for nickel ion.

The silica was then resuspended by sonication and shaking and a final pH reading was taken.

3.3.1.2 Titrations

Titration of the $Ni(II)-SiO_2$ system were performed in jacketed glass beakers. Temperature was maintained at $(25.0 \pm 0.2)^\circ C$ with a Haake constant temperature bath (model FS).

A freshly prepared 500 mL solution of 0.426 mM $Ni(ClO_4)_2$ was equilibrated under a N_2 atmosphere. 79 mg of Aerosil, dried at $110^\circ C$, were added and the suspension was stirred overnight.

The suspension was titrated with CO_2 -free NaOH to pH > 9. Periodi-

cally, 1 mL samples were removed by pipette, diluted to 5 mL with 0.1 M NaClO_4 , filtered through a 0.45 μm Millipore filter, acidified with 10 μL of concentrated HNO_3 and stored in a plastic vial. This solution was later analyzed for Ni(II).

Dissolved silica measurements were also made at various times by obtaining a 2 mL aliquot and diluting to 10 mL as above. One half of the resultant filtrate was used for Ni analysis and the rest for silica measurements.

Similar titrations were also performed on systems of Ni(II) in the absence of silica and silica in the absence of Ni(II). A 0.1 M NaClO_4 solution was titrated to determine the blank correction.

3.3.2 Nuclear Magnetic Resonance

3.3.2.1 Apparatus

Nuclear magnetic resonance (NMR) spectra were recorded on three different instruments. Measurements were initially made on a Varian HR-220 spectrometer. Most of the data was gathered using a modified Varian HA-100 spectrometer and a Bruker WM-500 spectrometer. Modifications to the Varian HA-100 spectrometer included a digital frequency sweep and accumulation of the signals in a Hewlett-Packard 5480 averager, both under the control of a Hewlett-Packard 2116 computer. Temperature was controlled using a Varian temperature controller (model V-6040). Temperature measurements were made before and after each spectrum was recorded by inserting a chromel-constantan thermocouple into the sample region of an outer sample tube. The thermocouple was encased in a 3/32 inch diameter brass tube attached to the plastic probe

cover. Three screws were arranged symmetrically around and perpendicular to the tubing near the top. These allowed the thermocouple to be positioned such that the tube could be spun while temperature measurements were taken. Spinner air flow was maintained at 7 L/m. Accuracy under these well-controlled conditions were $\pm 0.2^{\circ}\text{C}$. A complete description of the modifications is available in Manatt and Young (1980), and Cooper et al. (1971).

Samples were placed in 5 mm precision coaxial cells (No. 516) purchased from Wilmad Glass. The compound 2,2,4,4-tetramethylpentane (TMP) was used in the annulus as a standard and to provide the lock signal for the HA-100 spectrometer. Heat shrink tubing (3/16 inch) was applied around the opening of the annulus to prevent the loss of TMP at high temperatures.

3.3.2.2 Bulk Susceptibility Correction

Chemical shifts measured in externally referenced samples must be corrected for bulk susceptibility differences (Dickinson 1951). Live and Chan (1970) have shown that these corrections are a function of the magnet/sample geometry and that this fact can be used to correct observed chemical shifts.

NMR experiments were conducted on two spectrometers having different magnet/sample geometries. The Bruker WM-500 spectrometer's superconducting solenoid produces a magnetic field along the long axis of a cylindrical sample tube. The Varian HA-100 spectrometer's electromagnet produces field lines perpendicular to this long axis.

Equations describing corrections to the observed chemical shift as

a function of susceptibility for these two geometries are (from Live and Chan 1970)

$$\omega_{\text{corr}} = \omega_{\text{obs}} + \frac{2\pi}{3} (\chi_{\text{v}}^{\text{ref}} - \chi_{\text{v}}) \quad (3.6)$$

for the perpendicular geometry (HA-100) and

$$\omega_{\text{corr}} = \omega_{\text{obs}} - \frac{4\pi}{3} (\chi_{\text{v}}^{\text{ref}} - \chi_{\text{v}}) \quad (3.7)$$

for the parallel geometry (WM-500) where: ω_{obs} is the observed chemical shift in ppm, ω_{corr} is the value of the shift corrected for susceptibility effects in ppm, and χ_{v} and $\chi_{\text{v}}^{\text{ref}}$ are the volume magnetic susceptibilities of the sample and reference solutions, respectively.

Combining these equations by eliminating the susceptibility term yields

$$\omega_{\text{corr}} = \frac{1}{3}\omega_{\text{obs}||} + \frac{2}{3}\omega_{\text{obs}\perp} \quad (3.8)$$

The subscripts $||$ and \perp indicate parallel and perpendicular geometries, respectively. Susceptibility corrections now become a simple linear combination of observed chemical shift values recorded by the two different spectrometers.

CHAPTER 4

ADSORPTIVE BEHAVIOR OF Ni(II) ON SILICA

4.1 Introduction

In order to conduct a meaningful NMR investigation of adsorbed Ni(II), it is necessary to have a detailed understanding of the speciation of Ni(II) in the presence of a silica surface. Data on the position of the pH adsorption edge (a steep rise in percent adsorption of a metal ion with increasing pH) in this system are inconclusive. There is no information regarding adsorption densities at high concentrations of nickel relative to surface sites. In light of these facts, an experimental program was undertaken to determine the behavior of a Ni(II) - SiO₂ aqueous system. Two aspects studied in detail were the pH-dependent nature of the adsorption and the capacity of the silica surface to adsorb nickel ions.

Modeling the behavior of this system was accomplished by considering two simple subproblems: the acid-base nature of silica in solution and the solubility of Ni(OH)₂(s). They were examined experimentally and modeled successfully before attempting to describe to the entire system.

4.2 Design Considerations

Conditions under which the experiments were run were quite different from those usually encountered in studies of metal ion adsorption onto surfaces. In particular, the ratio of the total amount of nickel ion in solution to the total available surface sites, $\rho \equiv \text{Ni}^{2+}_{\text{T}}/\text{SiOH}_{\text{T}}$, ranged from 0.04 to 2.0. This is to be contrasted with values of 10^{-3} to 10^{-1} typically used in other investigations.

A study of high $[\text{Ni}^{2+}]_{\text{T}}/[\text{SiOH}]_{\text{T}}$ ratios was dictated by certain experimental constraints. Success of the NMR experiment rested on the ability to measure chemical shifts accurately. The magnitude of this shift is a linear function of concentration. Preliminary experiments indicated that concentrations in excess of 10^{-3} M nickel ion are necessary to produce measurable differences in the chemical shift (section 5.3.1). These high concentrations, coupled with the small sample volume of a 5 mm NMR tube, necessitated large adsorption densities and a high-surface-area adsorbent.

Consideration of the transport of metal ions in soils and sediments likewise generated interest in the response of surfaces to very high metal ion loadings. In and around landfills and ocean outfalls, metal ion concentrations can be orders of magnitude larger than those encountered in natural aquatic systems. The ability of surfaces to bind metal ions plays a crucial role in immobilizing toxic metals in these systems. Depending on the strength of the binding, adsorption onto surfaces can either retard transport through successive sorption/desorption processes or completely remove metals from the solution phase.

4.3 Silica Titrations

Alkalimetric titrations were performed on silica suspensions in order to quantify proton release from the surface and to understand the mechanisms by which the surface is charged. Surface charge was calculated and compared to literature values and theoretical predictions.

4.3.1 Choice of the Solid Phase

Silicon is the most abundant element in the earth's crust.

The bulk of the element is incorporated in various silicas and silicate minerals. A number of crystalline states of silica are known; quartz, opal, cristobalite, and tridymite are examples. Man has produced many additional types of silica. Generally, these are amorphous materials which can be found as gels, colloids, precipitates, vitreous and glassy materials, and pyrogenic solids. Qualitatively, the many forms of SiO_2 behave similarly. On a quantitative level, there are differences. The choice of the particular silica used in this work was made with the following considerations in mind:

- 1) uniformity: a widely available product with a well-defined and well-known composition was sought to ensure reproducibility;
- 2) non-porosity: porosity complications were to be avoided;
- 3) surface area: a large surface area would insure high concentrations of adsorbed Ni(II) per volume;
- 4) known behavior: a silica whose surface properties have been studied and reported in the literature would guide experimental design and provide a data base to which results could be compared.

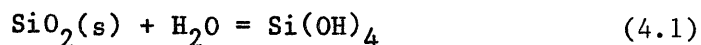
With these factors in mind, Aerosil 200 was chosen as the experimental surface. The properties of Aerosil 200 have been described in section 3.1.1.

4.3.2 Physical and Chemical Characteristics of Silica

4.3.2.1 Solution Chemistry

The solubility of silica at 25°C is relatively large compared to that of other environmentally interesting oxides like iron, manganese and aluminum. It ranges from 2 mM for amorphous materials to

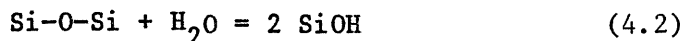
0.1 mM for crystalline quartz. Interaction of the solid phase with water forms orthosilicic acid as defined by equation 4.1.



Orthosilicic acid is a weak acid. Its first two acidity constants have been determined previously and are presented along with constants for some simple polymeric species in Table 4.1. In solutions whose concentrations are in excess of 2 mM (pH's less than 10), polymerization of the monomer, $\text{Si}(\text{OH})_4$, occurs. The stability of monomeric forms of silica increases at higher pH. Continued polymerization initially produces colloidal material which can be stable or can coagulate and settle. Stable particles can grow in size through condensation of monomeric and/or polymeric species in solution onto their surfaces.

4.3.2.2 Surface Chemistry

Chemistry of the silica surface presents another facet of the behavior of SiO_2 . Siloxane bonds (Si-O-Si) on the surface are easily hydrolyzed and react in solution with water producing surface hydroxyl (silanol) groups (equation 4.2).



Silanol groups have a pK_a of 6.8 and are, therefore, more acidic than orthosilicic acid (Schindler and Kamber 1968). Further reactions of these groups with hydrogen and hydroxide ions provide a means for charging the surface, equations 4.3, 4.4.



Table 4.1

Solution equilibria for selected silica species at 25°C, I = 0 (1)

		<u>log K</u>
K_{s0}	$\text{SiO}_2(\text{am}) + 2\text{H}_2\text{O} = \text{Si}(\text{OH})_4$	-2.7
$*K_1$	$\text{Si}(\text{OH})_4 = \text{SiO}(\text{OH})_3^- + \text{H}^+$	-9.86
$*K_2$	$\text{SiO}(\text{OH})_3^- = \text{SiO}_2(\text{OH})_2^{2-} + \text{H}^+$	-13.1
β_{22}	$2\text{SiO}_2(\text{OH})_2^{2-} + 2\text{H}^+ = \text{H}_6\text{Si}_2\text{O}_8^{2-}$	26.16(2)
β_{44}	$4\text{SiO}_2(\text{OH})_2^{2-} + 4\text{H}^+ = \text{H}_{12}\text{Si}_4\text{O}_{16}^{2-}$	55.9
β_{46}	$4\text{SiO}_2(\text{OH})_2^{2-} + 6\text{H}^+ = \text{H}_{14}\text{Si}_4\text{O}_{16}^{2-}$	78.2

(1) From Smith and Martell (1976)

(2) I = 3.0 molal



The pH_{zpc} , pH of the zero point of charge, is typically reported as 2, with values ranging from 1.0 to 4.0. Using this information, one can predict that the concentration of species SiOH_2^+ is vanishingly small at pH values greater than 2. Thus, silica surfaces found in most aquatic environments either carry no charge or are negatively charged. A comprehensive and up-to-date review of the chemistry of silica has been published by Iler (1979).

4.3.2.3 Surface Site Density

Coordination chemistry modeling to describe adsorption requires a value for the number of surface groups present per unit area. A number of experimental methods have been used to determine this value. These include chemical, titrimetric, deuterium and tritium exchange, and infrared spectroscopic techniques. Theoretical analyses, which assume the surface to be composed of various sets of crystal planes, have also been employed. Iler (1979) has listed thirty references on this subject covering all of the above methods and concludes, "It now seems generally agreed that on the smooth, nonporous heat-stabilized amorphous silica surface that is fully hydroxylated there are 4 to 5 SiOH groups nm^{-2} (100 \AA^2) which remain when the sample is dried at 120 to 150°C." Experimental values reported for the site density of Aerosil 200 are, 5.0 to 5.2 nm^{-2} by Davydov et al. (1964) using deuterium exchange in vacuo at 150°, and 5.46 nm^{-2} by Schindler et al. (1976) using an alkalimetric titration in 1 M NaClO_4 . A value of 5.0 sites nm^{-2} will be used for the density of silanol groups on a fully hydroxylated Aerosil 200 surface in

all calculations.

4.3.3 Previous Studies of the Silica Surface

Titrimetric techniques for the determination of surface charge were pioneered by Bolt (1957) and have been applied to the silica surface by Tadros and Lyklema (1968), Schindler and Kamber (1968), Allen and Matijević (1970), Abendroth (1970), and Yates and Healy (1976). Experiments must be carefully designed to avoid the suspension effect (the influence, as reported by Bolt (1957), of charged particles on the transference numbers of electrolyte ions in and around the liquid junction, which effects junction potentials), and corrected for protons consumed by dissolved silica species according to the reactions listed in Table 4.1. Titrimetric procedures are additionally complicated by the fact that surface charge measurements are a function of ionic strength and the background electrolyte cation. Thus, surface charge calculations in this work can only be compared to previous studies of amorphous nonporous silica at 0.1 M ionic strength in a NaX electrolyte. Two such studies exist.

Abendroth (1970) conducted potentiometric titrations of Cab-O-Sil M-7, a pyrogenic silica with an argon BET surface area of $170 \text{ m}^2/\text{g}$. The pH_{zpc} was reported to be between 1.7 and 3.5. Surface charge and differential capacity were reported as functions of ionic strength and background electrolyte at various values of pH. Silica loading was 5 g/400 mL. Bolt (1957) performed a similar study of a commercial silica sol, Ludox, an amorphous precipitated silica with a specific surface area of $180 \text{ m}^2/\text{g}$. Bolt's titrations were conducted on 3, 10, and 30%

silica suspensions in NaCl. Data were reported for the 10% suspension only, as surface charge calculations were found to be unaffected by silica loading. The ionic strength was varied from 0.004 to 4 M. Both the experiments of Abendroth and of Bolt show that surface charge begins to develop at pH 4 and increases with increasing pH. The data indicate a greater surface charge density for the precipitated silica used by Bolt.

4.3.4 Experimental Results

Experiments were conducted with 500 mL of a 1 g/L suspension of Aerosil 200 in 0.1 M NaClO₄. The silica solid was allowed to dissolve to equilibrium with the dissolved species Si(OH)₄ by bringing the solution to pH 8.25 for at least one day. Measurements of dissolved silica as a function of time at two pH values indicate this is sufficient time (Figure 4.1). The measured value of the equilibrium concentration of dissolved silica in this system was 1.85 mM. The standard error of the mean for twenty one measurements was 0.03 mM. The pH was then lowered to less than 5 and the suspension was titrated to pH greater than 10 with 0.1 N NaOH. Titrations were rapidly completed (2 to 3 hours) to avoid further dissolution of the solid phase; yet concentrations of Si(OH)₄ in excess of 1.85 mM were observed. Measurements of silica at the end of titration LM13 indicate the concentration of dissolved silica was 2.31 mM (elapsed time two hours). 1.2 hours after the end of titration LM12, the concentration of dissolved silica was 3.43 mM (elapsed time 4.6 hours). Data are presented in Figure 4.2 and compared to theoretical titrations of: i) water, ii) a silica suspension in which the total concentration of dissolved silica is fixed at 1.85 mM, and

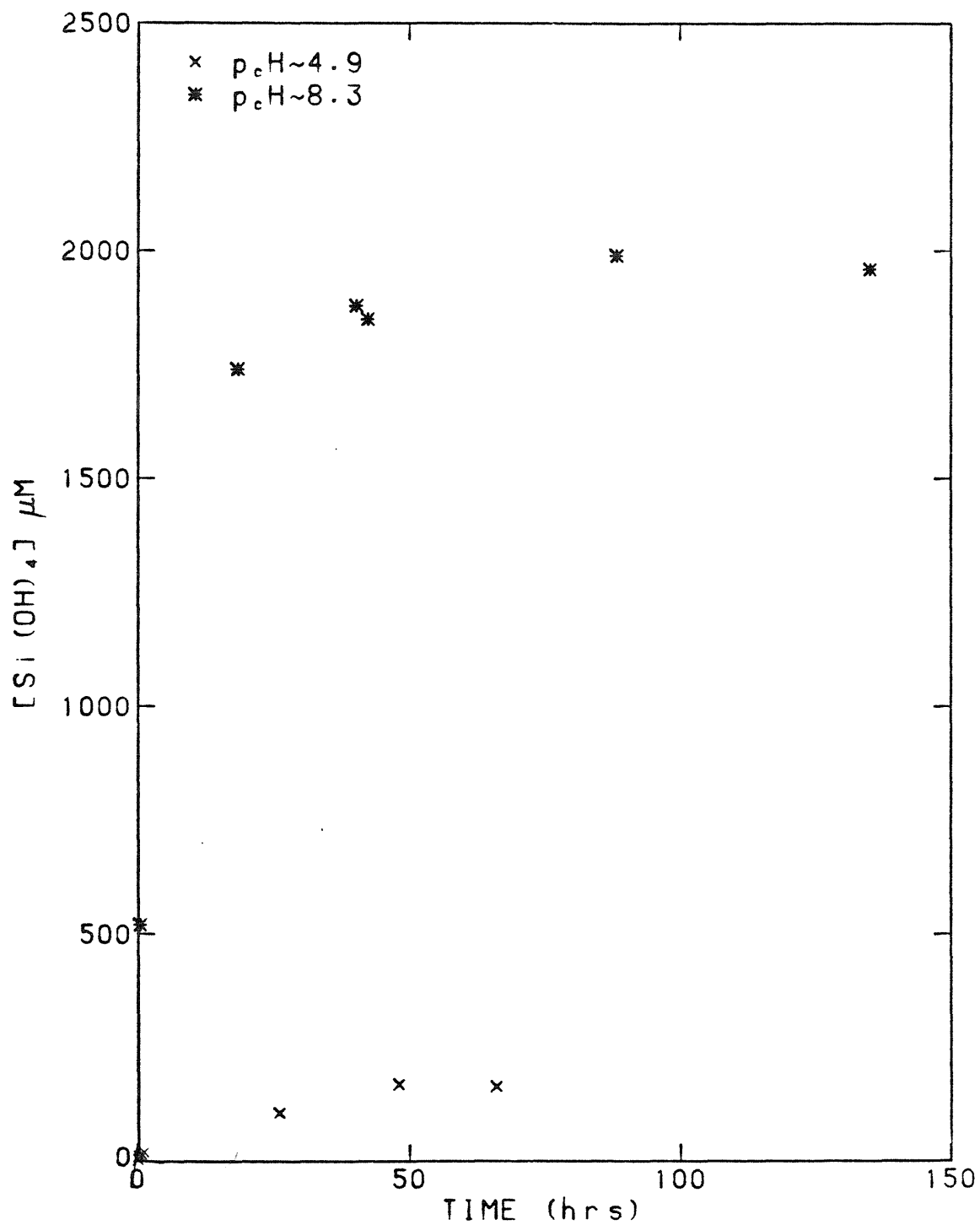


Figure 4.1 Measured dissolved silica plotted as a function of time at 2 different pH values. Silica loading was 1 g/L.

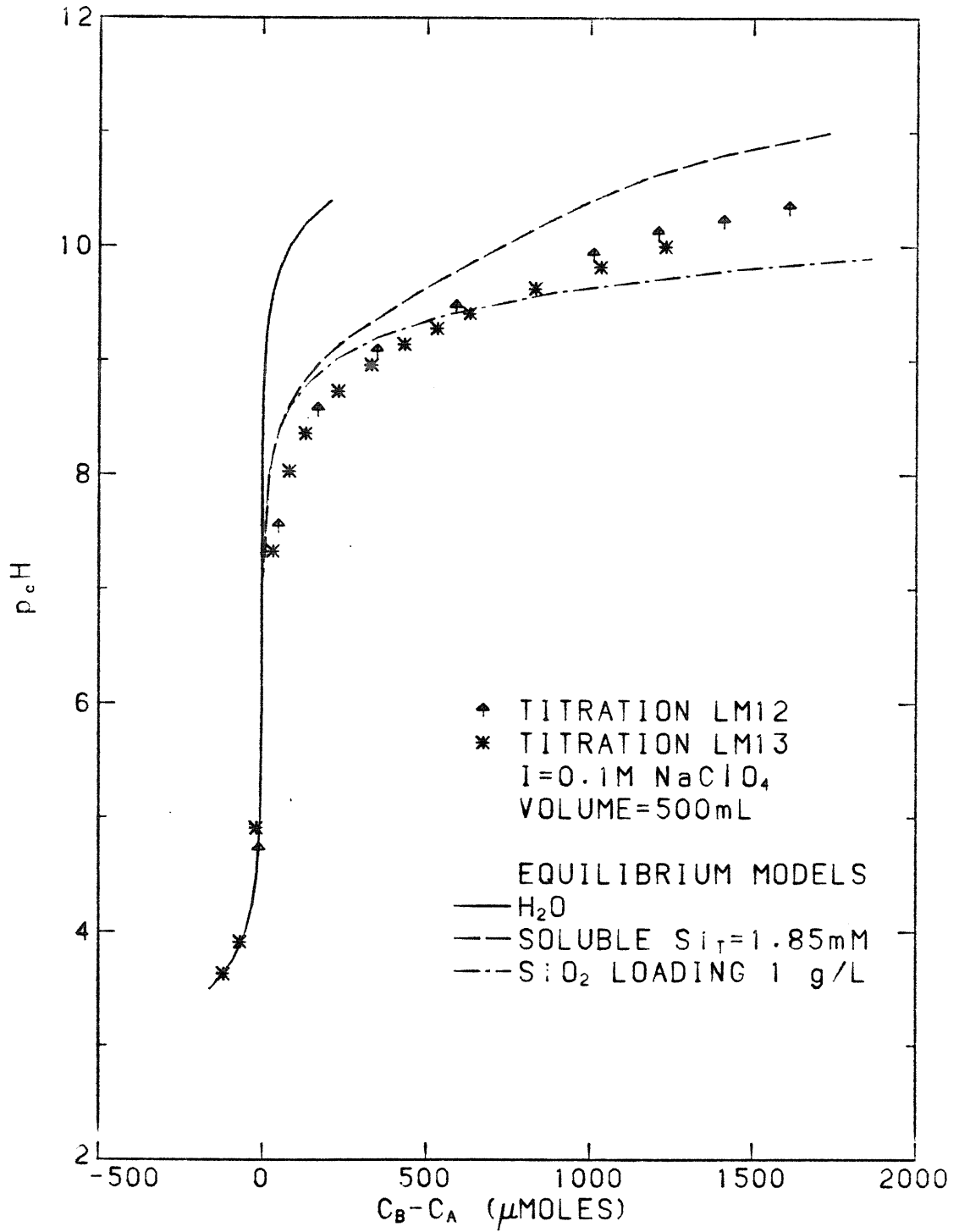


Figure 4.2 Titration data for 1 g/L silica suspensions titrated with 0.1 N NaOH. Calculated titration curves for various equilibrium systems are shown for comparison.

iii) a 1 g/L suspension in equilibrium with the liquid phase. Equilibrium constants for the soluble silica species considered were those in Table 4.1.

Values for the surface charge were calculated and compared to those published by Abendroth (1970) and Bolt (1957). Surface charge, in $\mu\text{C}/\text{cm}^2$, is the difference in adsorption densities of H^+ and OH^- . Specifically,

$$\sigma = F(\Gamma_{\text{H}} - \Gamma_{\text{OH}}) \quad (4.5)$$

where Γ_{H} and Γ_{OH} are the adsorption densities of H^+ and OH^- respectively in $\mu\text{moles}/\text{cm}^2$ and F is the Faraday. Acidimetric titrations of the silica sol to determine the pH_{zpc} produced uncertain results. Therefore, data were referenced to a zero charge condition by setting the value of σ to $-0.65 \mu\text{C}/\text{cm}^2$ at a p_cH of 5. This is the average of Abendroth's and Bolt's values at this point, -0.7 and $-0.6 \mu\text{C}/\text{cm}^2$, respectively. A value of 2.31 mM for Si_{T} was used to correct the data for protons consumed by soluble silica. This is strictly correct for titration LM13. Only an estimate can be made for titration LM12 as a measurement of the concentration of dissolved silica was not made immediately after the last addition of titrant. Surface charge is plotted against p_cH in Figure 4.3.

Surface charge calculations for titration LM12 reveal a discontinuity at p_cH 8.6. An equilibrium calculation using SURFEQL predicted the silica to dissolve at this point producing a large concentration of titratable $\text{Si}(\text{OH})_4$ not present in titration LM12. The resulting underestimation of surface charge is evident. This fact, and the lack

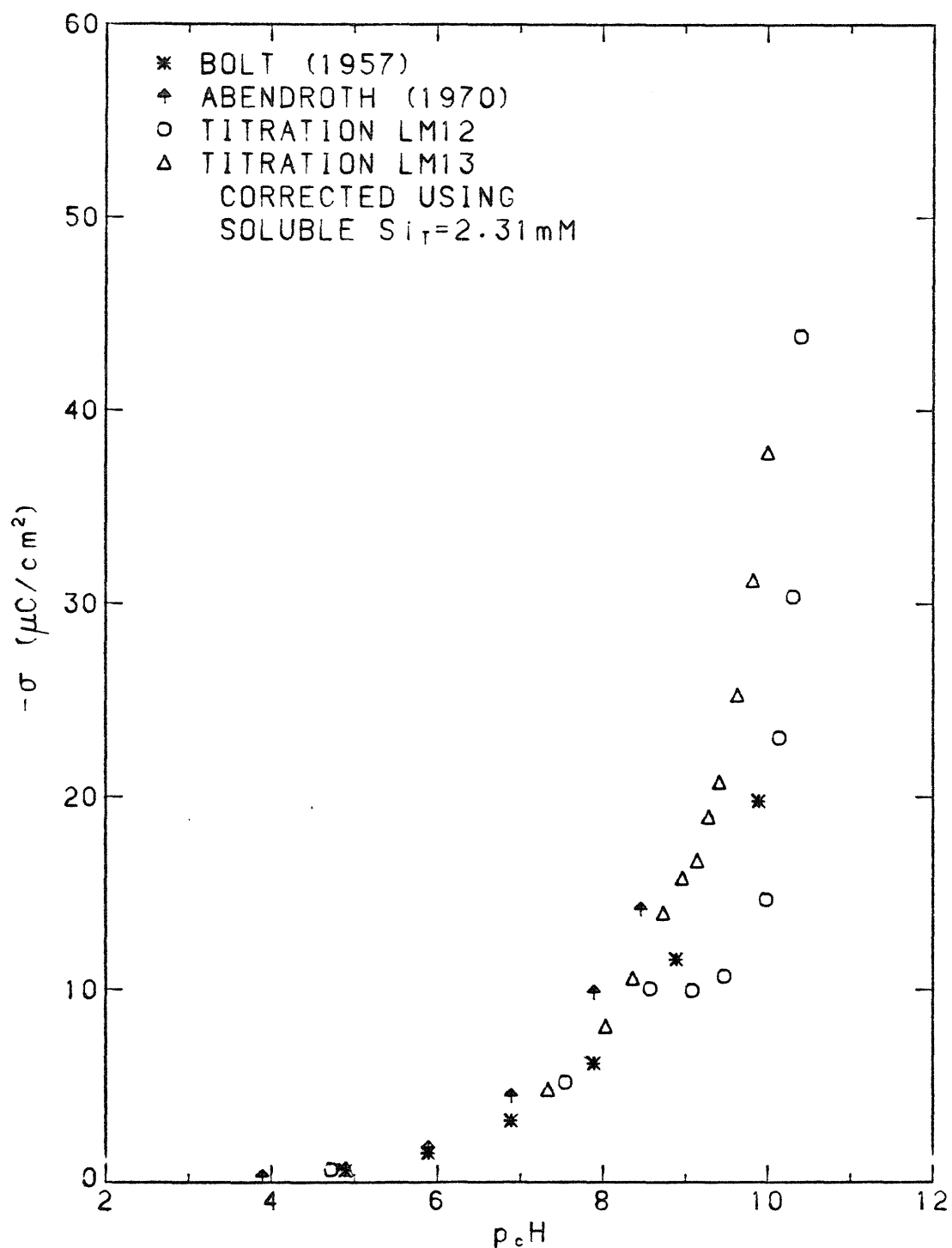


Figure 4.3 Surface charge calculations for titrations LM12 and LM13 compared to literature values for equivalent systems.

of a measured value for the concentration of dissolved silica at the conclusion of titration LM12, preclude the use of the data from this titration for modeling studies.

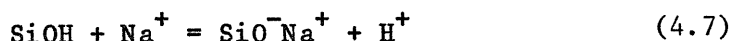
A lower limit for the charge density on Aerosil 200 in 0.1 M NaClO₄ is calculated to be -38 μC/cm² or 3.9 μmoles/m² or 2.4 negatively charged sites/nm².

4.3.5 Modeling the Observed Surface Charge

Surface charge calculations for titration LM13 were modeled with both the constant capacitance model (CCM) and the triple layer model (TLM). Two mechanisms for the development of surface charge were investigated. Along with the surface hydrolysis reaction common to both models,



an exchange reaction of surface protons for background electrolyte cations was considered when the TLM was used.



These reactions have interesting implications with regard to the detailed ways in which electrostatic corrections are formulated. The CCM and the TLM treat the surface hydrolysis reaction in the same fashion. Electrostatic corrections are equivalent and the intrinsic equilibrium constants have the same form.

$$c_{a2}^s(\text{int}) = \frac{\{\text{SiO}^-\}[\text{H}^+]}{\{\text{SiOH}\}} \cdot \exp(-z_o) \quad (4.8)$$

The electrostatic correction is more complex for the exchange reaction in the TLM because the background electrolyte ions are located in a different plane than H^+ and OH^- . The TLM requires,

$$c_{1Na}^{*s} (int) = \frac{\{SiO^- Na^+\} [H^+]}{\{SiOH\} [Na^+]} \cdot \exp(z_1 - z_0) \quad (4.9)$$

As the potentials ψ_0 and ψ_1 are not equal, a net electrostatic correction remains.

The inadequacy of these models to explain the behavior of the silica system, regardless of the model under consideration, is evident in Figure 4.4. Any combination of values for the constants or capacitances will not change the linear relationship between surface charge and pH which occurs at pH's greater than $p^{CK_{a2}^s}$. Surface parameters held constant during the generation of these curves were surface area, 182 m²/g, surface loading, 1 g/L, and the capacitances; C_1 was set equal to 125 F/m² in the CCM and C_1 and C_2 were set equal to 125 and 20 F/m², respectively, in the TLM.

In order to fit the data, (therefore, having the means to account for the acid-base behavior of a silica surface in later calculations) a variation of the CCM was considered. This variation, designated CCM', places all adsorbing ions in the σ_0 plane. In the CCM' framework, the form of the surface hydrolysis constant (equation 4.8) remains unchanged. When an exchange reaction with Na^+ is considered, the correction for a leaving H^+ is equal to and opposite from that of the bound Na^+ , resulting in an intrinsic equilibrium constant that is not a function of potential. The form of this constant is shown below.

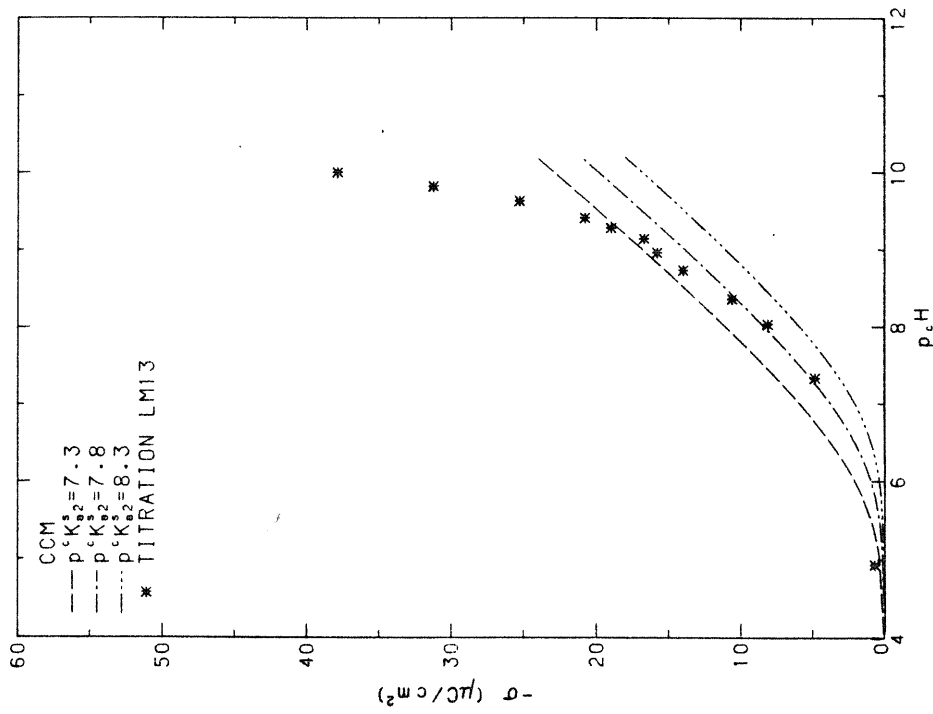
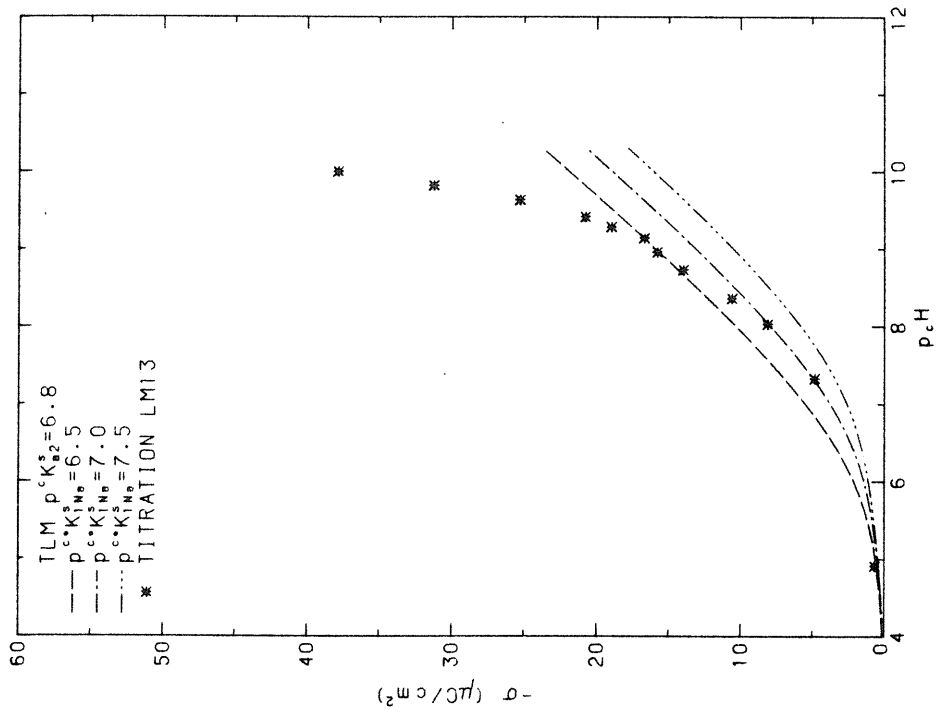


Figure 4.4 A comparison of values predicted for σ by the CCM and the TLM to calculated values from titration LM13.

$$c_{1\text{Na}}^{*K^S}(\text{int}) = \frac{\{\text{SiO}^- \text{Na}^+\}[\text{H}^+]}{\{\text{SiOH}\}[\text{Na}^+]} \quad (4.10)$$

Results from the CCM' (Figure 4.5) are much more satisfactory in describing the surface charge/pH relationship of silica. Values of -7.8 for $\log c_{a2}^{K^S}$ and -9.5 for $\log c_{1\text{Na}}^{*K^S}$ provide a very good fit.

4.3.6 Discussion

Modeling the generation of surface charge on silica has led to two interesting results: i) surface charge was found to be logarithmically related to pH; ii) two surface charging mechanisms, deprotonation of silanol groups and surface complexation with the background cation, were necessary to explain the observed behavior.

Studies of other metal oxide and oxyhydroxide surfaces generally show surface charge to be a linear function of pH at ionic strengths of 0.1 M or greater. For nonporous silica surfaces, the calculations in Figure 4.3 show a relationship between surface charge and pH that is not linear. When these calculations are replotted as $\log(-\sigma)$ vs. pH, linear relationships are obtained (Figure 4.6). Regression lines are plotted for each set of calculations, r^2 values are all greater than 0.99. Wirth and Gieskes (1979) noted, using the calculations of Bolt (1957), that the logarithmic nature of the surface charge/pH relationship held over ionic strengths ranging from 0.001 to 1 M NaCl. It can be seen in Figure 4.6 that this relationship not only holds for one type of silica at differing ionic strengths but also for a variety of nonporous amorphous silicas at $I = 0.1$ M. It can be concluded that surface charge/pH relationships are logarithmic over a wide range of ionic

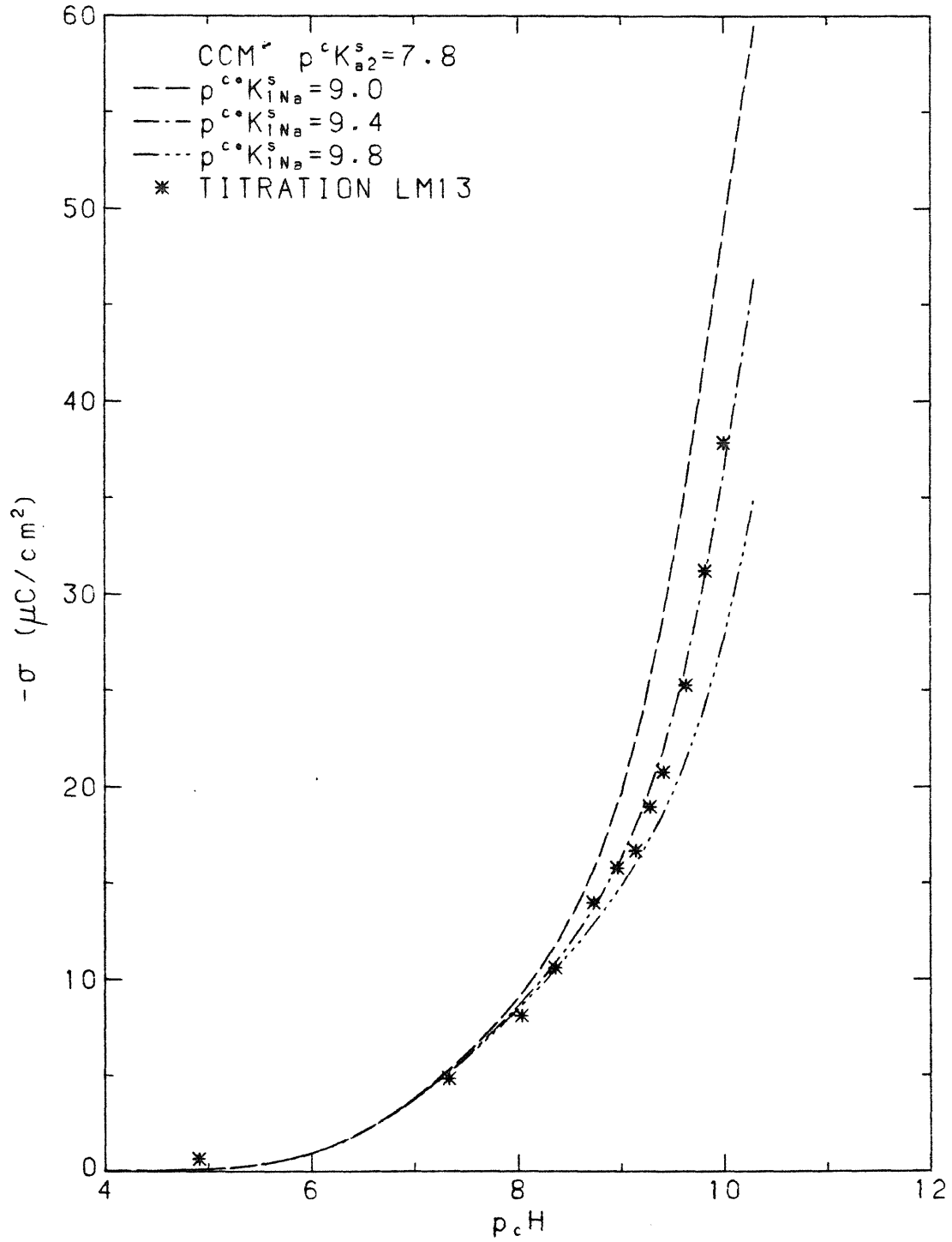


Figure 4.5 A comparison of values predicted for σ by the CCM to calculated values from titration LM13. Both surface hydrolysis and exchange reactions are considered.

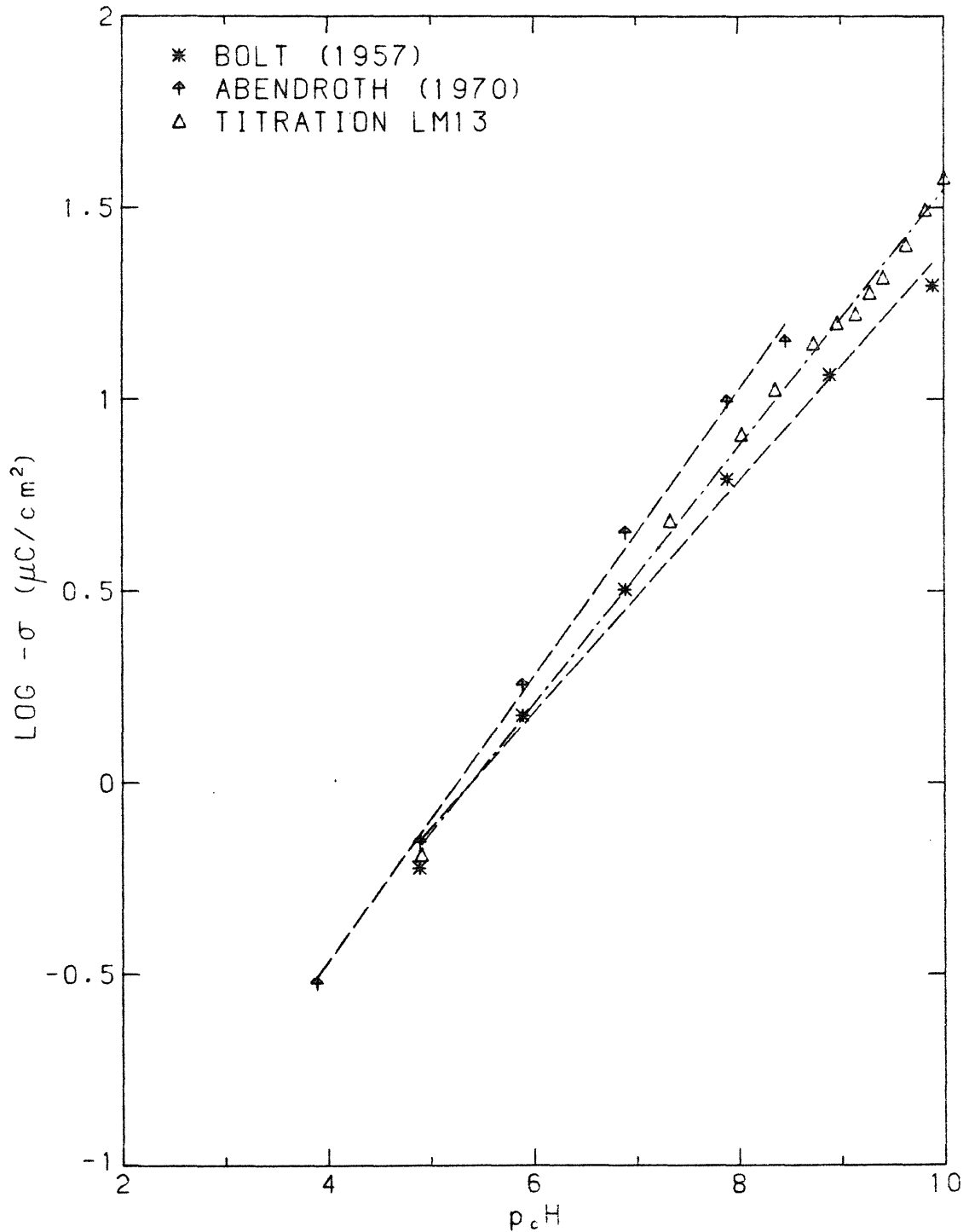


Figure 4.6 Calculations for Figure 4.3 replotted as $\log -\sigma$ vs. $p_c H$. Linear regressions from each set of points are shown.

strengths for nonporous amorphous silicas.

In order to assess the capabilities of the models to reproduce the logarithmic relationship, results from titration LM13 along with the best fits to them from both the CCM' and the TLM or CCM, are shown in Figure 4.7. Here, σ has been normalized with respect to total available surface sites, SiOH_T . The ordinate now represents $\log \alpha$, where α is the fraction of surface sites neutralized. Results from titration LM13 show the logarithmic relationship holds up to $\alpha = 0.5$. The CCM' predicts this will continue to be true until $\alpha \geq 0.6$, while the TLM or CCM show this behavior only up to a value of $\alpha = 0.1$.

The difference in the capabilities of the models to describe this behavior successfully is directly related to the difference in the way the electrostatic corrections are made and, ultimately, on the differences in the descriptions of the double layer structure. As mentioned previously, electrostatic corrections to c_{Na}^{S} in the CCM' cancel as the exchange of H^+ for Na^+ takes place at the same mean plane of adsorption. The TLM places the Na^+ farther from the surface, resulting in a net electrostatic correction, $\exp(z_1 - z_0)$. As a consequence, the apparent value of c_{Na}^{S} will not decrease with increasing pH in CCM' calculations as it does in TLM calculations.

The relative importance of each species contribution to the surface charge is shown in Figure 4.8 for the CCM'. At a pH of 10.2 the SiO^-Na^+ species becomes prevalent. The apparent value of $\log c_{\text{a2}}^{\text{S}}$ has dropped from -7.8 to -10.5 at this point.

Efforts of previous investigators to model the surface charge on a silica surface have resulted in the following interpretations. Allen et

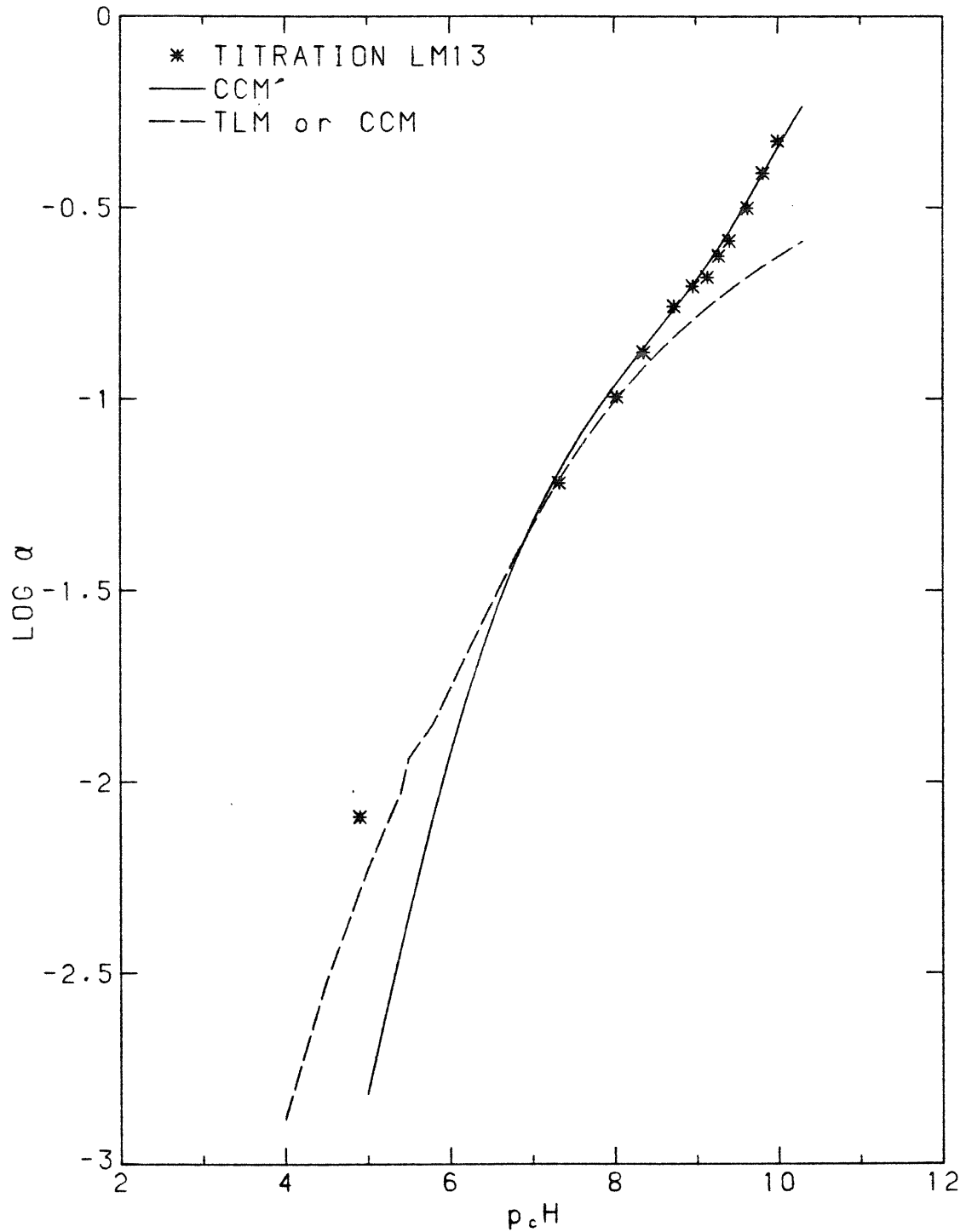


Figure 4.7 The logarithm of the fraction of surface sites neutralized, α , is plotted against $p_c H$. The curves are the best fits to the data using the CCM^c and the TLM or CCM.

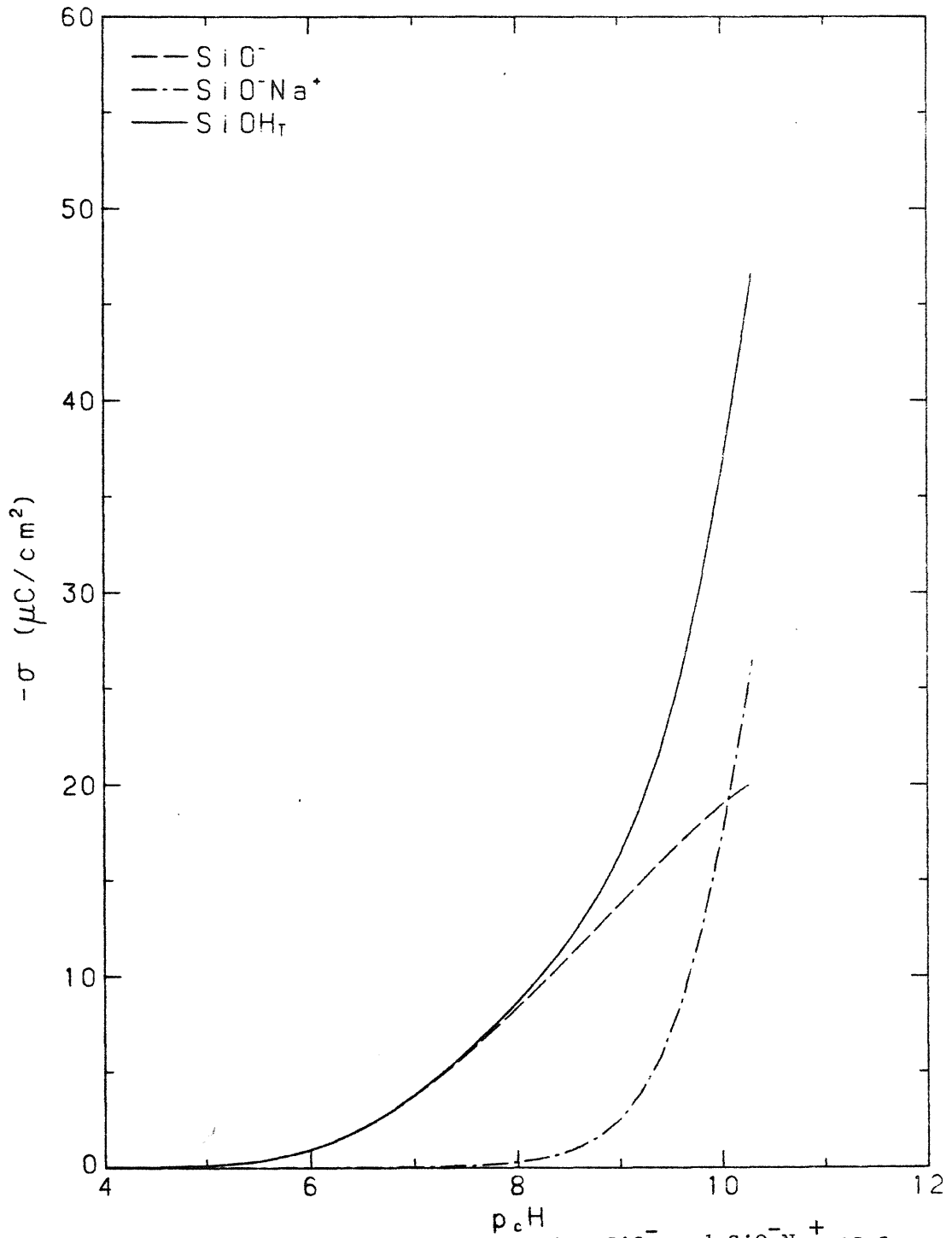


Figure 4.8 The distribution of surface species SiO^- and SiO^-Na^+ as a function of p_cH . Calculations were made with the CCM^r using values for $p_cK_{a2}^S$ and $p_cK_{1Na}^S$ of 7.8 and 9.4, respectively.

al. (1971), modeling their alkalimetric titrations of suspensions of Ludox HS in 1.0 M NaCl, examined three assumptions which attempted to describe the exchange of Na^+ for silanolic protons. The first assumed the surface consisted of two types of silanol groups with different reactivities. In the second, the equilibrium constant for a single type of silanol group was supposed to decrease as the exchange process proceeded. The third was a combination of these two effects. The best fit to their data was realized using the third assumption. Intrinsic constants for exchange with two differing sites which provided the best fit were found, by a curve fitting process, to be $\log K_1 = 5.5$ and $\log K_2 = 9.0$.

Davis et al. (1976) found reasonable agreement with the data of Abendroth (1970) when using the TLM. An inner layer capacitance of $1.25 \pm 0.1 \text{ F/m}^2$ was used along with a surface acidity constant, $\log c_{a2}^{\text{K}^{\text{S}}}$, of -7.3 and surface complexation constant for exchange with K^+ , $\log c_{\text{IK}}^{\text{K}^{\text{S}}}$ of -6.7 . Both surface dissociation and surface complexation were found to be important charging mechanisms.

Smit et al. (1978) studied the adsorption of sodium ions into the compact part of the double layer with a radiotracer technique and zeta potential measurements. Sodium-24 and bromide-82 were adsorbed on vitreous silica rods at pH 4 and 10. The rods were equilibrated with 0.006 to 0.015 M NaBr solutions for at least 20 hours, rinsed seven times with water (4% by weight) in acetone, and etched three times in 1.5 M HF, each etch removing a layer of silica 0.3 nm thick. Results indicate that both Na^+ and Br^- are quantitatively removed by the washing process alone at pH 4. Residual activity in the first HF etch was

attributed to NaBr solution remaining in cracks. At pH 10, a fraction of the Na^+ was still associated with the rod after the seventh wash. The sodium was completely removed by the first HF etch. Non-zero Na^+ ion activity in the latter washings was attributed to Na^+ ion adsorption into the compact part of the double layer. The distribution of charge within the double layer was calculated. A lower value for σ_{Na} was estimated by summing Na^+ count rates in those washings and etchings where Na^+ desorption was occurring and converting to $\mu\text{C}/\text{cm}^2$ units. Values of σ_{d} were calculated from zeta potential measurements using the theory of the flat double layer, letting $\psi_{\text{d}} = \zeta$. σ_{o} follows from the charge balance for a silica surface:

$$\sigma_{\text{o}} + \sigma_{\text{Na}} + \sigma_{\text{d}} = 0 \quad (4.11)$$

Their results at pH 9.7, $I = 0.015 \text{ M}$, show 80% of the surface charge is neutralized by sodium ion adsorbed in the compact part of the double layer with the rest of the surface charge balanced in the diffuse layer. Their calculated value of σ_{o} agrees with that of Bolt (1957).

These researchers found a need to invoke a charging mechanism for the silica surface in addition to the deprotonation of one type of silanol group. This either takes the form of an additional set of surface groups capable of exchanging protons for sodium ions or the specific adsorption of sodium ions into the compact part of the double layer.

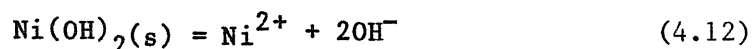
Surface charge calculated from the titration data presented here can be fit by including a specific chemical interaction between Na^+ and silanol groups in a variation of the CCM in which all adsorbing ions are

located at the σ_0 plane. Neither the CCM or the TLM is able to fit the experimental results obtained in this study, especially at the larger values of surface charge.

4.4 Nickel Hydroxide Solubility

4.4.1 Introduction

The solubility product for $\text{Ni(OH)}_2(s)$, K_{s0} , corresponds to the reaction

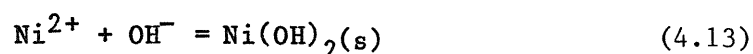


Values for $\log K_{s0}$ reported in the literature have been collected by Sillén and Martell (1964). Those values, corrected to ionic strength 0 at 25°C, range from -14.7 to -17.2. Using these values, one can predict a pH domain over which a 0.426 mM Ni^{2+} solution at $I = 0.1$ M would be unstable with respect to precipitation in the absence of complexing ligands. The calculated p_{cH} range is 7.24 to 8.48. The pH domain over which Ni^{2+} is expected to be removed from solution by adsorption processes is 6 to 8.5 (Vydra and Galba 1969, Richter and Theis 1978). Adsorption and precipitation are, therefore, potentially competitive removal mechanisms for nickel. Comparing the pH at which nickel is lost from solution in the presence and absence of silica will allow one to distinguish the operative process for nickel removal.

To test the applicability of the published values for K_{s0} in the system under study, solutions of $\text{Ni(ClO}_4)_2$ were titrated in the absence of a silica surface.

4.4.2 Results and Discussion

Solutions of 500 mL of $\text{Ni}(\text{ClO}_4)_2$ in 0.1 M NaClO_4 were titrated with 0.1 N NaOH under a N_2 atmosphere. Data from two titrations are presented in Figure 4.9. The measured concentration of Ni_T in LM10 was 0.357 mM. pH readings plotted were those taken after 5 to 6 minutes equilibration time. The titration curve possess two distinct regions. The initial, vertical, region is essentially a titration of water. The horizontal portion, which begins when the pH has increased to 8.6, describes the precipitation of the solid hydroxide phase. Most of the hydroxide ion added in this region is consumed by the precipitation process according to the reaction



Thus, the pH remains essentially constant during precipitation.

pH is plotted against time for selected additions of titrant in Figure 4.10 for titration LM10. The pH change was considerable after each perturbation during the precipitation process. An equilibrium state was not achieved after any of these additions.

Time-dependent pH readings are shown in a different manner in Figure 4.11. If one were to connect the points corresponding to equal time intervals, the family of curves thus generated would describe shifts in the titration curves with equilibration time. Two theoretical curves have been included in this figure. They were generated by SURFEQL, using the values for $c_{K_{s0}}$ indicated and the equilibrium constants for soluble nickel hydroxo-complexes listed in Table 4.2. The dashed line depicts a titration of active, freshly precipitated, $\text{Ni}(\text{OH})_2(\text{s})$ using a solubility product constant reported by Feitknecht and Hartmann (1954),

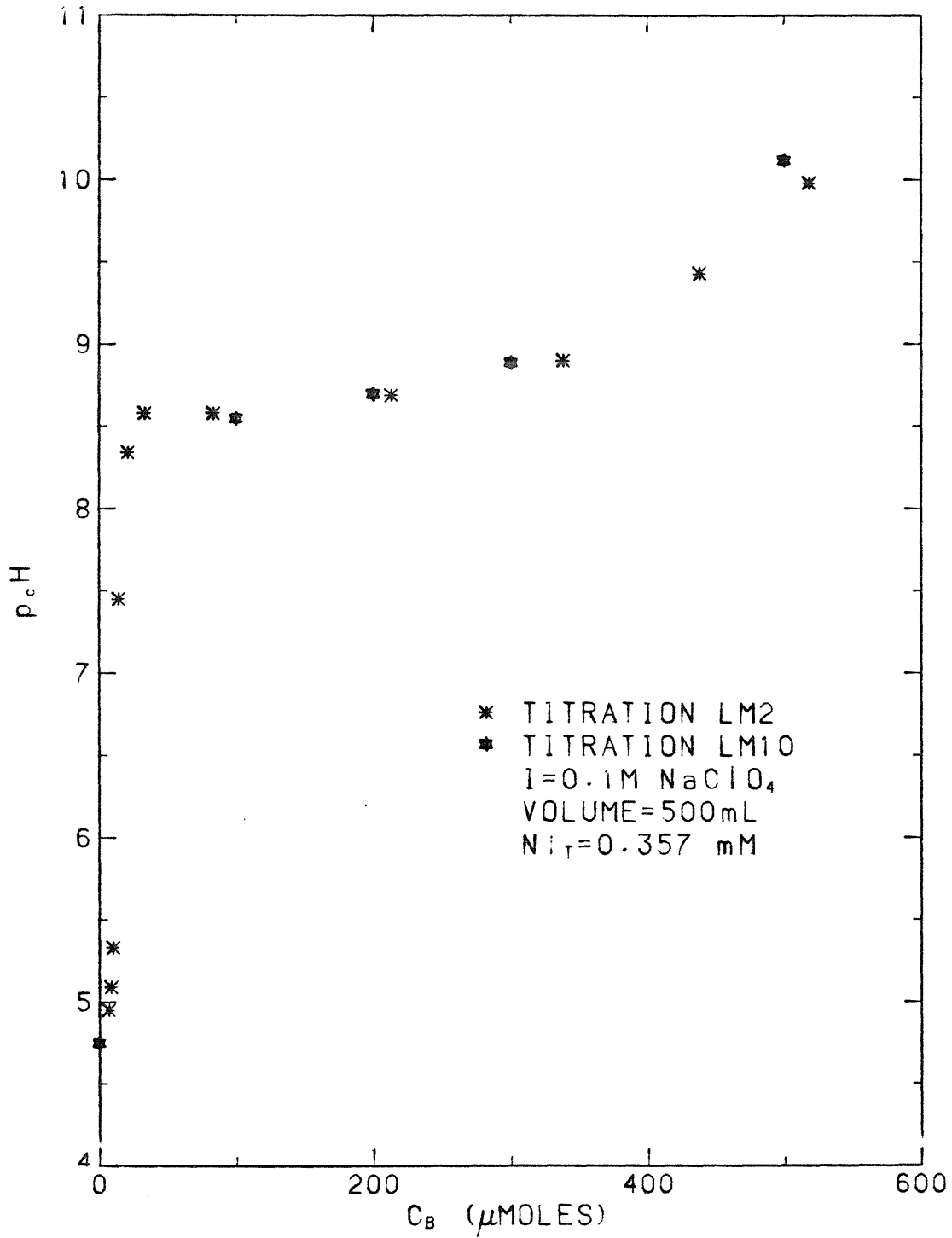


Figure 4.9 Titrations of 0.357 mM Ni(ClO₄)₂ in 0.1 M NaClO₄ with 0.1 N NaOH under N₂ in the absence of silica.

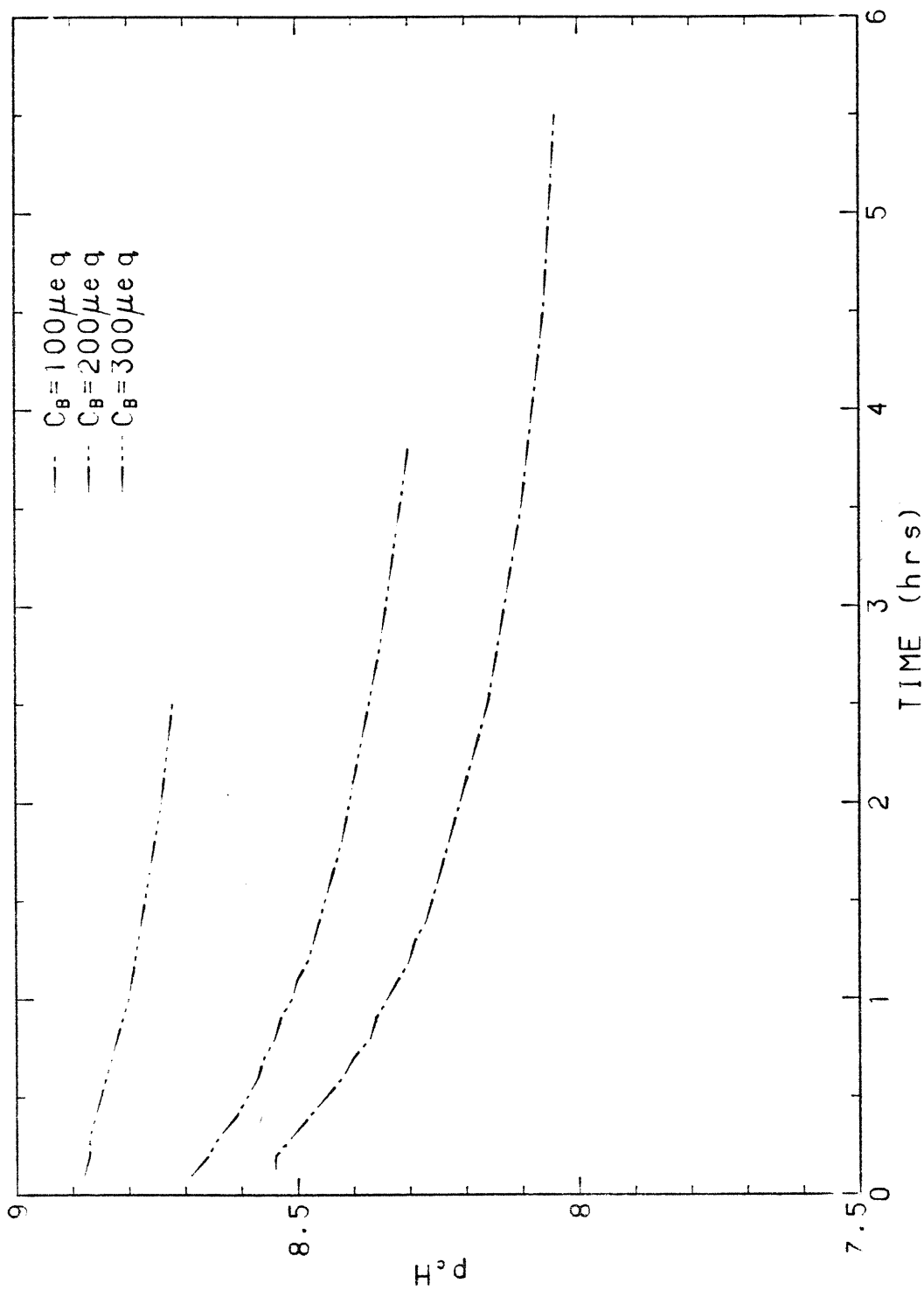


Figure 4.10 pH change with time is shown after selected additions of C_B during titration LM10. The values of C_B are cumulative.

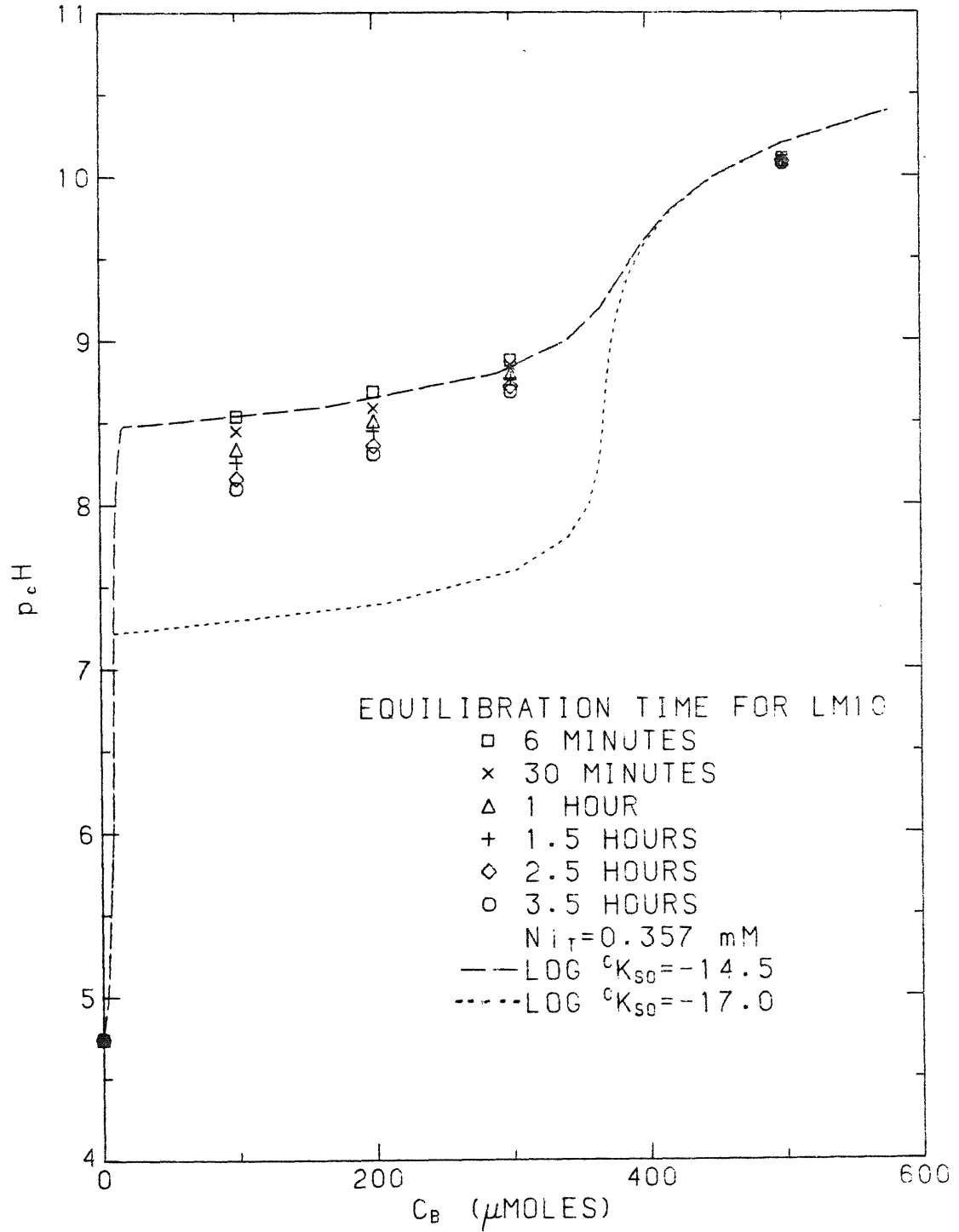


Figure 4.11 pH change with time is shown for each addition of C_B during titration LM10. The dashed line is a theoretical titration curve for a freshly precipitated $Ni(OH)_2(s)$ phase and the dotted line the titration curve for an aged solid.

Table 4.2

Solution equilibria for nickel hydroxo species
at 25°C, I = 0, from Smith and Martell (1976).

		<u>Log K</u>
* K_1	$\text{Ni}^{2+} + \text{H}_2\text{O} \rightleftharpoons \text{NiOH}^+ + \text{H}^+$	-9.9
* β_2	$\text{Ni}^{2+} + 2\text{H}_2\text{O} \rightleftharpoons \text{Ni(OH)}_2 + 2\text{H}^+$	-20.0
* β_3	$\text{Ni}^{2+} + 3\text{H}_2\text{O} \rightleftharpoons \text{Ni(OH)}_3^- + 3\text{H}^+$	-31.0
* β_{12}	$2\text{Ni}^{2+} + \text{H}_2\text{O} \rightleftharpoons \text{Ni}_2(\text{OH})^{3+} + \text{H}^+$	-10.7
* β_{44}	$4\text{Ni}^{2+} + 4\text{H}_2\text{O} \rightleftharpoons \text{Ni}_4(\text{OH})_4^{4+} + 4\text{H}^+$	-27.7

and the dotted line the titration of an aged solid whose constant has been reported by Gayer and Garrett (1949), Feitknecht and Hartmann (1954) and by Baes and Mesmer (1976). Although an equilibrium state was not attained in these experiments, the observed pH changes with time indicate this system is slowly approaching equilibrium. The final equilibrium state would seem to be consistent with the range of reported values for $\log K_{s0}$.

One could attempt to estimate a solubility product by extrapolating the curves in Figure 4.10 to larger times. The many factors which lead to a high probability of obtaining inaccurate results using data taken in the absence of stable equilibrium conditions have been described by Lewin (1964). A comparison of pH vs. time curves for this system and an adsorbed Ni(II) system will be adequate to differentiate between precipitation and adsorption. For this reason, a solubility product for nickel hydroxide will not be reported.

4.5 Adsorption Experiments

4.5.1 Adsorption Density Measurements

An adsorption isotherm was constructed in order to determine the maximum adsorption density, Γ_{\max} , of Ni(II) on a silica surface and the conditions under which it could be obtained.

No information could be found in the literature regarding measurements of Γ_{\max} in a Ni(II)-SiO₂ system. Coughlin and Matsui (1976) reported data which allows one to calculate the value of Γ_{\max} for a Mn(II)-SiO₂ system. At pH 8, 4.36 mM solutions of Mn²⁺ were equilibrated with 1 g/L suspensions of Cab-O-Sil EH-5, a 390 m²/g silica gel.

Langmuirian behavior was observed and Γ_{\max} was found to be 3.23 $\mu\text{moles}/\text{m}^2$.

4.5.1.1 Results

Adsorption density was determined experimentally by equilibrating successively higher added concentrations of Ni^{2+} with a fixed amount of silica. SiO_2 loading was 1.6 g/L. Experiments were run in the presence of atmospheric concentrations of CO_2 . Equilibration times were ten to twenty days.

Typically, pH was adjusted upwards to a value just less than that at which $\text{Ni}(\text{OH})_2(\text{s})$ was predicted to precipitate. The pH would fall during an overnight shaking process due to release of protons from the surface upon the binding of Ni^{2+} . pH measurements and adjustments were made daily until a value of 7.5 ± 0.2 was obtained after one day's equilibration. This value was chosen from analysis of similar batch experiments where pH was the independent variable (section 4.5.2.3).

Adsorption density, Γ in $\mu\text{moles}/\text{m}^2$, is plotted against total concentration of Ni^{2+} in Figure 4.12. Average values are shown for batch experiments conducted in triplicate. Some measurements from experiments conducted with a single sample are also included. The percentage of Ni_T removed from solution is greater than 93% in all but one case. At $\text{Ni}_T = 0.180$ mM, 14% of the Ni initially in solution remained at the end of the experiment. The maximum adsorption density observed was 9.8 $\mu\text{moles}/\text{m}^2$. This can be compared to the value for silanol group density of 8.3 $\mu\text{moles}/\text{m}^2$. At the highest nickel loading, 1.2 Ni^{2+} ions were lost from solution for each SiOH group present.

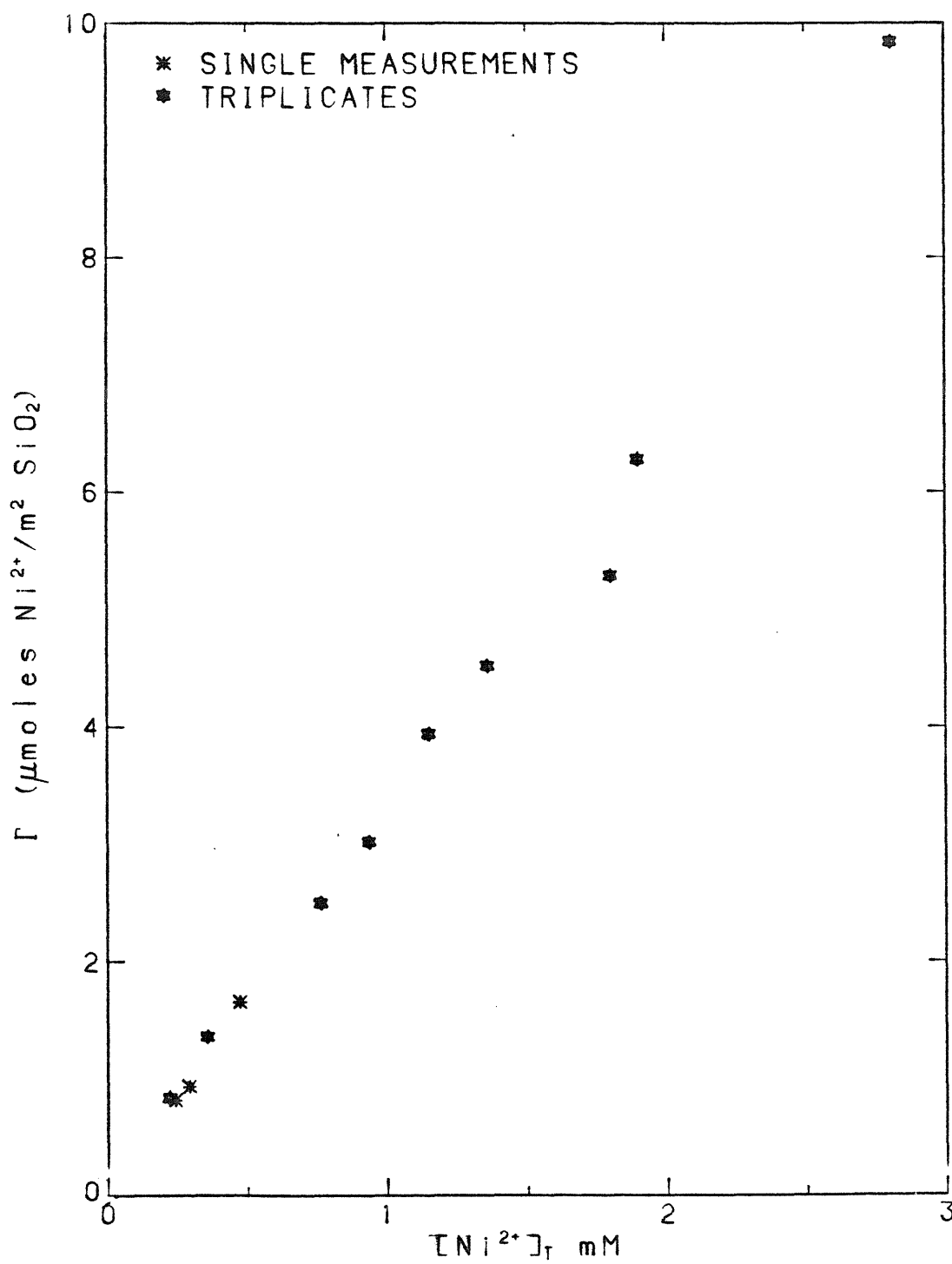


Figure 4.12 Adsorption density of Ni²⁺ on silica plotted against the total concentration of nickel present.

4.5.1.2 Discussion

A linear relationship between Γ and Ni(II)_{T} is evident in Figure 4.12. Such behavior over so great a range of Ni_{T} was not expected. Adsorption density calculations using the GCM or the TLM predict some maximum value for Γ as Ni_{T} is increased. It should be less than the density of silanol groups for monolayer adsorption (the actual value varying with the subset of possible surface complexes used in the modeling process). Upon observation of this trend, it was speculated that precipitation of the solid, Ni(OH)_2 , might be responsible for the large adsorption densities. Although considerable care was taken when adjusting the pH upwards, readings taken immediately after an addition of strong base would, at times, indicate the solubility product of $\text{Ni(OH)}_2(\text{s})$ had been momentarily exceeded. This condition never lasted for more than two minutes as the pH dropped rapidly after adjustment.

This set of experiments resulted in adsorption density measurements in excess of those reported by Coughlin and Matsui (1976) and those predicted by adsorption models. Precipitation of $\text{Ni(OH)}_2(\text{s})$ could not be conclusively ruled out as a removal mechanism for Ni(II) . In order to more precisely control the pH (allowing one to differentiate between adsorptive and precipitative removal mechanisms for Ni(II)), a titrimetric procedure was employed in future experiments. Ni_{T} and SiOH_{T} were lowered by an order of magnitude to increase the stability range of aqueous Ni(II) species.

4.5.2 pH dependence Studies

According to the literature, the adsorption edge for the

Ni(II) - SiO₂ system occurs somewhere between pH 2 and 8.5. No theory could predict such a wide range of pH values. The pH dependence of Ni²⁺ adsorption was investigated in this study using batch and titrimetric methods, in the presence and absence of CO₂. Values of ρ ranged from 0.038 to 2.0.

4.5.2.1 Previous Work on Nickel Adsorption on Silica

Literature references concerning the chemistry of the nickel-silica system are scarce and the information reported is sometimes contradictory. Vydra and Galba (1969) studied the adsorption of Co²⁺, Mn²⁺, Cu²⁺, Ni²⁺ and Zn²⁺. A chromatographic silica was prepared. The specific surface area was 310 m²/g, grain size was 0.15 to 20 μ m and pore diameter was 85 Å. Exchange capacity was reported as 1.90 meq/g. In batch experiments, 20 g/L suspensions were equilibrated for 2 to 3 hours with a 10⁻² M metal ion solution. Analysis was performed on the centrates and adsorption was calculated by difference. pH was controlled by acetate and borate buffer solutions. The adsorption edge was found to lie between pH 6 and 7 for Co²⁺, Mn²⁺, and Ni²⁺. They also found 0.74 protons released per Ni²⁺ adsorbed over the pH range 6.3 to 6.8. Adsorption of the hydrolysis product, NiOH⁺, was postulated.

Isaeva and Presnyakova (1973), working with an activated silica gel at 5 mg Si/mL concentration and a nickel chloride solution of 8.5 x 10⁻⁶ M concentration, reported attainment of equilibrium after 7 days. In solutions with no supporting electrolyte, adsorption began at pH 2 and approached 100% at pH 7. In 0.57 M NaCl, adsorption again began at pH 2 but after reaching 50% at pH 4 decreased to zero by pH 5. No further

adsorption was observed as the pH was increased to 7.

Taniguchi et al. (1973) reported a value of 1.9 for the ratio of protons released per Ni^{2+} adsorbed at a pH of 8.0.

Richter and Theis (1978) used an amorphous commercial grade silica with a specific surface area of $1.7 \text{ m}^2/\text{g}$. Ni^{2+} solutions, initially $1.7 \times 10^{-5} \text{ M}$, were equilibrated with $50 \text{ m}^2/\text{L}$ of silica. The adsorption edge was shown to be at pH 8 to 8.5; NiOH^+ was again postulated as the adsorbing species.

4.5.2.2 Prediction of the pH dependence of Nickel Adsorption on Silica

Schindler et al. (1976) studied the adsorption behavior of Fe^{2+} , Cu^{2+} , Cd^{2+} and Pb^{2+} on Aerosil 200 in 1 M NaClO_4 . They found linear correlations between the first and second hydrolysis constants of the metal ions in solution, *K_1 and $^*\beta_2$, and the corresponding constants for monodentate and bidentate surface complexes, $^*K_1^s$ and $^*\beta_2^s$. Values for the hydrolysis constants of Ni^{2+} are known, and allow one to estimate values for the surface constants. A prediction of the adsorptive behavior of Ni^{2+} on silica was made using these constants in the constant capacitance model. The system modeled has the following properties: $0.167 \text{ mM Ni(ClO}_4)_2$, 1.0 M NaClO_4 , 50 g/L SiO_2 , surface area = $160 \text{ m}^2/\text{g}$, hence 72.5 mM SiOH and $C_1 = 1.25 \text{ F/m}^2$. These conditions are those under which the data would have been taken if Schindler et al. had studied Ni^{2+} . Estimates from the correlations of Schindler et al. provided values of $\log ^*K_1^s = -6.58$ and $\log ^*\beta_2^s = -11.78$ for nickel surface complexes. Modeling was done neglecting electros-

tatic corrections for the surface complexes of Ni^{2+} , as Schindler et al. determined the constants by assuming $\psi_0 = 0$. Results are presented in Figure 4.13. Adsorption is predicted to begin at pH 6 and to approach 100% at pH 8.

Values of ρ in all of these studies of metal ion adsorption were less than one and ranged from 0.0023 in the work of Schindler et al. (1976) to 0.26 in the study of Vydra and Galba (1969).

4.5.2.3 Batch Experiments

Results of the batch experiments are shown in Figure 4.14(abc). Three sets of data are presented. All of the MG series were equilibrated for 1 day and the SiO_2 loading was 1.6 g/L. Experiments MG2 to MG6 (Figure 4.14a) were conducted under N_2 with $\rho = 0.038$ while MG9 and MG10 (Figure 4.14b) were equilibrated with atmospheric concentrations of CO_2 at $\rho = 0.11$. AH6 (Figure 4.14c) was again performed under N_2 at a ρ value of 0.20, with a three week equilibration time. The data indicate the adsorption edge lies between pH 6 and 7. There is no significant trend with respect to surface loading, equilibration time, or the presence of CO_2 . Measured concentrations of Ni^{2+} correlated well with the amount of base added, (increased additions of base produced decreased values of nickel in solution) while pH values did not. Scatter in the data is due largely to pH-measurement difficulties in these poorly buffered suspensions. These experiments were made to determine a pH value at which batch adsorption density experiments could be conducted. The pH value sought was one high enough so as to yield quantitative adsorption of nickel ion from solution but low enough to

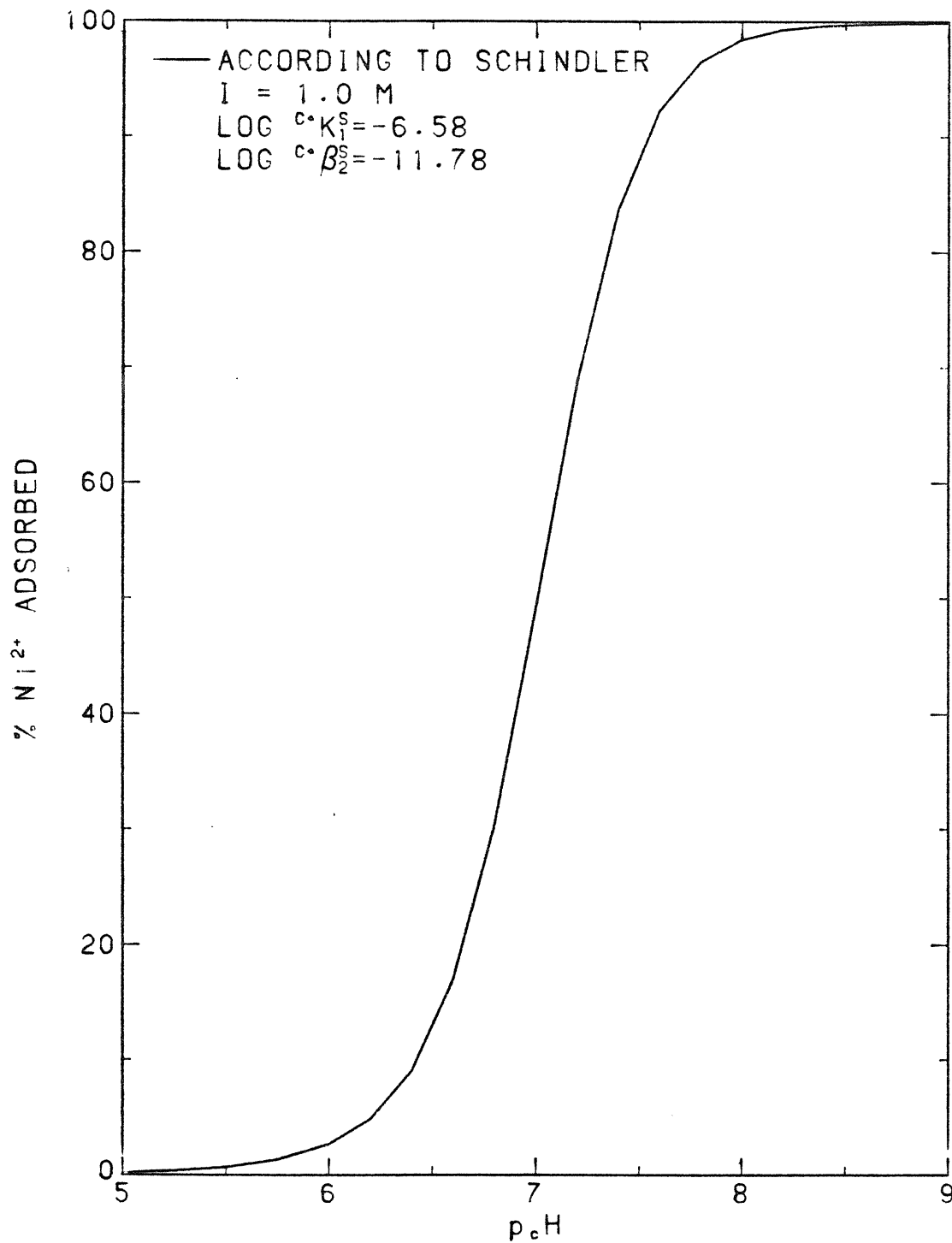


Figure 4.13 Predicted behavior of Ni²⁺ adsorbing onto silica at $\rho = 0.0023$. The CCM was used without correcting the surface complexation constants for electrostatic effects.

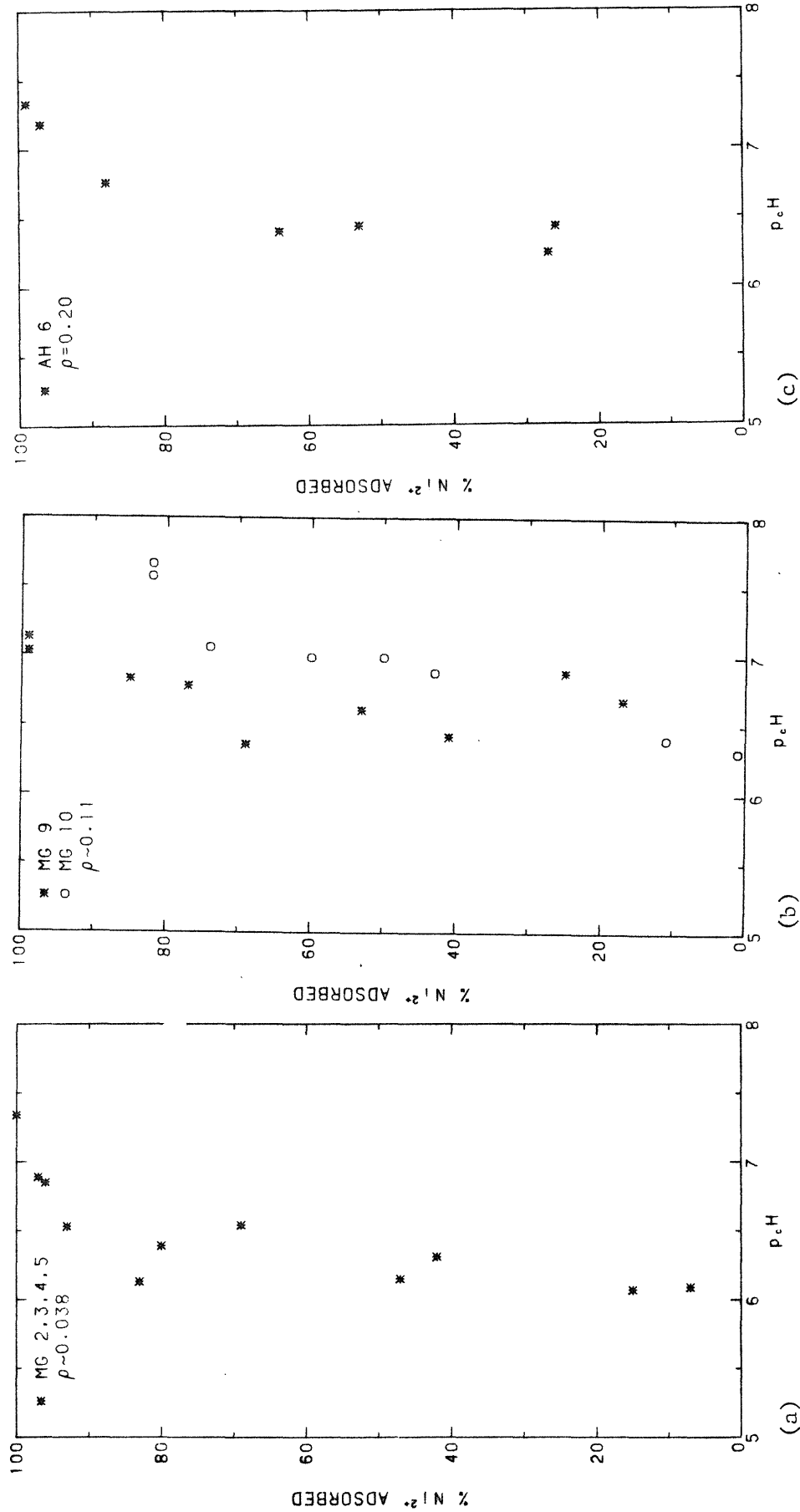


Figure 4.14 pH-dependence of Ni^{2+} adsorbing on silica as determined by batch experiments. SiO_2 loading 1.6 g/L. $I = 0.1 \text{ M NaClO}_4$. Data in 4.14b were taken under a CO_2/N_2 atmosphere.

avoid precipitating a solid hydroxide phase. These data coupled with the results from the nickel hydroxide solubility study suggested a pH value of 7.5 would satisfy these requirements.

4.5.2.4 Titrations

pH-dependent behavior was also tested with titrimetric procedures. Certain advantages were realized. pH control was more precise. Information about kinetic processes was obtainable. Chances of precipitating $\text{Ni}(\text{OH})_2(\text{s})$ after base additions were eliminated. Proton stoichiometry of the adsorption reactions could be investigated. Back titrations could provide evidence to assess the degree of reversibility.

4.5.2.4.1 Results

Surface titrations LM6 and LM15, and a back-titration LM7, are shown in Figure 4.15. In each, 5 mLs of a 42.6 mM $\text{Ni}(\text{ClO}_4)_2$ solution was added to 500 mLs of a 0.16 g/L suspension of Aerosil 200. Final system concentrations were designed to be 0.426 mM Ni^{2+} and 0.24 mM SiOH , giving a value of $\rho = 1.8$. Initial measurements of Ni_T were 0.406 and 0.470 mM for LM6 and LM15, respectively. Dilution errors are suspected to have caused the differences in measured values of Ni_T . The solid silica phase in LM15 was equilibrated with the aqueous phase for 2 days at pH 8.0 to 8.5 before returning to pH 4 for the addition of Ni^{2+} . This equilibration procedure was not used in LM6. In both titrations, the suspension was equilibrated for 2 hours after addition of Ni^{2+} and titrated with 0.1 N NaOH under N_2 . The back titration, LM7, was a continuation of LM6. All conditions remained the same except that 0.1 N HClO_4 was used in place of 0.1 N NaOH as the titrant.

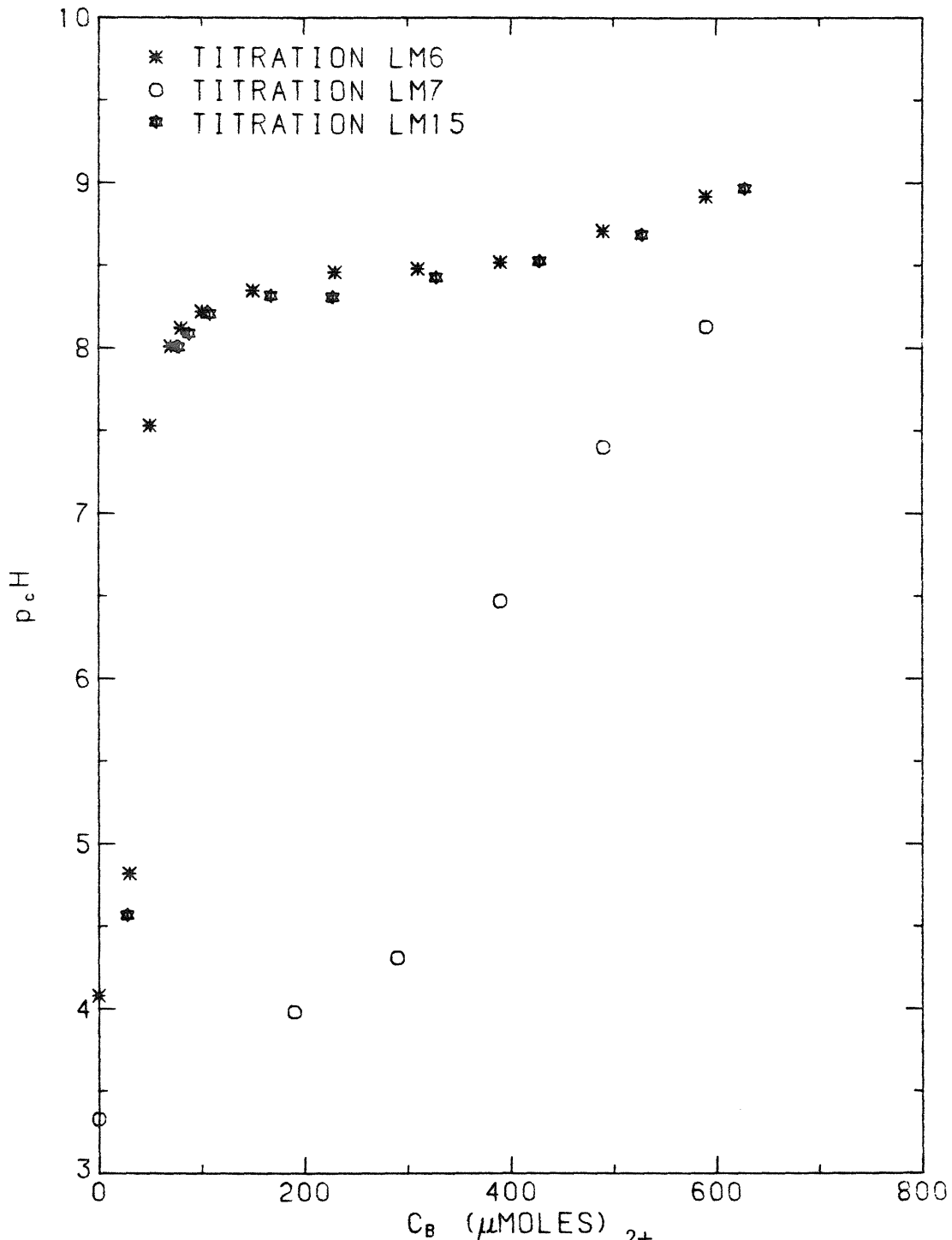
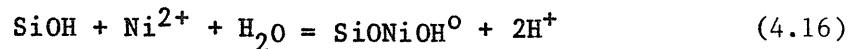
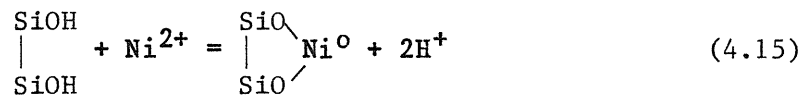
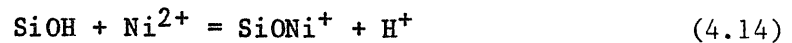


Figure 4.15 Forward and back titrations of Ni^{2+} in the presence of an 0.16 g/L suspension of silica. 500 mL suspensions were titrated with 0.1 N C_A and C_B . $\rho = 1.7$ for LM6 and 2.0 for LM15. $I = 0.1 \text{ M NaClO}_4$.

The features of the forward titration curve are very similar to those described for the titration of nickel without silica; the curve rises steeply and then becomes nearly horizontal between pH 8 and 8.5. Measured nickel concentrations decrease in the horizontal region as C_B is added. Formation of surface complexes as discussed in Chapter 2 will release protons to solution as shown here



Upon the onset of adsorption, base added to the system will be neutralized by the protons released during the adsorption processes with little or no resultant pH change. It is therefore reasonable to observe titration curves with similar shapes for both adsorption and precipitation reactions.

Removal of nickel from solution in the presence of silica is seen to be irreversible on a time scale of days. The back titration curve would lie atop the curve for the forward titration if the removal process was reversible. Not only has the curve been displaced to a lower pH but it has a significantly different shape. The initial pH reading of LM7, 8.13, represents a drop of 0.79 pH unit from the final measurement of LM6 over a period of four days. pH values plotted were those recorded after 24 hours. Much longer times were necessary to approach equilibrium than were observed for the forward titrations (Figure 4.16). An example of the pH data vs. time for LM7 at $C_B = 190 \mu\text{eq}$ is shown

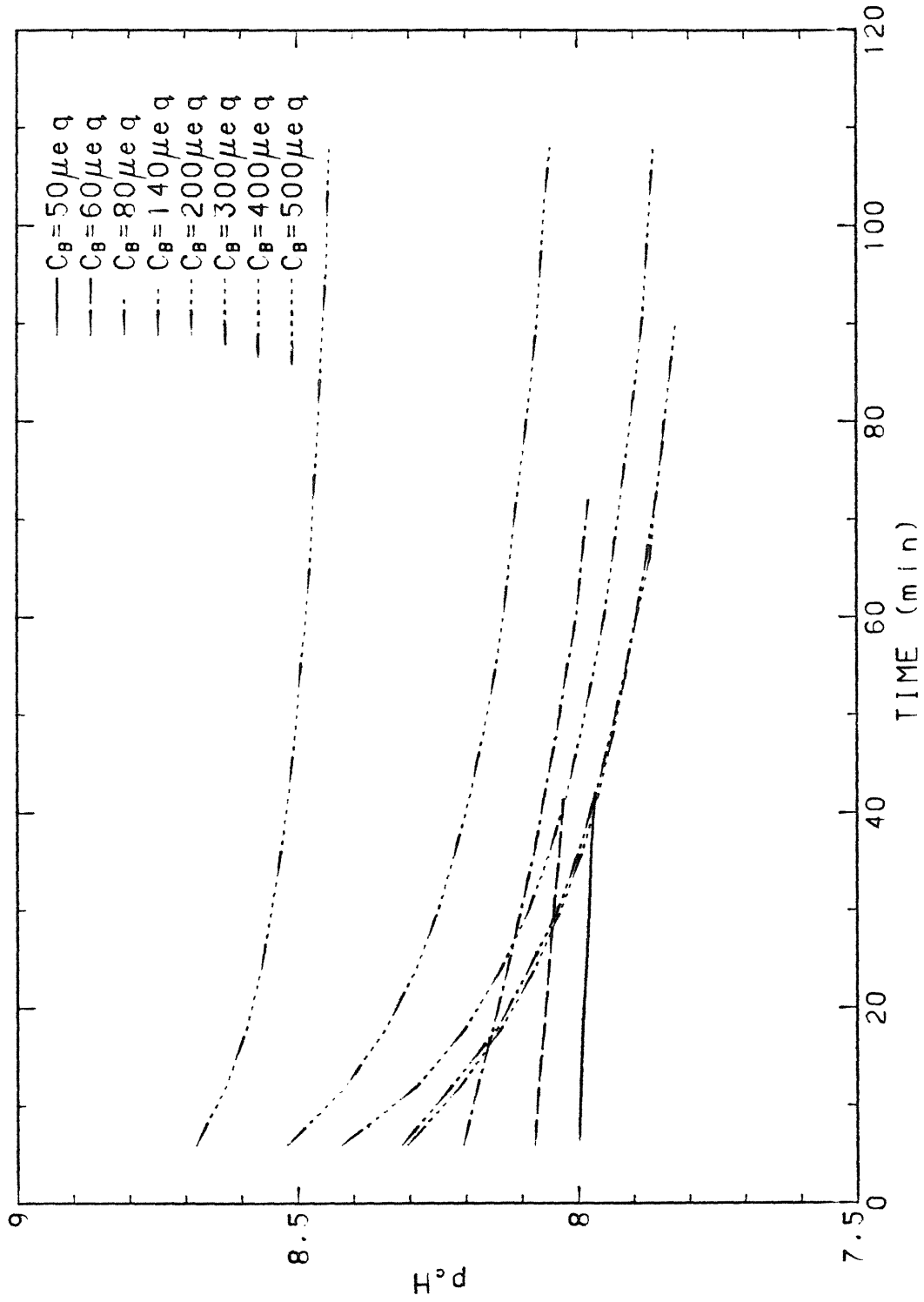


Figure 4.16 pH change as a function of time for each addition of titrant in titration LM15.

here.

P _c H	Time (hrs)
3.63	0.1
3.98	24
4.56	48
5.89	72
6.11	96

Thirty-one days after the end of this titration 10% of the Ni_T was still bound to the silica.

True equilibrium was never reached after additions of strong base. A quasi-stationary state, defined as $\Delta\text{pH}/\Delta t$ less than 0.3 mv/min, was achieved within 10 minutes during the the initial phase of the titration. Continued monitoring revealed a reproduceable pH change of 0.05 mv/min which continued for up to 2 hours. A different pH behavior with time was noticed during the adsorptive process, represented by the horizontal plateau of the titration curve. Here, 45 minutes to 1 hour was necessary to reach the quasi-stationary state and another hour to approach a change rate of 0.1 mv/min. The data plotted in Figure 4.15 for titrations LM6 and LM15 were obtained 5 to 6 minutes after base additions to allow for pH variations due to mixing processes.

pH is plotted against time, for successive additions of C_B in Figure 4.16 for LM15, a more extensively sampled replicate of LM6. pH values before 6 minutes time have been excluded to allow for variable readings due to inadequate mixing. Data for C_B = 50 and 60 μeq are linear with time and have a slope close to 0 while pH values for C_B = 140, 200, 300, 400, and 500 μeq decrease asymptotically towards some equilibrium value. Data at C_B = 80 μeq appear to be in an intermediate regime. This figure can be compared to the analogous figure from the

nickel hydroxide precipitation experiments (Figure 4.10). Experimental conditions are essentially the same but for the presence of a solid phase in these experiments. At C_B values of 200 and 300 μeq direct comparisons have been made (Figure 4.17). The p_c^H at which nickel is removed from solution is significantly lower in the presence of silica. The pH difference is not smaller than 0.4 pH units over the time scale of the experiment.

The ratio of protons released per nickel ion removed, \bar{n} , was calculated for that region of the titration curve where additions of C_B produced decreases in dissolved nickel. After accounting for the protons necessary to titrate soluble silica species and silanol groups, the value of \bar{n} was determined to be 1.9 ± 0.2 (mean \pm standard error for four measurements).

When surface complexes are formed, 1 proton released per Ni^{2+} bound would indicate the presence of monodentate surface species while a ratio of 2 would point to either hydrolyzed or bidentate species. Surface species in which three or more surface groups are bound to a single metal ion are generally not considered for steric reasons. These facts suggest that bidentate or hydrolyzed species predominate in this system.

During the course of titration LM15, aliquots were taken, filtered and acidified for subsequent analysis for dissolved Ni(II) by atomic absorption spectrophotometry. Samples were taken every 20 minutes after most titrant additions. A way to visualize these changes in conjunction with the simultaneously varying pH is exhibited in Figure 4.18. A set of curves displays the adsorption edge as it moves with time. Each of the groups of data are associated with an addition of titrant. If the

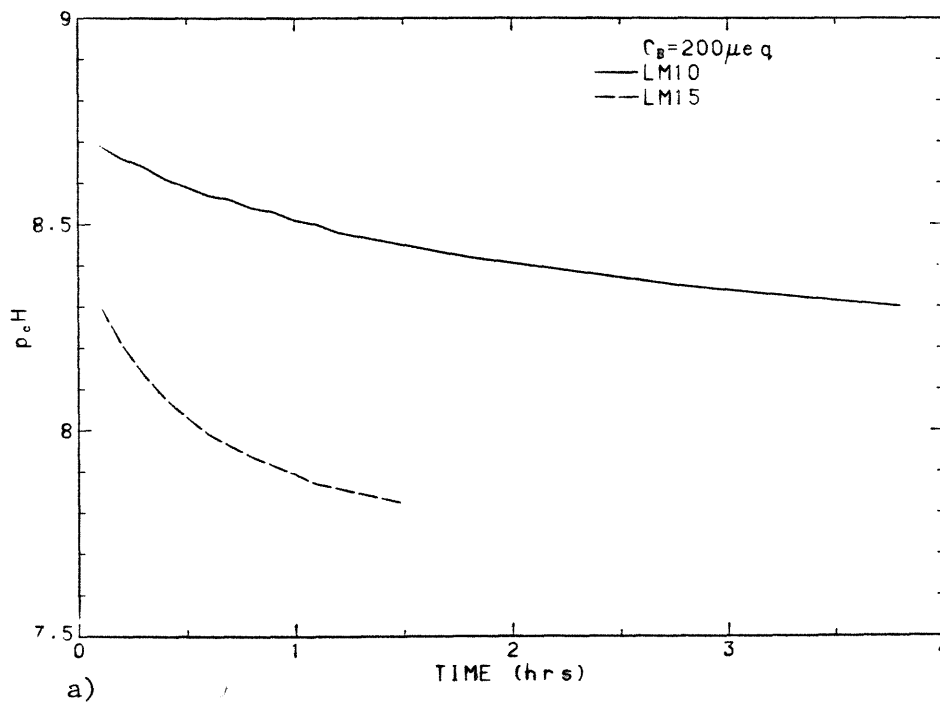
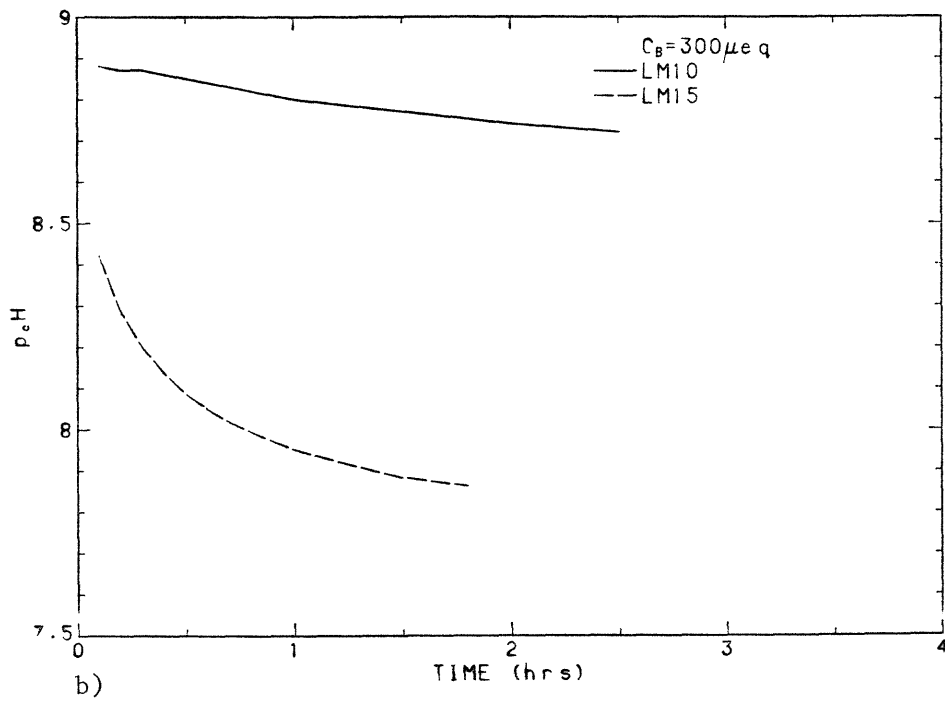


Figure 4.17 Direct comparisons of pH vs. time curves for titrations of nickel in the presence of silica (LM15) and in the absence of silica (LM10) at C_B total of 200 μeq (4.7a) and 300 μeq (4.17b).

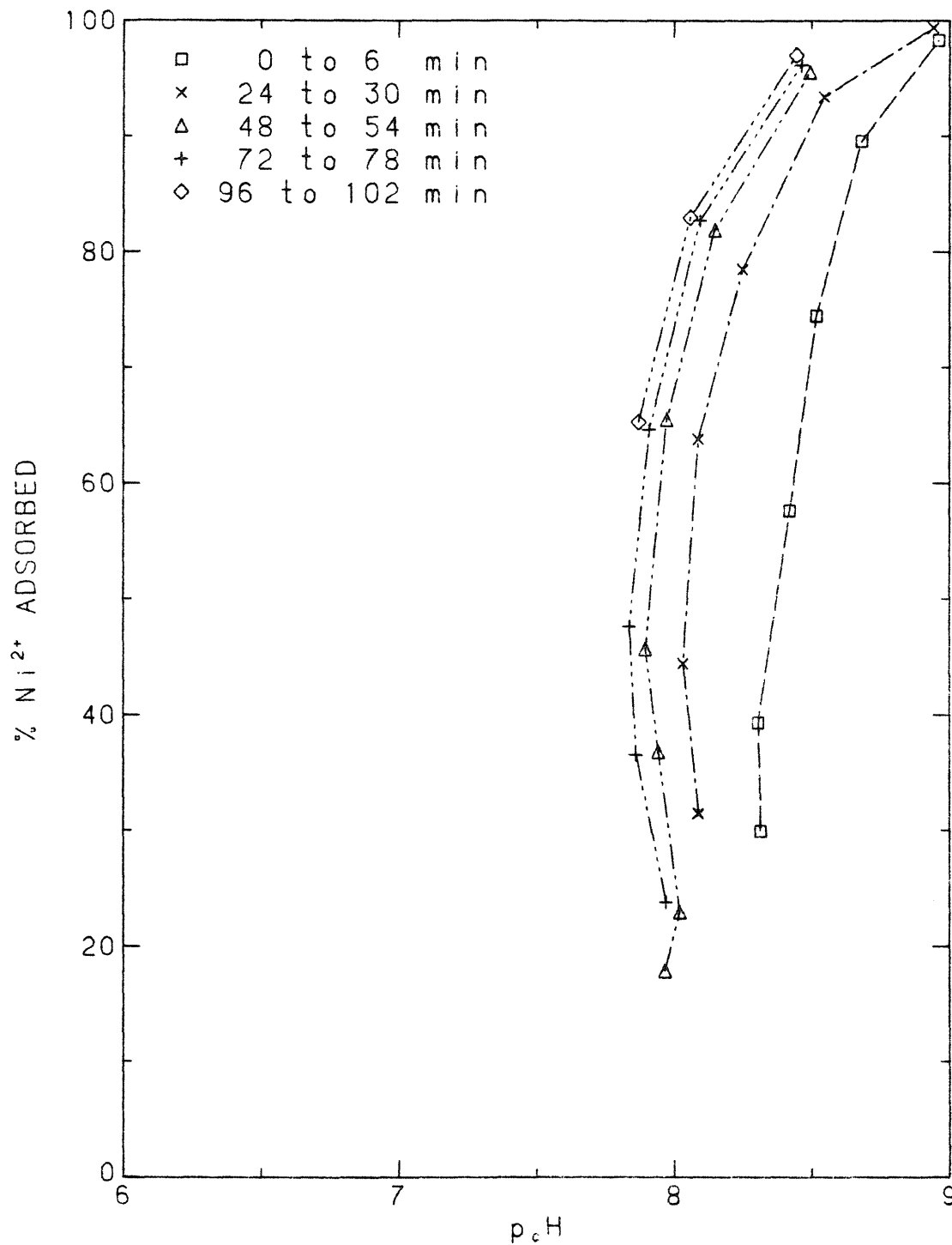


Figure 4.18 Percent adsorption calculations for titration LM15 at the equilibrium times shown.

rate at which the adsorption edge moves continues to decline in the observed manner, 96 to 102 minutes of equilibration time, after a perturbation by the addition of strong base, would produce data very similar to that obtainable at true equilibrium.

For the five additions after which sampling was continued for nearly two hours, one can calculate the percent Ni^{2+} removed with respect to the total Ni^{2+} removed at the end of the equilibration time. These numbers are presented in Table 4.3. Approximately 50% of the total nickel removed after each addition of base was removed within 6 minutes and 90% or more was removed within one hour. These observations agree well with other data from this laboratory (Vuceta 1976 and Sung 1981) and with the consensus of published data which addresses the kinetics of metal ion removal by adsorption processes.

The adsorption edge, as defined by this titrimetric procedure, occurs at a pH near 8 after two hours equilibration time. Longer equilibration times would undoubtedly lead to slightly lower values.

4.5.2.4.2 Discussion

The adsorption edge has moved to a higher pH value under the conditions of the adsorption titrations than that observed for the batch experiments. Longer equilibration times would have shifted the adsorption edge to lower pH's in the adsorption titrations. However, the kinetic data indicate that this lack of equilibrium conditions is insufficient to account for the additional one pH unit difference. The two experiments are not necessarily comparable though. A significant change in the parameter ρ has occurred. Batch experiments

Table 4.3

Percent nickel removed by adsorption
processes as a function of time.

cumulative C_B (μeq)	Time (min)				
	0 to 6	24 to 30	48 to 54	72 to 78	96 to 102
140	47	60	100	100	--
200	25	72	82	100	--
300	55	92	100	97	100
400	50	74	94	98	100
500	46	70	88	94	100

were performed on systems with values of ρ less than one while titrations were carried out with ρ greater than one. James and Healy (1972a), working with Co^{2+} adsorbing on silica, and Benjamin and Leckie (1980), investigating a variety of metals adsorbed on amorphous iron oxyhydroxide, have observed that the adsorption edge will move to higher pH's as the ratio of metal to surface increases. This phenomenon is in agreement with the observed behavior for nickel adsorbed on silica.

It was expected that in systems where ρ was greater than one an adsorption maximum would result from a depletion of available binding sites. Possible explanations for the absence of this behavior include: i) the existence of binding sites in internal structures, micropores or gel-like layers; ii) precipitation of a less-soluble hydroxide phase on the silica surface; iii) the creation of additional binding sites as adsorption proceeds (multilayer adsorption). These explanations are discussed below.

i) Existence of binding sites in internal structures, micropores or gel-like layers

Silanol groups are found within the pores of silicas, in intraskeletal structures and within gel-like layers which form on the surface of some silicas. Each situation is considered with respect to the nonporous, amorphous, pyrogenic silica used in these experiments.

Nonporous is a common adjective seen in the literature to describe pyrogenic silicas. Barby (1976) presents an extensive review of the structure of various silicas whose particle diameters range from Å's to mm's. When aerosil has been hydroxylated by immersion in water and

redried to a xerogel form he concludes, "There is little microporosity in such gels . . . Indeed, microporosity cannot be expected."

The lack of internal hydroxyl groups is demonstrated by Kiselev (1971). Infrared spectra of deuterium-exchanged aerosils with differing specific surface areas show a successive decrease in the fraction of intra-skeleton OH groups as specific surface area increases. A spectrum of aerosil with a specific surface area of $165 \text{ m}^2/\text{g}$, indicates intra-skeletal hydroxyl groups represent a vanishingly small fraction of the total silanol groups at this relatively large surface to volume ratio.

Questions concerning the presence of gel-like layers on the surface of silica have been frequently discussed in the literature. Development of a loosely-structured amorphous region, through dissolution and reprecipitation, may give rise to silanol groups within this structure in addition to those already on the surface. Those who put forth such ideas, Tadros and Lyklema (1968), Perram et al. (1974), and Yates and Healy (1976) do so in support of alkalimetric titrations of porous precipitated silicas which produced values of surface charge that are large when compared to other forms of silica.

Yates and Healy (1976) investigated BDH precipitated silica. When the silica was heat treated at 500°C , the calculated surface charge values were lower than those obtained using the untreated silica. They concluded that, as opposed to untreated precipitated silica, there is no evidence for gel layers on heated treated precipitated or pyrogenic silicas. Smit et al. (1978) conducted experiments designed to measure the penetration depth of counter ions adsorbed on vitreous silica, which is closer in nature to pyrogenic silica than to precipitated silica. At pH

10, specifically adsorbed sodium ion was completely removed with one etching in 1.5 M HF. The etching was calculated to remove a layer of silica 0.3 nm thickness. The diffusion of sodium ion out of a gel layer 2.0 nm in thickness as postulated by Perram et al. (1974) inadequately described the data. A site binding model proposed by Yates et al. (1974) where specific surface sites were postulated to interact with potential determining ions and counter ions forming surface ion pairs was judged a more appropriate description of the surface of nonporous silica.

The weight of evidence supports the conclusion that pyrogenic silicas are nonporous and contain few, if any, internal silanol groups accessible to protons or counter ions. Neither do they have a surface gel-layer located at the surface, as do precipitated silicas. Explanations for the large adsorption densities of Ni(II) on pyrogenic silica must exclude the existence of an accessible reservoir of silanol groups in addition to those on the surface.

ii) Precipitation of a less-soluble hydroxide phase in the presence of a surface

The idea that the solubility of a metal hydroxide solid phase will be decreased when the precipitate is formed on or near a surface has appeared in the literature previously. James and Healy (1972b) performed detailed electrophoretic studies on a Co(II)-SiO₂ system. Charge reversals on the surface were described as a function of pH and metal to surface ratios. A model was postulated to describe the (+/-) charge reversal associated with the formation, on the surface, of a Co(OH)₂ solid phase. The contribution to the standard free energy due to the

presence of an electric field, G' , was calculated for the individual species involved in the precipitation reaction at the surface. The important result was that G'_i is a function of the square of the valence of species i . Thus, it is positive for both anions and cations. The value of the corrected solubility product would always be less than its value in the absence of a surface.

One can, to first order, also calculate the effect of the electric potential on the activity of any species using the electrical double layer framework developed in Chapter 2. The true equilibrium constant for the solubility product of nickel hydroxide in bulk solution is expressed in terms of activities,

$$K_{s0} = (a_{Ni^{2+}})(a_{OH^-})^2 \quad (4.17)$$

The chemical potential of species i in bulk solution, μ_i is defined by

$$\mu_i = \mu_i^{\circ} + RT \ln a_i \quad (4.18)$$

where μ_i° is the standard state chemical potential. a_i defined in terms of chemical potentials is then

$$a_i = \exp\left(\frac{\mu_i - \mu_i^{\circ}}{RT}\right) \quad (4.19)$$

The electrochemical potential of species i at position x , $\bar{\mu}_{ix}$, where the electric potential is ψ_x , is defined by

$$\bar{\mu}_{ix} = \mu_i^{\circ} + RT \ln a_{ix} + n_i F \psi_x \quad (4.20)$$

which can be rearranged to give

$$a_{ix} = \exp\left(\frac{\bar{\mu}_{ix} - \mu_i^{\circ} - n_i F \psi_x}{RT}\right) \quad (4.21)$$

or

$$a_{ix} = A_{ix} \exp(-n_i z_x) \quad (4.22)$$

where

$$A_{ix} = \exp\left(\frac{\bar{\mu}_{ix} - \mu_i^o}{RT}\right) \quad (4.23)$$

and

$$z_x = \frac{F\psi_x}{RT} \quad (4.24)$$

At equilibrium,

$$\bar{\mu}_{ix} = \mu_i \quad (4.25)$$

that is, the electrochemical potential is the same everywhere. In particular, the chemical potential in bulk solution is equal to the electrochemical potential at any position. Thus,

$$a_i = A_{ix} \quad (4.26)$$

Substituting for A_{ix} in equation 4.22 gives

$$a_{ix} = a_i \exp(-n_i z_x) \quad (4.27)$$

The solubility product expression can now be formulated with the effects of the surface potential on the activity of the species included. Substituting 4.27 into 4.17

$$K_{s0} = [(a_{Ni^{2+}_x}) \exp(-2z_x)] [(a_{OH^-_x}) \exp(z_x)]^2 \quad (4.28)$$

$$K_{s0} = (a_{Ni^{2+}_x}) (a_{OH^-_x})^2 \quad (4.29)$$

$$K_{s0} = (a_{\text{Ni}^{2+}})(a_{\text{OH}^-})^2 \quad (4.30)$$

The resulting equation shows that an electric potential has no net effect on the solubility product. The contributions to the electrochemical potential are equal and opposite for ions of opposite charge.

The theoretical treatment of James and Healy (1972b) followed from a model developed to describe the "specific" adsorption of ions on metals from aqueous solutions by Anderson and Bockris (1964). They found that super-equivalent adsorption onto metal surfaces could be described by a non-chemibonding model. Contributions to the standard free energy changes were calculated for several physical processes. Evidence was presented that surface bonds were not covalent. The applicability of this purely physical model to a chemical system must be inadequate. The equivalence of corrections to free energy terms, for the effects of an electric field, on both positively and negatively charged species is counter-intuitive. The chemical approach described above seems more reasonable and so, without additional evidence to the contrary, the solubility product of $\text{Ni}(\text{OH})_2(\text{s})$ will be taken to remain unchanged in the presence of a surface.

iii) Multilayer adsorption

Isothermal analysis often provides useful information about the adsorption process. The Langmuir and BET isotherms will be examined briefly.

Monolayer adsorption onto a fixed number of equivalent sites with no exchange of adsorbate between sites is described by the Langmuir isotherm. A BET isotherm assumes a number of Langmuirian layers of

adsorbate molecules can form at the surface. Adsorption density, Γ , plotted against the concentration of adsorbate with which the solid was equilibrated, will produce the curves shown in Figure 4.19. for the two models. Comparing the Langmuir curve to Figure 4.12. could lead one, without further information, to the conclusion that the adsorption data might be described by the initial linear part of a Langmuir isotherm where Γ is less than Γ_{\max} . The problem with this interpretation is that the experimental values of Γ have already exceeded the value of Γ_{\max} for a 1:1 complex of nickel with surface groups by 18%. Agreement with the BET isotherm would be indicated by a linear plot of $(C/(C_s - C)) \Gamma$ vs. C/C_s where C is the adsorbate concentration initially in solution and C_s is its saturation concentration in solution. Figure 4.20 indicates this model does not fit the data.

Isothermal analysis has shown that adsorption of nickel on silica has exceeded monolayer coverage, yet cannot be described by the BET model for multilayer adsorption.

The CCM and the TLM, although not capable of describing multilayer adsorption per se, can be useful in trying to understand the phenomenological data on nickel adsorption. A system where new adsorption centers are generated at the locations of adsorbed nickel ions will be investigated. Adsorption centers would not be depleted but rather regenerated as the adsorption process proceeds.

It was postulated, using the proton release data, that hydrolyzed or bidentate surface species were preferentially formed during the adsorption process. The hydrolyzed species is particularly well suited to serve as a new adsorption center. Considering the following two

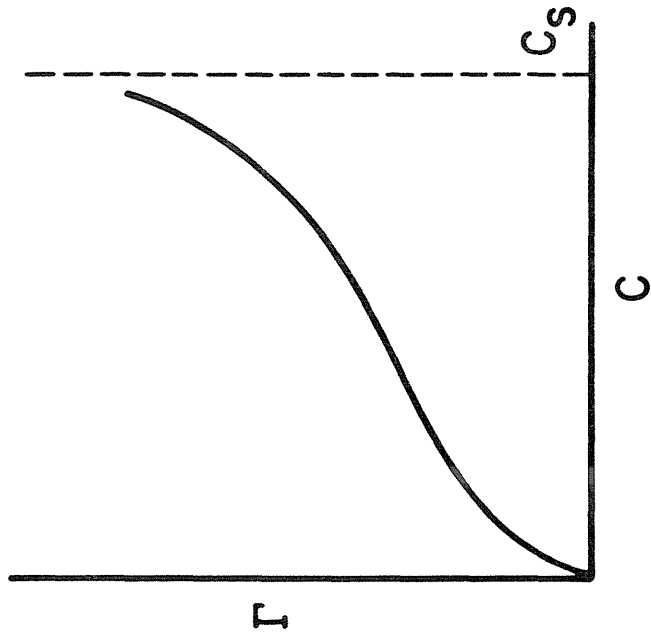
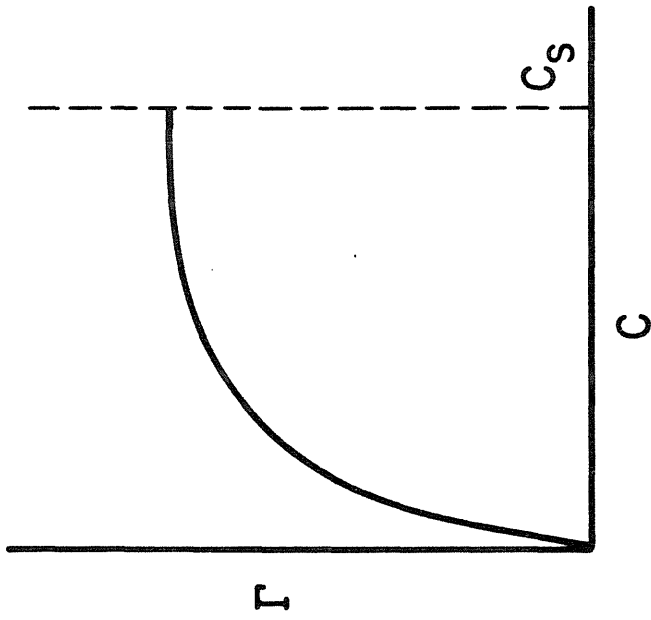
**a. LANGMUIR****b. BET**

Figure 4.19 Plots of adsorption density Γ versus the total concentration of adsorbate for Langmuir (a) and BET (b) isotherms.

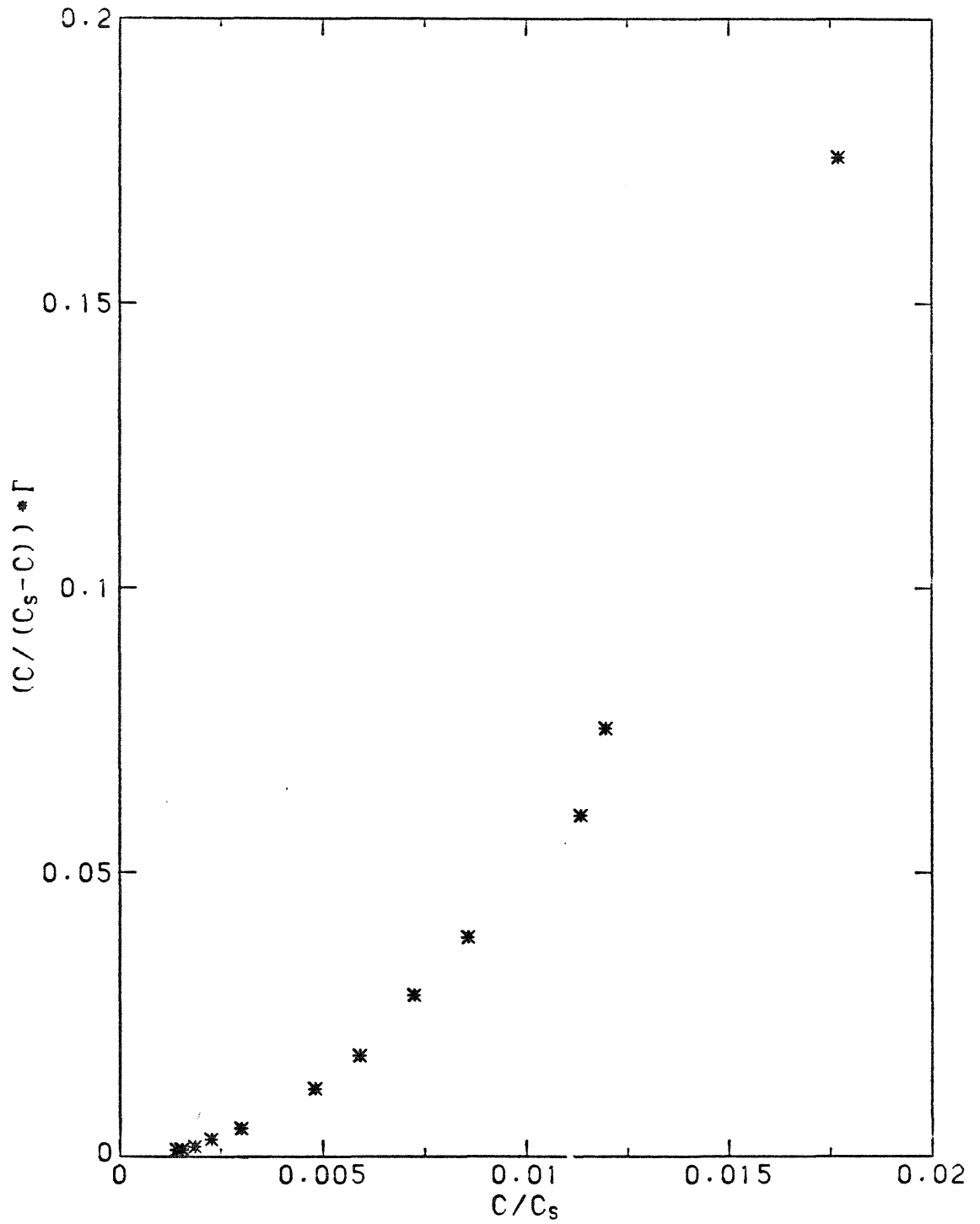
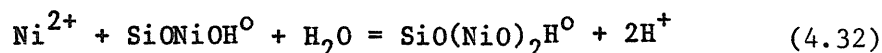
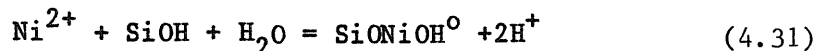
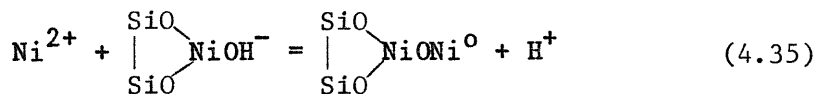
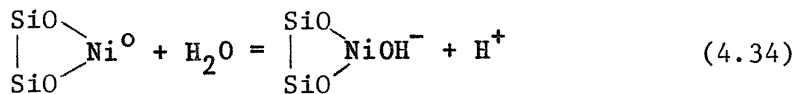
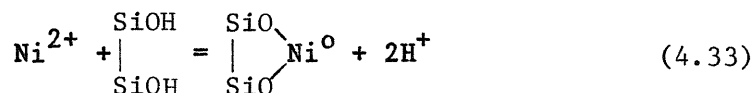


Figure 4.20 Linearized BET plot of adsorption data from Figure 4.12.

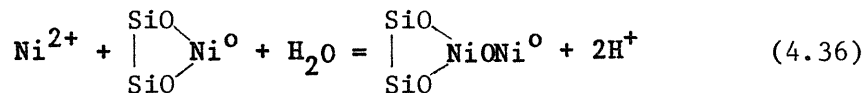
reactions,



one can see similarities in the interactions between Ni^{2+} and SiOH and Ni^{2+} and SiONiOH° : both consume a surface site while producing a new surface site (NiOH), and release two protons for each nickel ion bound. Analogous reactions can be written when bidentate surface complexes are considered.



The chemistry is different for the bidentate species. Although combining reactions 4.34 and 4.35 produces a net reaction very similar to 4.32,



the intermediate surface species, $\begin{array}{c} \text{SiO} \\ \diagdown \\ \text{NiOH}^{-} \\ \diagup \\ \text{SiO} \end{array}$, and in particular, the NiOH^{-} group, produced in surface hydrolysis reaction 4.34, has no analog in the SiOH family.

Modeling a system where hydrolyzed surface complexes can act as adsorption centers will be accomplished by adding, at each iteration in SURFEQL, the concentration of newly formed hydrolyzed surface complexes to

the initial concentration of SiOH_T . As the first hydrolysis constant of nickel ion and the first acidity constant of silicic acid are the same, it is reasonable to assume that this chemical similarity of solution species would apply to the equivalent surface species. Results are shown in Figure 4.21 using the CCM'. The following conditions apply: $\text{Ni}_T = 4.70 \text{ mM}$, $I = 0.1 \text{ M}$, $C = 1.25 \text{ F/m}^2$, surface area = $182 \text{ m}^2/\text{g}$, surface loading = 0.16 g/L , initial $\text{SiOH}_T = 2.4 \text{ mM}$, and $\log c_{K_1}^* = -6.0$. Theoretical curves are shown on top of the results from titration LM15 previously shown in Figure 4.18.

In order to see the usefulness of the above approach, a set of curves was produced using the unmodified SURFEQL program. Curves were calculated at differing values of SiOH_T with all other conditions the same as in Figure 4.21. These results are shown in Figure 4.22 for $\log c_{K_{\text{NiOH}}}^* = -12.0$. The values of SiOH_T shown range from the initial calculated 2.4 mM to four times that. As SiOH_T is increased, larger percentages of Ni(II) are adsorbed and the adsorption edge moves to lower values of pH reflecting a decrease in the parameter ρ . Qualitatively, increasing the number of surface sites can account for the large adsorption densities observed. A minimum of four times as many sites as were originally present are necessary to achieve 100% adsorption.

The major difference between the theoretical curves shown in Figure 4.21 and those in Figure 4.22 is their steepness. The curves in Figure 4.22 have a considerably greater slope which provides a much better fit to the percent adsorption calculations. A value for $\log c_{K_{\text{NiOH}}}^*$ of -11.8 describes the system after 96 to 102 minutes equilibration time. It was found that the results in Figures 4.21 and 4.22 were relatively

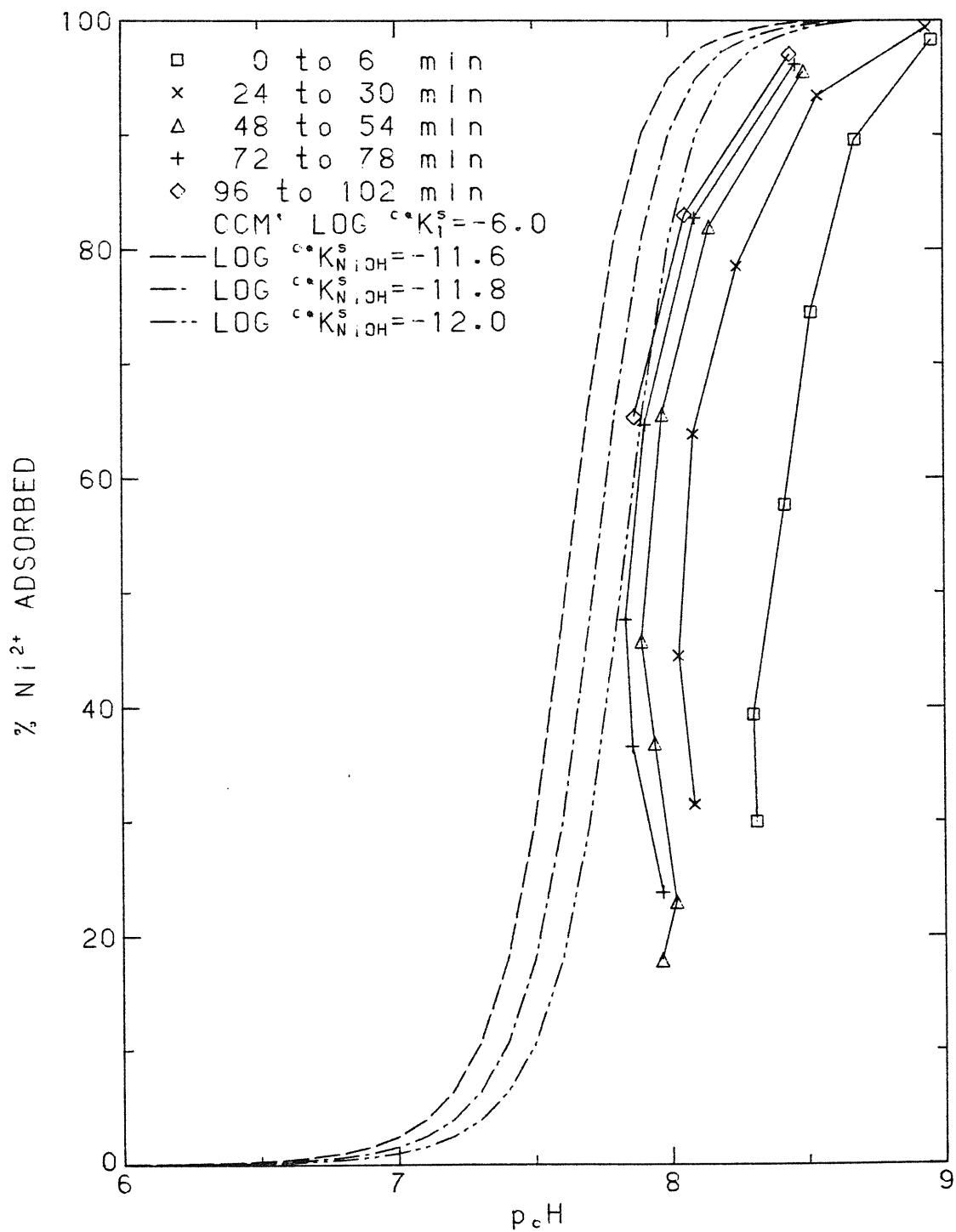


Figure 4.21 The shape and location of the adsorption edge predicted using SURFEQL when regeneration of surface sites is included. $c^*K_{NiOH}^s$ is varied as indicated while $\log c^*K_1^s$ is held constant at -6.0.

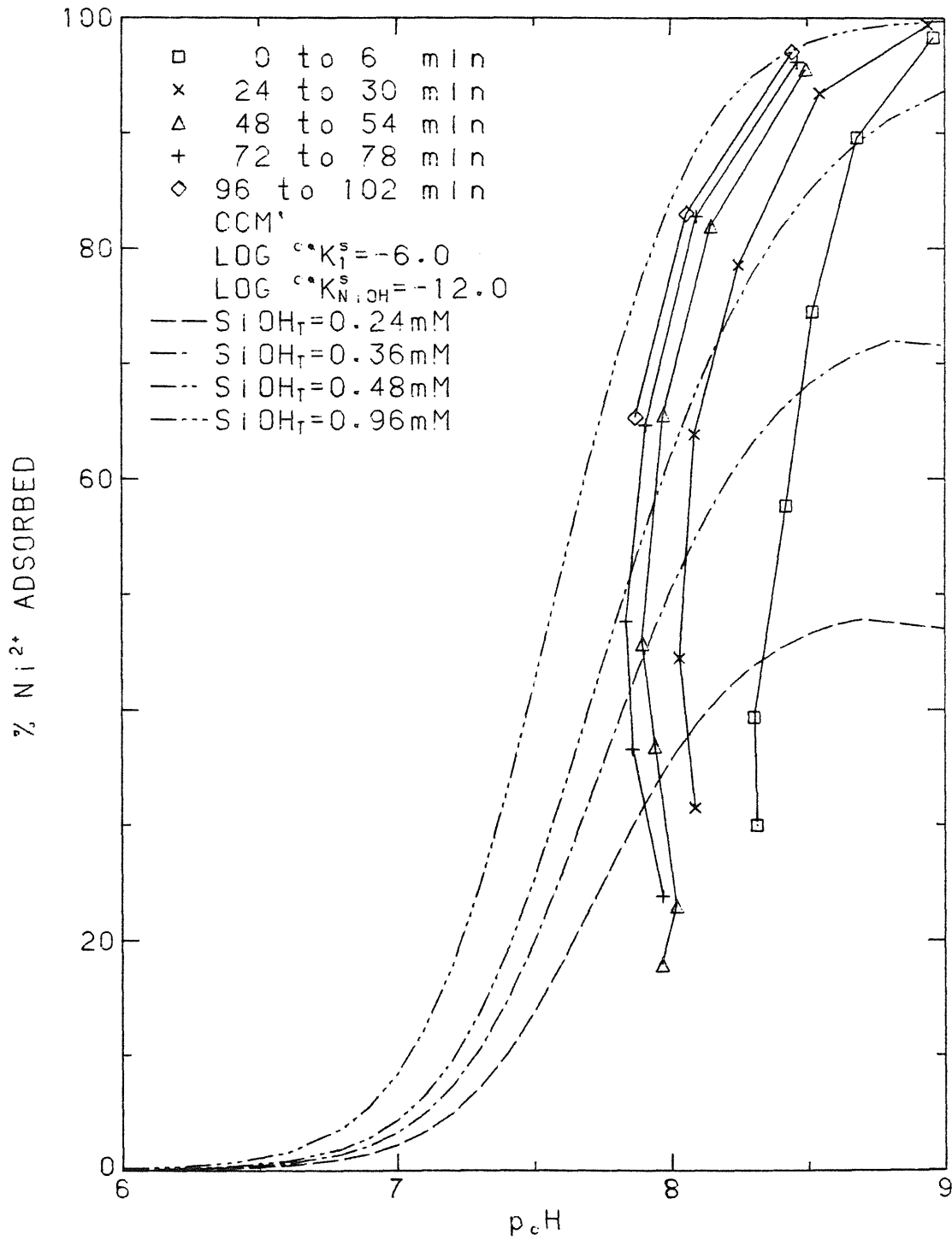


Figure 4.22 Adsorption edge predictions using the unmodified version of SURFEQL. The different theoretical curves correspond to different values of SiOH_T indicated on the plot.

insensitive to the value of $\log c_{K_1}^s$. Modeling these results using the TLM was unsatisfactory.

A coordination chemistry model developed to describe adsorption at very low values of ρ can be modified to model data obtained in systems where ρ is greater than one. No validation for the assumption on the manner in which adsorption centers are formed is possible as hydrolyzed and bidentate surface complexes have equivalent formulations in the CCM'.

4.6 Summary

Adsorption of Ni(II) onto a silica surface was studied by means of alkalimetric titrations. The experiments were designed to understand the speciation of Ni(II) under a set of experimental conditions which maximized adsorption density. Each component of the system with the capability to consume or release protons was considered individually, with the following results.

- i) Si(OH)_4 : The concentration of silicic acid in equilibrium with $\text{SiO}_2(\text{s})$ in 0.1 M NaClO_4 was determined to be 1.85 ± 0.03 mM.
- ii) SiOH : Titrations of silica suspensions, after correcting for the proton demand of soluble silica species, were modeled successfully with a variation of the constant capacitance model which included an exchange reaction between silanol protons and sodium ions. The original constant capacitance model (CCM) and the triple layer model (TLM) were not able to reproduce the data. Values of $\log c_{K_2}^s$ and $\log c_{K_{1Na}}^s$ used in the CCM' were -7.8 and -9.4, respectively. Titrations

provided a lower limit for surface site density of $3.9 \mu\text{moles}/\text{m}^2$.

iii) Ni^{2+} : The hydrolytic behavior of nickel ion was defined by the reactions and equilibrium constants in Table 4.2. A solubility product for the solid hydroxide phase was impossible to measure as stable equilibrium conditions were not reached. Reproducible data were obtained describing the pH change over time during the onset and initial phase of the precipitation. These data allowed a differentiation between precipitation and adsorption of nickel ion in the presence of silica.

With these results in hand, the following conclusions were drawn concerning adsorption of nickel onto a silica surface at values of the parameter $\rho = 2.0$.

- i) As the pH of an aqueous nickel solution is increased, nickel is removed from solution by adsorption processes before the precipitation of nickel hydroxide occurs.
- ii) Accompanying the adsorption of nickel onto the surface, results yield 1.9 ± 0.2 protons released to solution per nickel ion adsorbed.
- iii) Adsorption of nickel ion is not limited by the availability of silanol groups. Adsorption continues to occur after the concentration of uncomplexed silanol groups approaches zero. The maximum adsorption density observed was $16 \mu\text{moles Ni}/\text{m}^2 \text{SiO}_2$. It appears that the capacity of the surface to adsorb nickel ion has no upper bound.

(iv) Multilayer adsorption as defined by the BET isotherm does not fit the data. A coordination chemistry model, in which the total concentration of surface groups increases as adsorption occurs, does describe the experimental data. This increase in adsorption sites is postulated to be the result of the formation of hydrolyzed surface complexes: the resultant NiOH groups functioning in a chemically similar manner to SiOH groups.

CHAPTER 5

NUCLEAR MAGNETIC RESONANCE EXPERIMENTS

5.1 Introduction

A proton magnetic resonance experiment has been conducted to investigate the hydration state of nickel ion adsorbed onto a silica surface. The coordination number of surface complexes composed of silanol groups and an aqueous Ni(II) species was determined. The difference in the chemical shift of the exchange-averaged water line of a $\text{Ni}(\text{ClO}_4)_2$ solution in the presence and absence of a solid silica phase was the key experimental measurement. Bulk susceptibility corrections, necessitated by an external referencing technique, were accomplished by recording spectra with two different magnet/sample geometries.

5.2 Referencing of Spectra

The choice of an appropriate standard for referencing NMR spectra was influenced by several factors. A decision was made to use an external referencing technique in which a standard is held in the annular region of a coaxial sample tube. Potential chemical and magnetic interactions between the sample and standard were thereby eliminated. External referencing does necessitate a correction to the observed chemical shift for differences in bulk susceptibilities of the sample and the standard. Corrections were made by recording spectra on instruments with different magnet/sample geometries. The details have been discussed in Section 3.3.2.2.

While the external referencing process increased the number of possible standard compounds from which to choose, other considerations

imposed limitations. The standard compound was required to have: i) the capability to provide a lock signal for the HA-100 spectrometer, ii) a resonance frequency far enough upfield or downfield from the bulk water signal to be clearly visible, iii) a stable liquid phase over the temperature range 0 to 100 °C and iv) a small bulk susceptibility to minimize the development of sidebands accompanying the standard signal (see Hatada, et al. 1972). The compound, 2,2,4,4-tetramethylpentane (TMP), with 12 equivalent protons, a boiling point of 120°C, a low susceptibility compared to the other standards tested (tetramethylsilane (TMS) and cyclohexane) and a major resonance signal located 3.82 ppm upfield from the water resonance was chosen as the standard for referencing spectra recorded at higher-than-ambient temperatures.

5.3 Concentration-dependent Experiments

5.3.1 Investigation of the Chemical Shift of the Exchange-averaged Water Line in Diamagnetic and Paramagnetic Systems

Paramagnetic species containing unpaired electron spins produce chemical shifts many times larger than those observed for diamagnetic species. A comparison of the magnitude of the chemical shift of the exchange-averaged water line in solutions of the paramagnetic species Ni^{2+} and the diamagnetic species Na^+ , ClO_4^- and SiOH was made. It could then be determined whether or not significant contributions to the measured chemical shift values were made by any of the diamagnetic species.

5.3.1.1 Results

Spectra were recorded for 0.001 to 1 M solutions of

$\text{Ni}(\text{NO}_3)_2$, NaClO_4 and suspensions of Aerosil 200, to determine experimentally the magnitude of the chemical shift of the exchange-averaged water line under the influence of these different components. Experiments were conducted on a Varian HR-220 NMR spectrometer. Spectra were externally referenced with TMS and recorded at 22°C.

The results plotted in Figure 5.1 show the log of the absolute value of the chemical shift of the exchange-averaged water line, $|\Delta\omega|_{\text{std}}$ (ppm), versus the log of the concentration of the component present, x . Measurements of the chemical shift of the exchange-averaged water line were made relative to the position of the pure water resonance. In the case of the silica suspension, shifts are plotted against calculated concentrations of silanol groups. The concentration range investigated corresponds to silica loadings of 3.45 to 230 g/L.

Three phenomena are evident: i) in the presence of Ni^{2+} , exchange-averaged spectra were recorded; ii) the chemical shift, $\Delta\omega$, is seen to be a linear function of concentration for $\text{Ni}(\text{NO}_3)_2$ solutions, concentrated (greater than 0.1 M) NaClO_4 solutions and silica suspensions (where $[\text{SiOH}]$ is greater than 0.1 M) and iii) the magnitude of the chemical shift in the presence of the paramagnetic Ni^{2+} species ranges from ten times larger (at concentrations of 10^{-2} M) to 1000 times larger (at concentrations of 1 M) than shifts resulting from the presence of the diamagnetic species Na^+ , ClO_4^- or SiOH . The direction of the chemical shift also changes. The nickel solution resonance is located downfield from that of pure water while resonances for the diamagnetic samples are found upfield from pure water.

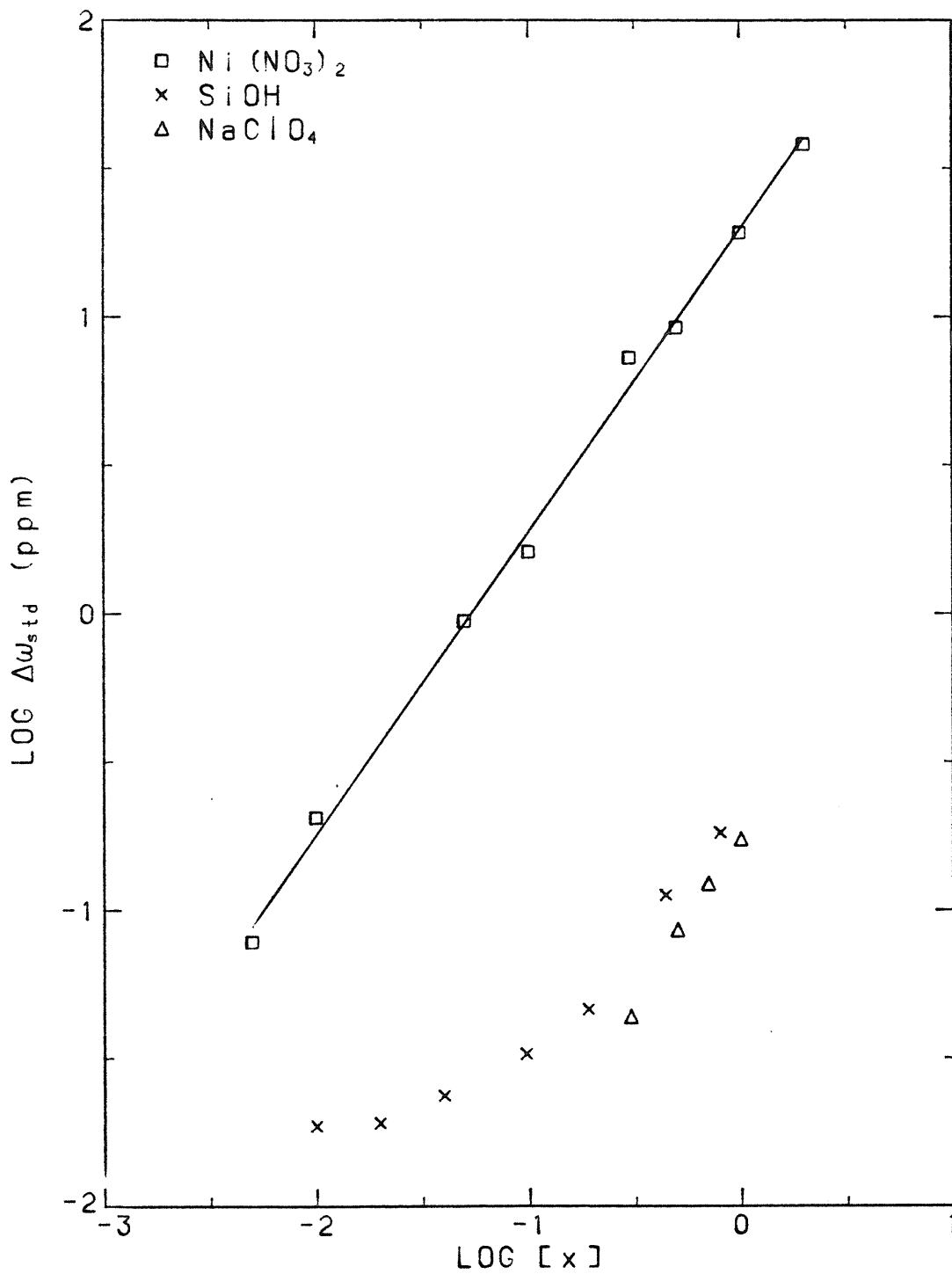


Figure 5.1 The absolute value of the log of the chemical shift of the water resonance for the components listed plotted against the log of their concentrations.

5.3.1.2 Discussion

Exchange-averaging of the resonance line in Ni(II) solutions can be inferred in two ways:

- 1) In an exchange-averaged system, increasing the concentration of a Ni^{2+} solution increases the fraction of protons located in coordinated water molecules. As the resonance frequency of coordinated water molecules is downfield from that of pure water (section 5.3.2.2), the resonance frequency of the exchange-averaged line should shift downfield from the location of the pure water resonance when $[\text{Ni}^{2+}]$ increases. This is the observed trend.
- 2) Exchange-averaging is predicted to occur when the rate constant for the exchange of nuclei between two environments, k_1 , exceeds the chemical shift, $\Delta\omega$, of their respective NMR lines.

$\Delta\omega$ can be calculated using the contact shift equation of Bloembergen and the value of the hyperfine coupling constant determined in section 5.3.2.2. At a temperature of 25°C, $\Delta\omega$ is listed in Table 5.1 as a function of the working frequency of the spectrometer.

Table 5.1

$\Delta\omega(\text{sec}^{-1})$	spectrometer frequency (MHz)
5.2×10^3	100
1.1×10^4	220
2.6×10^4	500

At both 100 and 220 MHz, the value of k_1 in Ni^{2+} solutions ($3 \times 10^4 \text{ sec}^{-1}$) is greater than $\Delta\omega$. Therefore, the resonance line of water molecules in solutions of paramagnetic Ni^{2+} ions is predicted to be exchange-averaged at frequencies up to 220 MHz. At 500 MHz, k_1 is

comparable to $\Delta\omega$ and the exchange-averaging process is not complete. Even so, no significant effect on the position of the water resonance in Ni^{2+} solutions investigated on the WM-500 was noticed. This is reasonable in that the fractional population of water in the first coordination sphere was never greater than 0.03.

In the Ni(II)-SiO_2 system investigated in Section 5.4.2, both paramagnetic and diamagnetic components were present in the following concentrations: $\text{Ni(ClO}_4)_2 = 0.042 \text{ M}$, $\text{NaClO}_4 = 0.1 \text{ M}$, and $\text{SiOH} = 0.025 \text{ M}$. The measured chemical shifts for solutions of these concentrations can be interpolated from Figure 5.1 and are shown below.

solution composition	$\Delta\omega_{\text{std}}$ (ppm)
0.042 M $\text{Ni(NO}_3)_2$	0.774
0.1 M NaClO_4	0.014
0.025 M SiOH	0.023

At these concentrations, chemical shifts of the diamagnetic species NaClO_4 and SiOH are only 2% and 3% as large as the shift due to $\text{Ni(NO}_3)_2$. Therefore, chemical shift measurements made on the Ni(II)-SiO_2 system will be, within experimental error, attributable solely to the presence of the paramagnetic Ni(II) species.

5.3.2 Determination of the Hyperfine Coupling Constant

5.3.2.1 Introduction

The electron-nuclear hyperfine coupling constant, A , is a measure of the amount of electron spin density transferred from a paramagnetic species to a nucleus of interest, in this case, the proton of a first coordination sphere water molecule. It is an important

experimentally-derived constant necessary in order to apply the Bloembergen equation to calculate hydration numbers. A measurement of the hyperfine coupling constant of $\text{Ni}(\text{ClO}_4)_2$ solutions was made here by measuring the chemical shifts of 0 to 0.271 M solutions, externally referenced with TMP, and assuming a hydration number of six for aqueous Ni^{2+} . Spectra were recorded at $(25 \pm 1)^\circ\text{C}$.

5.3.2.2 Results

Chemical shift measurements made on the HA-100 and WM-500 spectrometers, along with shifts corrected for bulk susceptibility effects, are shown in Figure 5.2. $-\Delta\omega_{\text{std}}$ (ppm) is plotted against the fraction of water coordinated to nickel ions, f_{coor} . All of the measured chemical shift values shown in Figure 5.2 are located downfield of the TMP standard. Downfield shifts are defined as negative shifts. The conversion from molarity to f_{coor} is made using equation 5.1.

$$f_{\text{coor}} = \frac{[\text{Ni(II)}] \cdot 6}{D_{[\text{Ni}]} \cdot 55.5} \quad (5.1)$$

where: 6 is the hydration number of Ni(II) and $D_{[\text{Ni}]}$ is the density of water at each nickel concentration. The numerator of equation 5.1 calculates the molarity of coordinated waters in a solution of known nickel concentration. The denominator calculates the molarity of water in that same solution. Concentrations, densities and f_{coor} values for the five nickel solutions investigated are listed in Table 5.2. $D_{[\text{Ni}]}$ was assumed to be unity for the three least-concentrated solutions used and measured for the two most-concentrated.

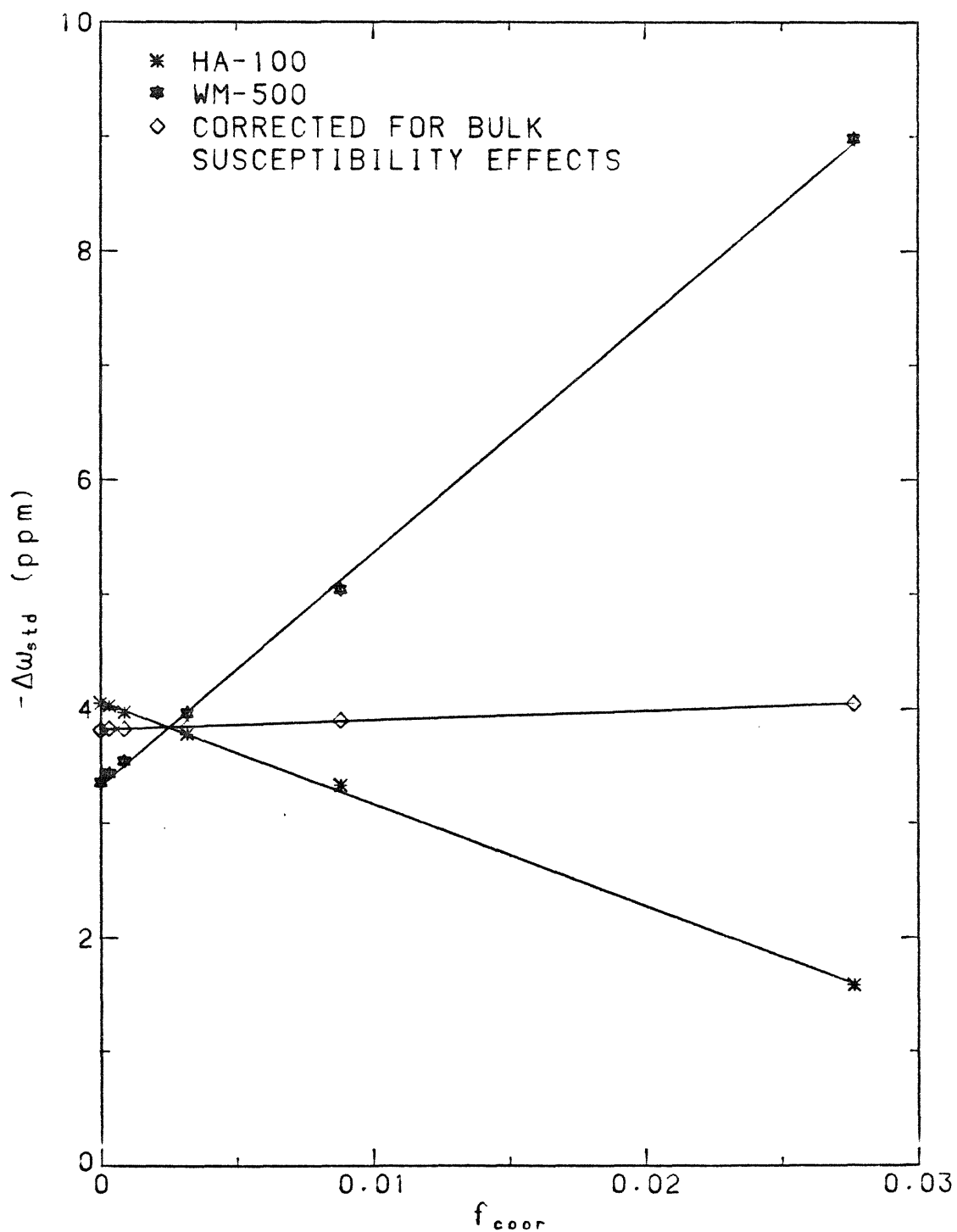


Figure 5.2 Chemical shifts for $\text{Ni}(\text{ClO}_4)_2$ solutions measured on both the HA-100 and WM-500 spectrometers, plotted against the fraction of coordinated water molecules in each solution studied.

Table 5.2

[Ni ²⁺] M	D _[Ni] g/mL	f _{coor}
0.00285	1	0.000308
0.00797	1	0.000862
0.0295	1	0.00319
0.0828	1.0132	0.00883
0.271	1.0571	0.0277

Linear regressions were performed on each set of experimental data and also on the chemical shift values corrected for bulk susceptibility effects. Values of r^2 are all greater than 0.99. The linear equation describing the bulk-susceptibility-corrected line is

$$-\Delta\omega_{\text{std}} = (8.22 \pm 0.43)f_{\text{coor}} + (3.82 \pm 0.006) \quad (5.2)$$

The errors shown for the regression parameters are at the 95% confidence level.

Bloembergen's equation describing the contact shift (equation 2.28) was rearranged in Chapter 2 (equation 2.30) so that it is in the same form as equation 5.2. The conversion between $\Delta\omega_{\text{std}}$ (ppm) in equation 5.2 and $\Delta\omega/\omega$ in equation 2.28 is shown below

$$-\Delta\omega_{\text{std}} = \frac{\Delta\omega}{\omega} \cdot 10^6 \quad (5.3)$$

Defining

$$Z = \frac{g_{\text{eff}} \beta S(S+1)}{g_N \beta_N 3kT} \cdot 10^6 \quad (5.4)$$

which has a value of $1.20 \times 10^{-10} \text{ erg}^{-1}$, using 2.26 for the value of g_{eff} (Neely and Connick 1972), and substituting equation 5.3 and equation 5.4 into equation 2.30 gives

$$\Delta\omega_{\text{std}} = AZf_{\text{coor}} \quad (5.5)$$

The slope of equation 5.2 can now be used to calculate A. The result, after converting from units of ergs to sec^{-1} , is $(6.5 \pm 0.3) \times 10^5 \text{ sec}^{-1}$. The error shown is at the 95% confidence level. This value agrees well with published values for A.

5.4 Temperature-dependent Experiments

5.4.1 Introduction

The temperature dependence of the position and linewidth of the exchange-averaged resonance line of water molecule protons was measured with respect to a TMP external standard for three systems: i) D_2O , ii) a 0.0274 M $\text{Ni}(\text{ClO}_4)_2$ solution and iii) Ni(II) adsorbed onto a silica surface. These experiments offer the potential to: i) determine the hydration number of an adsorbed Ni(II) species, ii) investigate the completeness of the exchange-averaging process at the higher frequency of the WM-500 spectrometer and iii) measure the hyperfine coupling constant for both systems ii and iii.

5.4.2 Results

Chemical shift determinations and linewidth measurements were made for the three systems described over the temperature range 5 to 88 $^\circ\text{C}$.

The temperature dependence of the chemical shift of D_2O was investigated so that the chemical shift of the exchange-averaged water resonance in the Ni(II) systems could be referenced to the position of the pure water resonance. A sample of 99.8% isotopically pure D_2O (0.1 M in

protons) was used in place of H_2O . Signals from H_2O samples were too intense to be measured accurately.

The measured concentration of the Ni^{2+} solution was 0.0274 M. The concentration was chosen to be as large as possible while still not causing excessive splitting of the TMP reference signal.

The Ni(II)- SiO_2 system was prepared by titrating, under an N_2 atmosphere, 500 mL of a 1 g/L Aerosil 200 suspension in 0.1 M $NaClO_4$ with 5 mL of a 0.252 M $Ni(ClO_4)_2$ solution. p_aH was maintained within the range 8.20 to 8.75 by adding 1 mL aliquots of 0.1 M NaOH. At the end of the titration the suspension was allowed to settle. The total amount of nickel added to the system was calculated to be 1.25×10^{-3} mole. The measured amount of Ni^{2+} in the supernatant at the end of the experiment was less than 4×10^{-6} mole. Essentially, 100% adsorption had been obtained. The volume of the settled suspension was 30 mL. The 'concentration' of Ni(II) in the settled suspension was calculated to be 0.042 M.

Chemical shifts, $-\Delta\omega_{std}$ (ppm), are plotted against inverse temperature ($10^3/^\circ K$) for all three experimental systems in Figures 5.3 and 5.4. Figure 5.3 shows data from the HA-100 spectrometer and Figure 5.4 from the WM-500 spectrometer. The lines drawn through each data set are obtained by regressing $-\Delta\omega_{std}$ against inverse temperature. Regression coefficients and r^2 values for the six sets of data are listed in the upper half of Table 5.3. Referring to the equation numbers used in Table 5.3, equations 5.8abc describe the results of correcting each of the three systems for bulk susceptibility effects and equations 5.9bc show the results of referencing the chemical shifts in the nickel

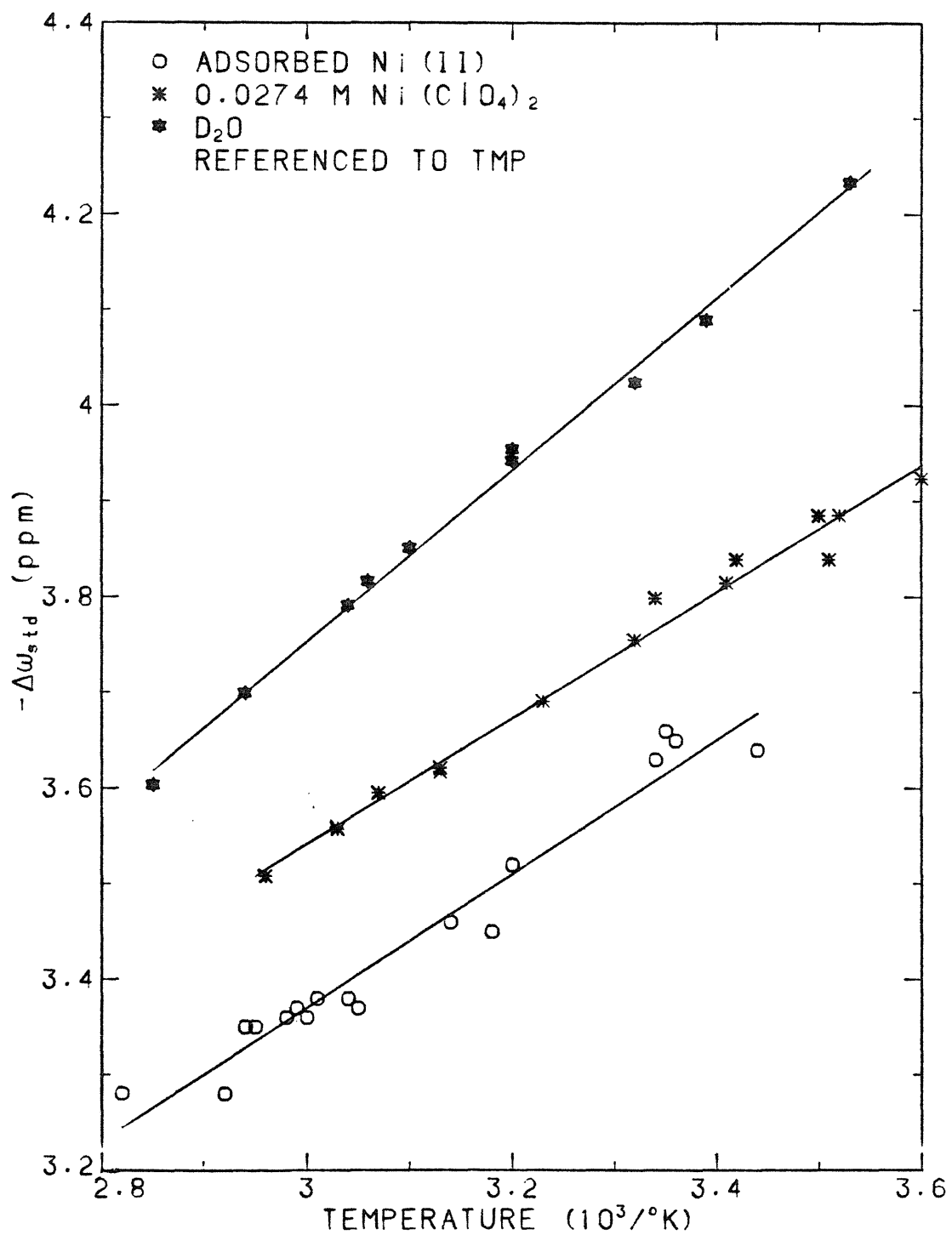


Figure 5.3 Chemical shifts are plotted against inverse temperature for the three systems listed. Measurements were made on the HA-100 spectrometer.

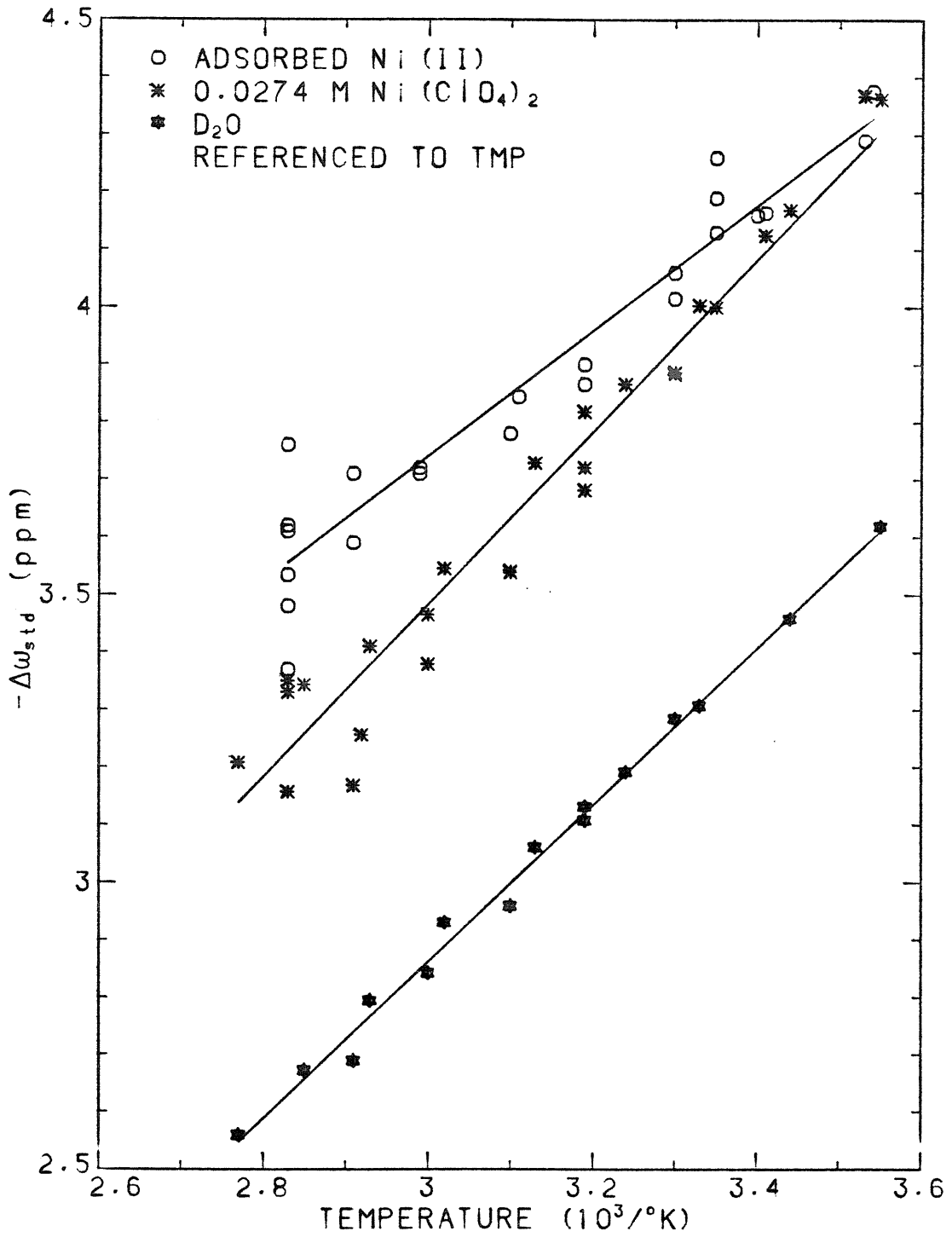


Figure 5.4 Chemical shifts are plotted against inverse temperature for the three systems listed. Measurements were made on the WM-500 spectrometer.

Table 5.3
 Linear Regression Parameters Describing
 the Variation of Chemical Shifts with Temperature⁻¹

System	$-\Delta\omega_{\text{std}} \text{ (ppm)} * = A(10^3/\text{°K}) + B$			r^2	Eq. #
	A	B			
HA-100 Data	D ₂ O	0.90 ± 0.04	1.06 ± 0.14	0.995	5.6a
	Ni ²⁺ solution	0.66 ± 0.04	1.56 ± 0.14	0.986	5.6b
	Adsorbed Ni(II)	0.70 ± 0.08	1.27 ± 0.24	0.953	5.6c
WM-500 Data	D ₂ O	1.36 ± 0.06	-1.23 ± 0.19	0.993	5.7a
	Ni ²⁺ solution	1.59 ± 0.12	-1.32 ± 0.36	0.965	5.7b
	Adsorbed Ni(II)	1.11 ± 0.12	0.40 ± 0.38	0.951	5.7c
Bulk Susceptibility Corrected Equations	D ₂ O	1.05 ± 0.05	0.30 ± 0.15	-	5.8a
	Ni ²⁺ solution	0.97 ± 0.07	0.60 ± 0.21	-	5.8b
	Adsorbed Ni(II)	0.84 ± 0.10	0.98 ± 0.29	-	5.8c
Referenced to D ₂ O i.e. $\Delta\omega_{\text{std}} = \Delta\omega_{\text{H}_2\text{O}}$	Ni ²⁺ solution	-0.08 ± 0.08	0.30 ± 0.25	-	5.9b
	Adsorbed Ni(II)	-0.21 ± 0.11	0.68 ± 0.32	-	5.9c

Errors shown are at the 95% confidence level.

* referenced to TMP

systems to the position of the pure water resonance. Equations 5.8 and 5.9 are linear combinations of equations 5.6 and 5.7. The appropriate combinations are shown below.

$$5.8a = 2/3(5.6a) + 1/3(5.7a) \quad (5.10)$$

$$5.8b = 2/3(5.6b) + 1/3(5.7b) \quad (5.11)$$

$$5.8c = 2/3(5.6c) + 1/3(5.7c) \quad (5.12)$$

$$5.9b = 5.8b - 5.8a \quad (5.13)$$

$$5.9c = 5.8c - 5.8a \quad (5.14)$$

Linewidths, $\delta_{\text{H}_2\text{O}}$ (Hz), of the exchange-averaged lines are plotted against inverse temperature, ($10^3/^\circ\text{K}$), in Figures 5.5 and 5.6. Measurements of the linewidths are made at half-maximum intensity of the resonance line.

Linewidths of the 0.0274 M $\text{Ni}(\text{ClO}_4)_2$ solution water resonance line are shown for the HA-100 and WM-500 spectrometers in Figures 5.5a and 5.5b, respectively. The trend of the data is qualitatively the same for each spectrometer, although there is more scatter in the WM-500 spectrometer data and the linewidths are 2 to 3 times as large. Linewidths increase linearly as the temperature decreases from 80 to 30 $^\circ\text{C}$ (2.8 to 3.3 in $10^3/^\circ\text{K}$ units), reach a maximum at 25 to 30 $^\circ\text{C}$ and then decrease at temperatures less than 25 $^\circ\text{C}$ (greater than 3.35 in $10^3/^\circ\text{K}$ units).

Linewidths measured on the $\text{Ni}(\text{II})\text{-SiO}_2$ system (Figure 5.6ab) increase linearly as temperature decreases over the entire temperature

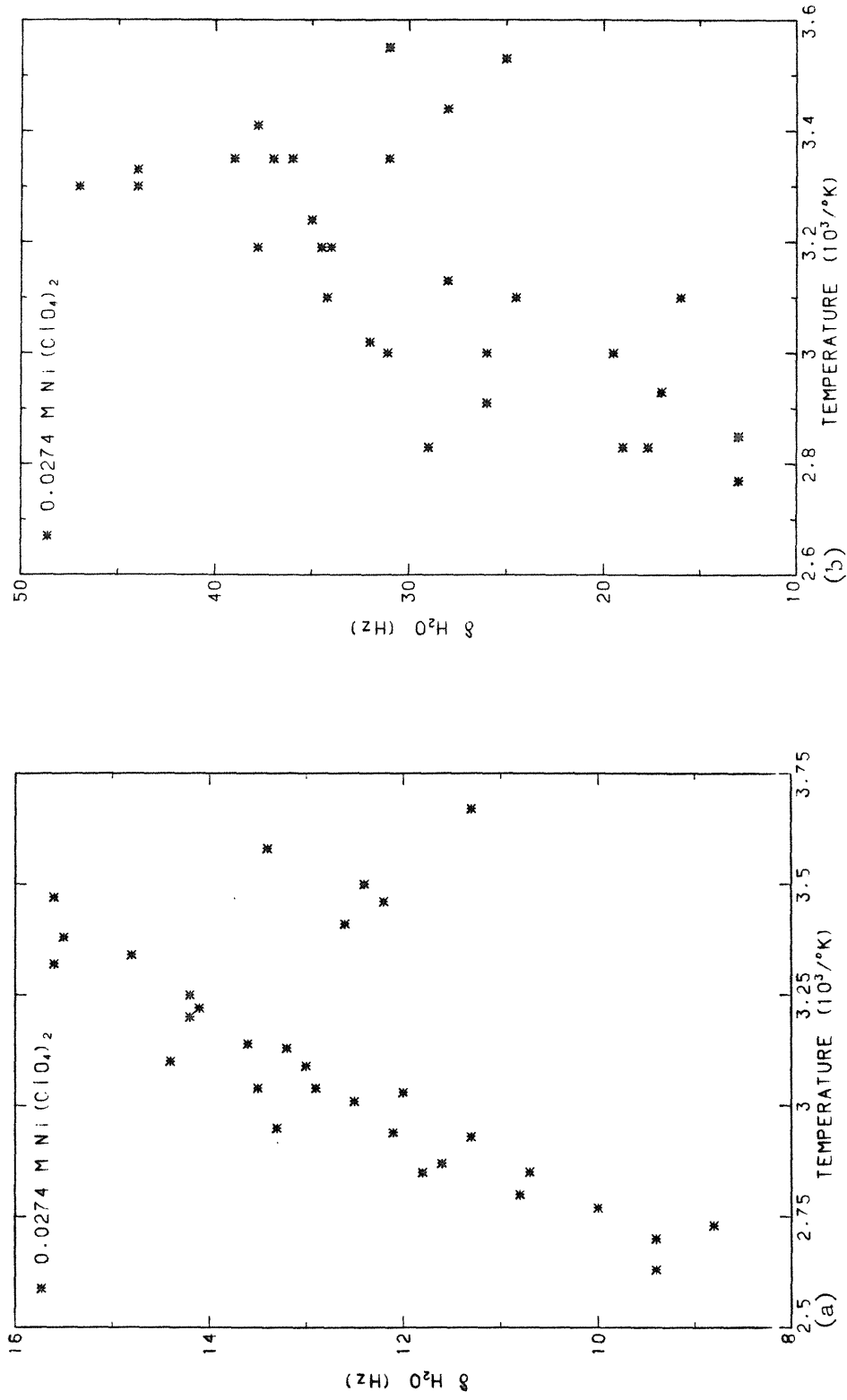
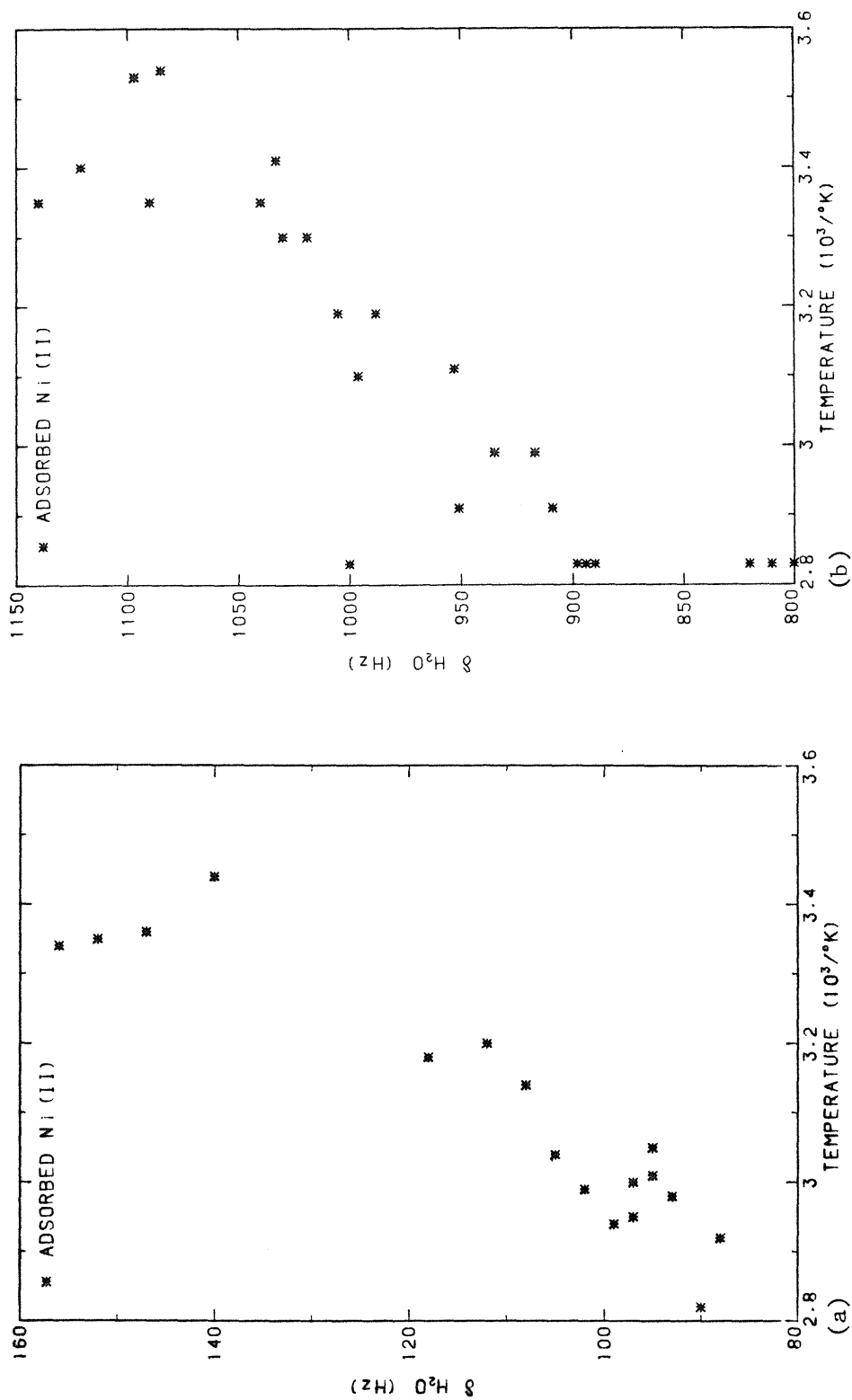


Figure 5.5 Linewidths of the water resonance in an 0.0274 M Ni(ClO₄)₂ solution are plotted against inverse temperature. Measurements were made on the HA-100 spectrometer (5.5a) and the WM-500 spectrometer (5.5b).



range studied and are 1 to 2 orders of magnitude larger than the corresponding measurements on the $\text{Ni}(\text{ClO}_4)_2$ solution. This behavior holds for both spectrometers. The increase in magnitude of the linewidths is a result of the adsorption of $\text{Ni}(\text{II})$ onto the surface. Rotational motion of the $\text{Ni}(\text{II})$ species is decreased when adsorption occurs. Averaging of molecular orientations with respect to the applied field therefore decreases, causing the observed line broadening.

5.4.3 Discussion

5.4.3.1 Water

The D_2O system was the most well-behaved. There is very little scatter in the chemical shift data in Figures 5.3 and 5.4. Values of r^2 greater than 0.99 for the regression lines attest to this. The value of the slope of the $-\Delta\omega_{\text{std}}$ versus inverse temperature line corrected for bulk susceptibility effects (equation 5.8a), is 1.05 ± 0.05 . Hindman (1966), making a similar measurement, reported a value of 1.02 for this slope. These two measurements are in good agreement.

5.4.3.2 The Ni^{2+} Solution

The position of the water resonance in the presence of 0.0274 M $\text{Ni}(\text{ClO}_4)_2$ has moved, with respect to the pure water resonance, over the entire temperature range studied. $\Delta\omega_{\text{H}_2\text{O}}$ of the Ni^{2+} solution has become more negative in spectra recorded on the WM-500 spectrometer and more positive on spectra recorded on the HA-100 spectrometer. At 25°C, this behavior is consistent with the results shown in Figure 5.2.

Examination of the linewidths, $\delta_{\text{H}_2\text{O}}$ (Hz), measured as a function of inverse temperature ($10^3/^\circ\text{K}$) for the 0.0274 M $\text{Ni}(\text{ClO}_4)_2$ solution

provides evidence for completeness of the exchange-averaging process.

Linewidths in dilute solutions of paramagnetic cations are controlled by the transverse or spin-spin relaxation time (T_2) of the system. Swift and Connick (1962) derived theoretical expressions describing the temperature dependence of the processes governing the overall relaxation rate ($1/T_2$). The overall relaxation process was found to be controlled by either the lifetime or the spin-spin relaxation time of protons within the first coordination sphere.

Measurements of the temperature dependence of the relaxation rate of Ni^{2+} solutions by Swift and Connick (1962) and Swift and Weinberger (1968) show the same maximum observed in the linewidth data in Figures 5.5ab ($1/T_2$ is directly proportional to the linewidth). The maximum was interpreted as a transition region between a lower-temperature slow-exchange regime and a higher-temperature fast-exchange regime. The temperature at which the transition takes place is a function of k_1 , f_{coord} and $\Delta\omega$. At the concentrations of Ni^{2+} and spectrometer frequencies used in this study, Ni^{2+} solutions are exchange-averaged at temperatures above 30°C.

A value for the hyperfine coupling constant, A , can be calculated from the slope of equation 5.9b (Table 5.3), in a manner similar to that used in section 5.3.2.2. The calculation would serve to corroborate the value of A reported in section 5.3.2.2. Unfortunately, the value of A determined from these data was too imprecise to be of any value and consequently is not given. Calculations of a value for A in the adsorbed $Ni(II)$ system suffers from the same difficulties.

5.4.3.3 The Ni(II)-SiO₂ System

Reproducible measurements of the chemical shift for the Ni(II)-SiO₂ system were difficult to obtain. The very wide lines observed for the adsorbed Ni(II) system made the center of the line, as defined by the maximum intensity, difficult to determine. Difficulties in obtaining correctly phased signals for both the standard and the water resonance line and irregular line shapes for the water resonance compounded the chemical shift measurement problem. Gas bubbles were noticed on occasion in the standard and the adsorbed Ni(II) samples at higher temperatures. Visible bubbles significantly changed the line shape and chemical shift by introducing inhomogeneity into the sample. Nevertheless, interesting conclusions can still be drawn.

The regression lines representing bulk-susceptibility-corrected equations referenced to D₂O for the Ni²⁺ solution and adsorbed Ni(II) system (equations 5.9b and 5.9c in Table 5.3) should be parallel if the hyperfine coupling constant A was the same and exchange-averaging was occurring in both systems. Displacement of these lines from the D₂O line, as measured by the intercepts of equations 5.9b and 5.9c, would then be a linear function of f_{coor} . As the concentration of Ni(II) and the density of the aqueous phase is known for each system, the hydration number of adsorbed Ni(II) could then be calculated using equation 5.1. Although the slopes of equations 5.9b and 5.9c are not statistically different at the 95% confidence level, the mean values are not nearly the same. There is a reason for this result.

The slope of the regression line for adsorbed Ni(II) calculated from data taken on the WM-500 spectrometer (equation 5.7c in Table 5.3)

is significantly smaller than the slope of equation 5.7b which describes the Ni^{2+} solution data from the same spectrometer. It was expected to be larger. The reasoning behind this expectation is as follows (equation numbers refer to the data described by them). It has been shown that equation 5.7a of Table 5.3 is correct in section 5.4.3.2. Data from section 5.3.1.1 indicate the position of equation 5.7b should be at larger values of $-\Delta\omega_{\text{std}}$ with respect to equation 5.7a; this is the case. The adsorbed Ni(II) system has a $[\text{Ni(II)}]$ 1.5 times that of the Ni^{2+} solution. At every temperature, equation 5.7c should be shifted 1.2 to 1.5 times farther from equation 5.7a (depending on the hydration number of the adsorbed Ni(II) species) than equation 5.7b is shifted. This last statement is true only if one assumes that the hyperfine coupling constant and the bulk susceptibility of the adsorbed Ni(II) system and Ni^{2+} solution are essentially the same and also that conditions for fast exchange are met. It is reasonable to make the first two assumptions but the third is not necessarily valid. It is suggested here that, at 500 MHz, exchange-averaging is not complete at 25°C in the adsorbed Ni(II) system and that this fact accounts for the smaller than expected chemical shifts at the lower temperatures.

The result of slow exchange, at any temperature, is to shift an incompletely-averaged water resonance towards the pure water resonance. Inspection of Figure 5.4 shows the expected shift of the adsorbed Ni(II) system at higher temperatures and no significant shift, compared to the Ni^{2+} solution, at lower temperatures. This results in a value of the slope of equation 5.7c which is smaller than expected.

At 500 MHz and 25°C , k_1 has been shown to be comparable to $\Delta\omega$ (Table

5.1). If $k_1(\text{ads})$ (the rate constant for exchange in the adsorbed Ni(II) system) is smaller than k_1 , slow exchange ($k_1 < \Delta\omega$) will be occurring at 500 MHz and 25°C. A smaller exchange rate is plausible on physical-chemical grounds. The movement of water molecules in and out of the first coordination sphere of an adsorbed Ni(II) species may be restricted by the presence of the surface, thus increasing their lifetime in the first coordination sphere and decreasing the exchange rate.

A lower limit can be placed on k_1 in the adsorbed Ni(II) system at 25°C by considering that exchange-averaging appears to be a valid assumption for this system at 100 MHz. At 100 MHz, $\Delta\omega$ is $5.2 \times 10^3 \text{ sec}^{-1}$. Fast exchange implies k_1 is greater than $\Delta\omega$, thus k_1 is greater than $5.2 \times 10^3 \text{ sec}^{-1}$.

k_1 is known to increase with temperature. Swift and Weinberger (1968) report the value of k_1 in an aqueous Ni^{2+} solution to be $2.1 \times 10^5 \text{ sec}^{-1}$ at 59°C. This is a seven-fold increase in the exchange rate compared to the value reported at 25°C. Assuming this increase in exchange rate can be applied to the adsorbed Ni(II) system (when the temperature is increased by the same amount), the exchange-averaging process would become operative again at temperatures above 60°C.

As exchange-averaging is incomplete at temperatures below 60°C in the adsorbed Ni(II) system at 500 MHz, the intended method of calculating the hydration number of an adsorbed Ni(II) species is not applicable. However, an estimate of this hydration number can be made at higher temperatures, where the exchange-averaging assumption is potentially valid, by considering data at individual temperatures. Bulk-susceptibility-corrected chemical shifts of an exchange-averaged water

line for the adsorbed Ni(II) system and the Ni²⁺ solution are linearly related to f_{coor} (equation 2.30). f_{coor} is related to the hydration number, h_n , by equation 5.1. Constructing a ratio of the chemical shifts, referenced to D₂O, of adsorbed Ni(II), $-\Delta\omega_{\text{H}_2\text{O}}(\text{Ni(II)})$, and Ni²⁺ solutions, $-\Delta\omega_{\text{H}_2\text{O}}(\text{Ni}^{2+})$, results in the following relationship:

$$R_\omega \equiv \frac{-\Delta\omega_{\text{H}_2\text{O}}(\text{Ni(II)})}{-\Delta\omega_{\text{H}_2\text{O}}(\text{Ni}^{2+})} = \frac{\frac{[\text{Ni(II)}] h_n(\text{ads})}{D_{[\text{Ni}]} \cdot 55.5}}{\frac{[\text{Ni}^{2+}] \cdot 6}{D_{[\text{Ni}]} \cdot 55.5}} \quad (5.15)$$

where $h_n(\text{ads})$ is the hydration number of the adsorbed Ni(II) species. $[\text{Ni(II)}]$ for the adsorbed Ni(II) system was 0.042 M and $[\text{Ni}^{2+}]$ in the Ni²⁺ solution was 0.0274 M. $D_{[\text{Ni}]}$ of the aqueous phase was essentially unity at the concentrations of Ni(II) used in each system (Table 5.2). As h_n is 6 for Ni²⁺ solutions, $h_n(\text{ads})$ is

$$h_n(\text{ads}) = R_\omega \left[\frac{6}{1.5} \right] \quad (5.16)$$

$h_n(\text{ads})$ was calculated for the three highest temperatures at which data are taken. Results of these calculations are shown in Table 5.4.

$h_n(\text{ads})$ in Table 5.4 represents the average hydration number of all adsorbed Ni(II) species. Values of $h_n(\text{ads})$ of 2.4 at 61°C and 3.6 at 70°C indicate that the exchange-averaging process is not complete at these temperatures. At 80°C, $h_n(\text{ads})$ has reached the lower limit of the range of predicted values listed in Table 1.1. The rate at which the hydration number is increasing with temperature has dropped 50% in going from 70 to 80 °C. Attainment of fast exchange would be indicated by a value of $h_n(\text{ads})$ which remained constant as temperature was increased.

Table 5.4
 Calculation of the Hydration Number of the
 Adsorbed Ni(II) Species at Higher Temperatures

T°C	$-\Delta\omega_{\text{H}_2\text{O}}(\text{Ni}^{2+})^1$	$-\Delta\omega_{\text{H}_2\text{O}}(\text{Ni(II)})^2$	R_ω	$h_n(\text{ads})^3$
61	0.061	0.04	0.6	2.4
70	0.067	0.06	0.9	3.6
80	0.074	0.08	1.1	4.4

- 1) Calculated from equation 5.9b.
- 2) At each temperature shown, chemical shifts for the adsorbed Ni(II) system taken from Figure 5.4 have been averaged and combined with values of HA-100 chemical shifts calculated from equation 5.6c producing chemical shift values corrected for bulk susceptibility effects. These chemical shift values are referenced to H₂O by subtracting the appropriate chemical shift values calculated from equation 5.8a.
- 3) Errors for these values are estimated to be ±50%. They result largely from the process by which the spectra are referenced to H₂O.

It cannot be concluded from these calculations whether or not the fast-exchange regime was reached at 80°C. It is more likely that the exchange-averaging process is not complete and that data taken at higher temperatures would lead to larger values of $h_n(\text{ads})$. More data, taken at higher temperatures, would be needed to reach a definite conclusion.

5.5 Summary

Chemical shift and linewidth measurements were made on solutions of paramagnetic Ni(II) ions as a function of concentration and temperature. The effect of adding certain diamagnetic species, Na^+ , ClO_4^- and SiOH to Ni(II) solutions was investigated. Lastly, chemical shift and linewidth measurements were made as a function of temperature on a system in which Ni(II) species were adsorbed onto a silica surface to determine the hydration number of the Ni(II) surface complexes.

These NMR experiments produced the following results:

- i) The paramagnetic Ni^{2+} ion shifts the exchange-averaged water resonance line downfield from the pure water resonance. The diamagnetic species, Na^+ , ClO_4^- and SiOH shift the resonance upfield. The paramagnetic shifts are 2 to 3 times larger than the diamagnetic shifts.
- ii) The hyperfine coupling constant in a solution of $\text{Ni}(\text{ClO}_4)_2$ was determined to be $(6.5 \pm 0.3) \times 10^5 \text{ sec}^{-1}$, in agreement with reported literature values.
- iii) The rate constant for exchange of water molecules between the first coordination sphere of Ni(II) adsorbed onto a silica surface and bulk solution ($k_1(\text{ads})$) is smaller than the rate constant for exchange of

water molecules between the first coordination sphere and Ni^{2+} ions in solution (k_1) at all temperatures studied. Upper and lower limits for $k_1(\text{ads})$ were determined. At 25°C , it was found that $5.2 \times 10^3 \text{ sec}^{-1} < k_1(\text{ads}) < 3 \times 10^4 \text{ sec}^{-1}$.

iv) The data suggest that exchange-averaging is still incomplete for the adsorbed $\text{Ni}(\text{II})$ system at 80°C . Therefore, the value of 4.4 calculated for $h_n(\text{ads})$ is only a lower limit.

The following conclusions can be drawn from these results:

- i) The method of Live and Chan (1970) used to correct chemical shift values, measured in externally referenced samples, for bulk susceptibility effects provides accurate results.
- ii) In the $\text{Ni}(\text{II})\text{-SiO}_2$ system, a mixture of paramagnetic and diamagnetic components, the magnitude of the chemical shift of the exchange-averaged water line is solely attributable to paramagnetic $\text{Ni}(\text{II})$ species.
- iii) With this experimental design, the observation that the value of $k_1(\text{ads})$ was less than the reported value of k_1 , over the entire temperature range studied, made the determination of a theoretically useful value for $h_n(\text{ads})$ impossible.
- iv) Since the adsorbed $\text{Ni}(\text{II})$ system is not exchange-averaged at 80°C , $k_1(\text{ads})$ must increase with temperature at a slower rate than does k_1 .

CHAPTER 6

CONCLUSIONS

The experimental program of this thesis was designed to determine the hydration number of Ni(II) species adsorbed onto a silica surface using a nuclear magnetic resonance (NMR) technique.

In order to make this determination possible, the speciation of Ni(II) in the presence of a silica surface was determined by batch and titrimetric chemical methods. The following experiments were conducted on Ni(II) systems using NMR methods: i) the effect of paramagnetic Ni(II) species on the chemical shift and linewidth of the exchange-averaged water resonance line, in the presence and absence of a silica surface, was investigated; ii) the value of the electron-nuclear hyperfine coupling constant was determined; and iii) the effects of temperature and the presence of the silica surface on the exchange rate for water molecules between the first coordination sphere of Ni(II) and bulk solution were examined. All of these individual experiments provided valuable results. However, the key NMR data that would allow the calculation of the hydration number of adsorbed Ni(II) species lay just beyond the limitations of the NMR experiment as it was designed. Nevertheless, a lower limit for this value was determined.

6.1 The Adsorption of Ni(II) onto a Silica Surface

The study of the adsorptive behavior of a Ni(II)-SiO₂ system under the condition of high nickel ion loading, $\rho > 1$, found adsorption densities greater than those predicted assuming one nickel ion was bound to one surface group. This phenomenon was explained by postulating the

presence of hydrolyzed surface complexes whose NiOH moiety had the capability to function, in a chemically-similar manner, like a silanol group. The result is a continual regeneration of adsorption centers. Each nickel ion that adsorbs to the surface consumes one surface site and produces one new chemically-similar surface site. Thus, adsorption, as described by a surface complex formation process, has the potential to continue after the original surface has become completely covered with adsorbate. Adsorption densities appear to have no upper bound.

This phenomenon provides a satisfying mechanism to link the processes of adsorption and surface precipitation. It describes, in some detail, a chemical process which begins with the binding of a metal ion to an oxide surface, and continues to operate as additional layers of adsorbate, which comprise the beginnings of a new solid phase, are formed.

There is a significant ramification of this process when considering the importance of adsorption as a sink for metals in various environmental systems. The capacity of silica to bind nickel ions has been shown to be greater than what calculations, based on monolayer coverages of adsorbate, suggest. The pH at which adsorption occurs in the Ni(II)-SiO₂ system is lower than the pH at which the solid hydroxide phase precipitates in the absence of silica. These two facts result in an adsorptive removal process which behaves very much like the precipitation of a fresh solid hydroxide phase but occurs at a pH value 0.5 units lower. The stability, with respect to precipitation, of aqueous Ni²⁺ ion in the presence of a solid silica phase is reduced by approximately 0.5 pH units by an adsorption process which includes a mechanism

to regenerate adsorption centers. The capacity of siliceous soils and sediments to remove nickel ions from an associated aqueous phase may be larger than previously thought.

Additional studies on adsorption of metal ions onto oxide surfaces at high metal ion loadings would be valuable. Continued work should focus on determining the extent to which regeneration of adsorption centers occurs in other systems. Studies which surveyed a number of combinations of transition metal ions and surfaces for evidence of this process would be of greatest interest. The effects on the adsorption process of changes in ionic strength and the addition of complexing ligands might also prove useful to investigate.

6.2 NMR Spectroscopy

The capability of NMR spectroscopy to investigate the hydration number of an adsorbed paramagnetic ion was demonstrated. The mean values of $h_n(\text{ads})$, determined at higher temperatures, were reasonable for a system in transition between slow and fast exchange. At the highest temperature at which measurements could be made (80°C), the calculated value of $h_n(\text{ads})$ was just entering the range of predicted values (4.5 to 6.0). The data suggest that the calculated value for $h_n(\text{ads})$ will increase as the temperature is increased above 80°C . As the exchange-averaging process becomes complete at higher temperatures, the value of $h_n(\text{ads})$ will become constant with temperature.

With the knowledge that $k_1(\text{ads})$ is less than k_1 and the realization that temperature must be known more accurately than it was in this work to reduce the uncertainty in the calculated value of $h_n(\text{ads})$, the fol-

lowing suggestions are made to guide future work:

- i) parallel magnet/sample geometry experiments should be conducted on a spectrometer with a lower working frequency. Two hundred MHz spectrometers with superconducting solenoids exist and would be much better suited for this type of experiment.
- ii) a compound with a temperature dependent chemical shift might be included in the annulus of the sample tube to allow direct temperature measurements to be made while a spectrum is being recorded.
- iii) investigation of an ion with a larger hyperfine coupling constant would increase the measured values of $-\Delta\omega_{\text{H}_2\text{O}}$ with a resulting decrease in uncertainty. Good candidates from this point of view would be Mn(II) and Fe(III) with coupling constants of 5.9 and 7.7 x 10^5 Hz, respectively.

REFERENCES

- Abendroth, R. P. 1970. Behavior of a Pyrogenic Silica in Simple Electrolytes. *J. Colloid Interface Sci.* 34, 591-596.
- Allen, L. H., and E. Matijević. 1970. Stability of Colloidal Silica. II. Ion Exchange. *J. Colloid Interface Sci.* 33, 420-429.
- Allen, L. H., E. Matijević, and L. Meites. 1971. Exchange of Na^+ for the Silanolic Protons of Silica. *J. Inorg. Nucl. Chem.* 33, 1293-1299.
- Anderson, T. N., and J. O'M. Bockris. 1964. Forces Involved in the "Specific" Adsorption of Ions on Metals from Aqueous Solution. *Electrochim. Acta.* 9, 347-371.
- Baes, C. F., and R. E. Mesmer. 1976. *The Hydrolysis of Cations.* Wiley, New York.
- Barby, D. 1976. Silicas. In: *Characterization of Powder Surfaces.* G. D. Parfitt and K. S. W. Sing, editors. Academic Press, New York.
- Bechtold, D. B., G. Liu, H. W. Dodgen, and J. P. Hunt. 1978. An Oxygen-17 Nuclear Magnetic Resonance Study of the Aquo Nickel(II) Sulfate System. *J. Phys. Chem.* 82, 333-337.
- Benjamin, M. M., and J. O. Leckie. 1981. Multisite Adsorption of Cd, Cu, Zn, and Pb on Amorphous Iron Oxyhydroxide. *J. Colloid Interface Sci.* 79, 209-221.
- Bloembergen, N. 1957. Comments of "Proton Relaxation Times in Paramagnetic Solutions". *J. Chem. Phys.* 27, 595-596.
- Bolt, G. H. 1957. Determination of the Charge Density of Silica Sols. *J. Phys. Chem.* 61, 1166-1169.
- Brunauer, S., P. H. Emmett and E. Teller. 1938. Adsorption of Gases in Multimolecular Layers. *J. Amer. Chem. Soc.* 60, 309-319.
- Chan, D., J. W. Perram, L. R. White, and T. W. Healy. 1975. Regulation of Surface Potential at Amphoteric Surfaces during Particle-Particle Interactions. *J. Chem. Soc. Faraday Trans.* 1, 1046-1057.
- Chmelnick, A. M., and D. Fiat. 1971. Oxygen-17 Magnetic Resonance Study of the Hydration of the Ferrous and Nickelous Ions. *J. Amer. Chem. Soc.* 93, 2875-2877.
- Connick, R. E., and D. Fiat. 1966. Oxygen-17 Nuclear Magnetic Resonance Study of the Hydration Shell of Nickelous Ion. *J. Chem. Phys.* 44, 4103-4107.

- Cooper, M. A., H. E. Weber, and S. L. Manatt. 1971. The ^{19}F NMR Spectra of Some Fluoroaromatic Compounds. Studies Using Noise Decoupling of Protons. *J. Amer. Chem. Soc.* 93, 2369-2380.
- Coughlin, R. W., and I. Matsui. 1976. Catalytic Oxidation of Aqueous Mn(II). *J. Catalysis* 41, 108-123.
- Cozar, O., V. Znamirovechi, and V. V. Morariu. 1976. E.P.R. of Cu(II) into Layers of Water Adsorbed on Silica Surface. *Rev. Roum. Phys.* 21, 579-584.
- Davis, J. A., R. O. James, and J. O. Leckie. 1978. Surface Ionization and Complexation at the Oxide/Water Interface. 1. Computation of Electrical Double Layer Properties in Simple Electrolytes. *J. Colloid Interface Sci.* 63, 480-499.
- Davis, J. A., and J. O. Leckie. 1978. Surface Ionization and Complexation at the Oxide/Water Interface. 2. Surface Properties of Amorphous Iron Oxyhydroxide and Adsorption of Metal Ions. *J. Colloid Interface Sci.* 67, 90-107.
- Davis, J. A., and J. O. Leckie. 1980. Surface Ionization and Complexation at the Oxide/Water Interface. 3. Adsorption of Anions. *J. Colloid Interface Sci.* 74, 32-43.
- Davydov, V. Y., A. V. Kiselev, and L. T. Zhuravlev. 1964. Study of the Surface and Bulk Hydroxyl Groups of Silica by Infra-red Spectra and D_2O -exchange. *Trans. Faraday Soc.* 60, 2254-2264.
- Desai, A. G., H. W. Dodgen, and J. P. Hunt. 1969. Water Exchange between Solvent and Aquoethylenediaminenickel(II) Complexes. *J. Amer. Chem. Soc.* 91, 5001-5004.
- Dickinson, W. C. 1951. The Time Average Magnetic Field at the Nucleus in Nuclear Magnetic Resonance Experiments. *Phys. Rev.* 81, 717-731.
- Fanning, K. A., and M. E. Q. Pilson. 1973. On the Spectrophotometric Determination of Dissolved Silica in Natural Waters. *Anal. Chem.* 45, 136-140.
- Feitknecht, W., and L. Hartmann. 1954. Die Löslichkeitprodukte von Nickel- und Cobalhydroxyden. *Chimia.* 8, 95.
- Gayer, K. H., and A. B. Garrett. 1949. The Equilibria of Nickel Hydroxide, $\text{Ni}(\text{OH})_2$, in Solutions of Hydrochloric Acid and Sodium Hydroxide at 25°C . *J. Amer. Chem. Soc.* 71, 2973-2975.
- Grahame, D. C. 1947. The Electrical Double Layer and the Theory of Electrocapillarity. *Chem. Rev.* 41, 441-501.
- Granot, J., A. M. Achlama (Chmelnick), and D. Fiat. 1974. Proton and

- Deuterium Magnetic Resonance Study of the Aqueous Nickel Complex. *J. Chem. Phys.* 61, 3043-3047.
- Hatada, K., Y. Terawaki, and H. Okuda. 1972. A New Method for the Determination of the Volume Magnetic Susceptibility by NMR. *Bull. Chem. Soc. Jap.* 45, 3720.
- Hathaway, B. J., and C. E. Lewis. 1969. Electronic Properties of Transition Metal Complex Ions Adsorbed on Silica Gel. Part 1. Nickel(II) Complexes. *J. Chem. Soc. (A)*, 1176-1182.
- Hausser, R., and G. Laukin. 1959. Messung und Deutung der Temperaturabhängigkeit der Kernmagnetischen Protonenrelaxation in Wässrigen Lösungen von Ionen der I. Gruppe der Übergangselemente. *Z. Physik* 153, 394-411.
- Hindman, J. C. 1966. Proton Resonance Shift of Water in the Gas and Liquid State. *J. Chem. Phys.* 44, 4582-4592.
- Hohl, H., and W. Stumm. 1976. Interaction of Pb^{2+} with Hydrous $\gamma - Al_2O_3$. *J. Colloid Interface Sci.* 55, 281-288.
- Iler, R. K. 1979. *The Chemistry of Silica*. John Wiley and Sons, New York.
- Isaeva, A. A., and O. E. Presnyakova. 1973. Adsorption of Traces of Nickel on Hydrated Oxide Adsorbents. *Russ. J. Phys. Chem.* 47, 1327-1329.
- James, R. O., and T. W. Healy. 1972a. Adsorption of Hydrolyzable Metal Ions at the Oxide-Water Interface. I. Co(II) Adsorption of SiO_2 and TiO_2 as Model Systems. *J. Colloid Interface Sci.* 40, 42-52.
- James, R. O., and T. W. Healy. 1972b. Adsorption of Hydrolyzable Metal Ions at the Oxide-Water Interface. II. Charge Reversal of SiO_2 and TiO_2 Colloids by Adsorbed Co(II), La(III), and Th(IV) as Model Systems. *J. Colloid Interface Sci.* 40, 53-64.
- James, R. O., and T. W. Healy. 1972c. Adsorption of Hydrolyzable Metal Ions at the Oxide-Water Interface. III. A Thermodynamic Model of Adsorption. *J. Colloid Interface Sci.* 40, 65-81.
- Kiselev, A. V. 1971. The Effect of the Geometric Structure and the Chemistry of Oxide Surfaces on their Adsorption Properties. *Trans. Faraday Soc. Disc.* 52, 14-32.
- Lewin, S. 1960. *The Solubility Product Principle*. Interscience Publishers, Inc., New York.
- Live, D. H., and S. I. Chan. 1970. Bulk Susceptibility Corrections in NMR Experiments Using Superconducting Solenoids. *Anal. Chem.* 42,

791-792.

- Luz, Z., and R. G. Shulman. 1965. Proton Magnetic Resonance Shifts in Aqueous Solutions of Paramagnetic Metal Ions. *J. Chem. Phys.* 43, 3750-3756.
- Lyklema, J. 1968. The Structure of the Electrical Double Layer on Porous Surfaces. *J. Electroanal. Chem.* 18, 341-348.
- Manatt, S. L., and J. R. Young. 1980. A Measurement of the Absolute NMR Frequencies of CCl_3F and C_6F_6 Relative to TMS. *J. Mag. Res.* 40, 347-350.
- Morel, F. J. Yeasted, and J. Westall. 1981. Adsorption Models: A Mathematical Analysis in the Framework of General Equilibrium Calculations. In: *Adsorption of Inorganics at the Solid Liquid Interface*, M. Anderson and A. Rubin, editors, Ann Arbor Science Publications, Ann Arbor, Michigan.
- Neely, J. W., and R. E. Connick. 1972. Oxygen-17 Nuclear Magnetic Resonance Studies of Aqueous Nickel Ion. *J. Amer. Chem. Soc.* 94, 3419-3424.
- Perram, J. W., R. J. Hunter, and H. J. L. Wright. 1974. The Oxide-Solution Interface. *Aust. J. Chem.* 27, 461-75.
- Rablen, D. P., H. W. Dodgen, and J. P. Hunt. 1976. Water Exchange Studies by Oxygen Nuclear Magnetic Resonance on Nickel(II) Complexes with Diethylenetriamine, Triethylenetetramine, and Tetraethylenepentamine. *Inorg. Chem.* 15, 931-933.
- Richter, R. O., and T. L. Theis. 1978. Adsorption Reactions of Nickel Species at Oxide Surfaces. Presented before the Division of Environmental Chemistry, American Chemical Society, Anaheim, California March 1978.
- Schindler, P. W. 1981. Surface Complexes at Oxide Water Interfaces. In: *Adsorption of Inorganics at the Solid Liquid Interface*, M. Anderson and A. Rubin, editors, Ann Arbor Science Publications, Ann Arbor, Michigan.
- Schindler, P. W., B. Fürst, R. Dick, and P. Wolf. 1976. Ligand Properties of Surface Silanol Groups. I. Surface Complex Formation with Fe^{3+} , Cu^{2+} , Cd^{2+} , Pb^{2+} . *J. Colloid Interface Sci.* 55, 468-475.
- Schindler, P. W., and H. R. Kamber. 1968. Die Acidität von Silanolgruppen. *Helv. Chimica Acta.* 51, 1781-1786.
- Sillén, L. G., and A. E. Martell. 1964. Stability Constants of Metal Ion Complexes, Special Publication No. 17, Chemical Society, London.

- Smit, W., C. L. M. Holten, H. N. Stein, J. M. M. DeGoejj, and H. M. J. Theelen. 1978. A Radiotracer Determination of the Adsorption of Sodium Ion in The Compact Part of the Double Layer of Vitreous Silica. *J. Colloid Interface Sci.* 63, 120-128.
- Smith, R. M., and A. E. Martell. 1976. *Critical Stability Constants*, Vol. 4. Plenum Press, New York.
- Sung, W. 1981. Catalytic Effects of the γ -FeOOH(Lepidocrocite) Surface on the Oxygenation Removal Kinetics of Fe(II) and Mn(II). Ph.D. Thesis, California Institute of Technology, Pasadena, California.
- Stern, O. 1924. *Z. fur Elektrochem. und Angew. Physik. Chem.* 30, 508.
- Stumm, W. and J. J. Morgan. 1981. *Aquatic Chemistry*, 2nd edition, Wiley, New York.
- Swift, T. J., and R. E. Connick. 1962. NMR-Relaxation Mechanisms of ^{17}O in Aqueous Solutions of Paramagnetic Cations and the Lifetime of Water Molecules in the First Coordination Sphere. *J. Chem. Phys.* 37, 307-320.
- Swift, T. J., and T. A. Stephenson. 1966. The Kinetics of Protonation of Nickel and Chromium Hexaquo Cations in Aqueous Solution. *Inorg. Chem.* 5, 1100-1105.
- Swift, T. J., and Weinberger. 1968. Proton Magnetic Resonance Determination of the Primary Solvation Number of Nickel(II) in Aqueous Solution. *J. Amer. Chem. Soc.* 90, 2023-2026.
- Tadros, Th. F., and J. Lyklema. 1968. Adsorption of Potential Determining Ions at the Silica Aqueous Electrolyte Interface and the Role of Some Cations. *J. Electroanal. Chem.* 17, 267-275.
- Taniguchi, K., M. Nakajima, S. Yoshida, and K. Tarama. 1971. Coordination States of Some Metal Ions on Silica Gel Surface. *Bull. Inst. Chem. Res., Kyoto Univ.* 49, 212-221.
- Vuceta, J. 1976. Adsorption of Pb(II) and Cu(II) on α -Quartz from Aqueous Solutions: Influence of pH, Ionic Strength, and Complexing Ligands. Ph.D. thesis, California Institute of Technology, Pasadena, California.
- Vydra, F., and J. Galba. 1969. Sorption von Metallkomplexen an Silicagel. Sorption von Hydrolysenprodukten des Co^{2+} , Mn^{2+} , Cu^{2+} , Ni^{2+} , Zn^{2+} an Silicagel. *Collection Czech. Chem. Comm.* 34, 3871-3878.
- Wayland, B. B., and W. L. Rice. 1966. Contact Shift Studies of Some Paramagnetic Hexaquo Metal Ion Complexes. *Inorg. Chem.* 5, 54-57.

- Westall, J., and H. Hohl. 1980. A Comparison of Electrostatic Models for the Oxide/Solution Interface. *Adv. in Coll. Interface Sci.* 12, 265-294.
- Westall, J., J. Zachary, and F. Morel. 1976. MINEQL: A Computer Program for the Calculation of Chemical Equilibrium Composition of Aqueous System. Technical Note No. 18, Ralph M. Parsons Laboratory, MIT, Cambridge, MA.
- Wirth, G. S., and J. M. Gieskes. 1979. The Initial Kinetics of the Dissolution of Vitreous Silica in Aqueous Media. *J. Colloid Interface Sci.* 68, 492-500.
- Yates, D. E., and T. W. Healy. 1976. The Structure of the Silica/Electrolyte Interface. *J. Colloid Interface Sci.* 55, 9-19.
- Yates, D. E., S. Levine, and T. W. Healy. 1974. Site Binding Model of the Electrical Double Layer at the Oxide/Water Interface. *J. Chem. Soc. Faraday Trans. I* 70, 1807-1818.